

Integrating PV systems directly on metro traction networks

Focussing on the metro traction network of Amsterdam

W.M. van Dijk



Integrating PV systems directly on metro traction networks

Focussing on the metro traction network of Amsterdam

by

W.M. van Dijk

to obtain the degree of Master of Science
at the Delft University of Technology,
to be defended publicly on July 15, 2021 at 10:00 AM.

Student number:	4464346
Project duration:	November, 2020 – July, 2021
Thesis committee:	Prof. Dr. O. Isabella, PVMD group TU Delft
	Dr. H. Ziar, PVMD group TU Delft, supervisor
	Dr. J. Dong, DCE&S group TU Delft
	Dr. E. Veldman, AMS Institute, supervisor
	Ir. W. de Jager, Municipality of Amsterdam, supervisor

An electronic version of this thesis is available at <http://repository.tudelft.nl/>.

Preface

The MSc thesis project covered in this report is a collaboration between the municipality of Amsterdam, the Amsterdam Institute for Advanced Metropolitan Solutions (AMS) and the Photovoltaic Materials and Devices group (PVMD) of the TU Delft. The aim of this report is to give a better understanding of DC metro traction networks and the effect of PV systems connected to the DC-side of these traction networks, to explore the challenges and possibilities of the integration of PV systems directly on the traction network and to get a step closer to the realisation of more integrated PV systems and a more sustainable way of powering public transit.

I want to thank my supervisors Ir. W. de Jager, Dr. E. Veldman and Dr. H. Ziar for their input and interesting discussions during the meetings we had. I'm very grateful for the opportunity to do this project and the time they invested to guide and support me during the project. Further I want to thank Dr. J. Dong and Prof. Dr. O. Isabella for participating in the thesis committee and their effort to review my work. Lastly I want to thank my family and my wife in particular for their support during my study.

*W.M. van Dijk
Delft, July 2021*

Abstract

Although the metro is a very energy efficient option for passenger transportation compared to internal combustion vehicles, it is still a very prominent energy consumer. Further, due to the global pressure to reduce CO_2 emissions, there is a worldwide demand for efficiency and sustainability improving solutions and approaches for railway traction systems. Also, in Amsterdam, the municipality sets great ambitions regarding installed PV power in the city and the emissions related to public transit. The municipality of Amsterdam has the goal to have an installed PV power capacity of 250 MW in 2022 and to reduce CO_2 emissions with 55% by 2030 compared to 1990. Also, the metro system has to become 35% more energy efficient in 2030 compared to 2013. Moreover, the municipality wants to offer emission free public transport in 2025. To reach these ambitious goals, no piece of land suitable for PV can be left unused.

In the past, PV systems have already been installed on metro station roofs, connected to the AC-side of the metro traction network. However, no PV systems have yet been connected to the DC-side of the traction network, which would have enabled the connection of PV systems anywhere along the track. Also, there is still a lot of unused land along the metro tracks in Amsterdam, with a total available surface of 47991 m^2 . This land could potentially be used to install PV systems with a total installed power of 4511 kWp [1]. To increase the amount of installed PV power and to fully utilise the available land along the metro tracks, this report focuses on the connection of PV systems directly to the metro traction system, at the DC-side of the traction network, to accelerate the energy transition and to reach the sustainability goals in Amsterdam.

This report includes a comprehensive study on the challenges related to the integration of PV systems at the DC-side of the traction network, as well as possible solutions to mitigate these challenges. To further increase the energy efficiency of the traction network with PV systems, the integration of additional solutions like energy recuperating inverters in power substations and energy storage systems are discussed as well.

To study the energy saving effects as well as challenges of PV systems connected to the DC-side of the traction network, a Simulink model of the traction network is created, using measurement data of an M5 metro, the metro timetables and traction network parameters as an input. The input data for a specific pilot location, located nearby station *Amsterdam RAI*, is used for the simulations. Also different PV systems, with sizes of 202 to 799 kWp are simulated with PVsyst, using meteorological data for the pilot location. The simulation results are used in the Simulink model, to simulate a PV system connected to the traction network. Also inverters and storage systems are simulated using the Simulink model.

The results show an energy saving enhancement effect, due to decreased ohmic losses in the network as a result of the injection of PV power, meaning that more energy is saved than supplied by the PV system. However, due to the intermittency of the load and regenerative braking, only 51.5-83.0% of the potential PV energy yield can be supplied to the traction network, depending on the PV system size, resulting in a waste of PV energy. A variable PV output control strategy is proposed, which can increase the energy output of the PV system with about 13-22%.

When using an inverter in a substation, the amount of supplied PV energy can be increased to 83.4-97.6%, by exporting the surplus of energy to the power grid. Also, using the inverter, a significant amount of braking energy can be recuperated, which would otherwise have been wasted in the braking resistors of the metros, leading to even more energy savings. Also, an energy storage system is simulated. The results show that the storage system could theoretically prevent any waste of PV energy, while also saving braking energy and decreasing ohmic losses even more.

Using the results for an economical feasibility study on a PV system with and without inverter shows that a PV system operating alone would have payback period of 11 years, which can be reduced to 5 years by using an inverter.

Although this research focuses on integrating PV systems on the metro network of Amsterdam, the methodology can be applied to DC traction systems worldwide.

Contents

List of Figures	ix
List of Tables	xi
1 Introduction	1
1.1 Background	1
1.2 Previous studies	2
1.3 Problem statement	3
1.4 The research objective	3
1.5 Thesis outline	4
2 The Amsterdam metro traction network and its PV potential	5
2.1 The Amsterdam metro traction network	5
2.2 PV potential	7
2.3 The pilot location	8
3 System Topology	11
3.1 Topologies without storage	11
3.1.1 PV system with grid connection	11
3.1.2 Direct DC/DC connection	12
3.1.3 Back to back converter	13
3.1.4 Inverter at substation	13
3.2 Topologies with storage	14
3.2.1 PV system with super-capacitor	14
3.2.2 Flywheels	16
3.2.3 PV system with batteries	16
3.2.4 Hybrid storage	16
3.2.5 Back to back converter with storage	16
4 Traction Network Model	19
4.1 The Traction Network	19
4.1.1 Substation	20
4.1.2 Metro	21
4.1.3 Resistance	22
4.2 The PV system	23
4.3 Inverter at substation	23
4.4 The ESS system	24
4.5 Model outputs	25
5 Power Flow Management	27
5.1 PV system control	27
5.2 Inverter control	29
5.3 PV with storage control	31
6 Results	33
6.1 Conventional operation of traction network	33
6.2 Traction network with PV	37
6.2.1 Normal power consumption in adjacent power sections	37
6.2.2 Low power consumption in adjacent network	40
6.2.3 Decreased consumption	41
6.2.4 Variable PV output	42

6.3	Traction network with inverter	45
6.3.1	Inverter without PV	45
6.3.2	PV + Inverter	48
6.4	Storage	50
6.4.1	ESS without PV.	50
6.4.2	ESS with PV	51
7	Case Study	53
7.1	The PV system	53
7.2	Additional equipment.	54
7.3	Results	55
7.4	Economical evaluation	56
8	Conclusions	57
8.1	Conclusion	57
8.2	Discussion	58
8.3	Future work	58
	References	64
A	Power substations metro traction network Amsterdam	65
B	Profile of free space	67
C	Power consumption and ohmic losses	69
D	Main results from PVsyst simulation	71
E	Costs and profit for three different systems	73

List of Figures

1.1	83 kWp PV system on roof of metro station Reigersbos [6]	1
2.1	Metro network of Amsterdam [17]	5
2.2	Schematic overview of metro traction network	6
2.3	Power consumption of M5 metro Amsterdam	6
2.4	Energy flow diagram for DC traction network [21]	7
2.5	Pilot location next to station RAI, Amsterdam [25]	9
2.6	Pilot location next to station RAI, Amsterdam [25]	10
3.1	PV system connected at the AC-side of the traction network	12
3.2	DC and DC/AC-AC/DC topologies	13
3.3	Inverter in substation	14
3.4	PV system with super-capacitors	15
3.5	PV with ESS	15
3.6	Back to back converter with storage	17
4.1	The modelled part of the traction network in Amsterdam [25]	19
4.2	A simplified overview of the modelled traction network [46].	20
4.3	Rectifier unit external characteristic curve [47].	20
4.4	Substation model	21
4.5	Metro model	21
4.6	The M5 metro owned by the GVB [16]	22
4.7	Computation of network resistances	23
4.8	PV system model	23
4.9	Inverter model as current source	24
4.10	Inverter model as IGBT	25
4.11	PV and ESS model	26
5.1	Control scheme for PV	28
5.2	PV power output response	29
5.3	Control scheme for PV with variable output	30
5.4	PV power output response with PI control	30
5.5	Control scheme for inverter	31
5.6	Control scheme for PV & an ESS	32
6.1	Energy consumption of substations	34
6.2	Power consumption of substations	34
6.3	Power consumption of substations with and without regenerative braking	35
6.4	Power consumption of substations compared to ohmic losses	36
6.5	Power consumption of substations compared to PV power supplied to traction network	38
6.6	Voltage and ohmic losses after PV connection	39
6.7	East-west configuration for PV systems	39
6.8	Power consumption of substations compared to PV power supplied to traction network	41
6.9	Power consumption of substations compared to PV power supplied to traction network	43
6.10	Power consumption of substations compared to PV power supplied to traction network	43
6.11	1.5 MW INGEBER inverter [60]	45
6.12	Braking energy recuperated by the inverter during a weekday	46
6.13	Power consumption substations vs recuperated power by inverter	46
6.14	Relation between potential recuperated energy and maximum power rating of the inverter	47

6.15	Relation between potential recuperated energy and maximum power rating of the inverter	48
6.16	Relation between potential recuperated energy and maximum power rating of the inverter	49
6.17	Relation between potential recuperated energy and maximum power rating of the inverter	50
6.18	Traction network voltage with ESS	51
6.19	State of charge of the ESS during a day	51
7.1	The chosen PV module and setup	54
7.2	Horizon profile of pilot location	54
7.3	ERS inverter and proposed implementation by ABB [61]	55
A.1	Locations of substations	65
B.1	Profile of free space	67
C.1	Power consumption and ohmic losses in traction network during an entire day	70
E.1	Profit and costs for PV system	73
E.2	Profit and costs for inverter	74
E.3	Profit and costs for PV system + inverter	74

List of Tables

6.1	Results south facing PV systems	37
6.2	Results east-west oriented PV systems	40
6.3	Results south facing PV systems	40
6.4	Results east-west oriented PV systems	41
6.5	Results for halved power consumption	42
6.6	Results for different south facing PV systems	43
6.7	Comparison potential recuperated energy for different inverters	47
6.8	Results for different south facing PV systems and inverter	48
6.9	Results for different south facing PV systems and inverter	49
7.1	Energy savings of the different systems for a year	56
7.2	Return of investment	56

Introduction

1.1 Background

Although the metro is a very energy efficient option for passenger transportation compared to internal combustion vehicles, it is still a very prominent energy consumer. Further, due to the global pressure to reduce CO_2 emissions, there is a worldwide demand for efficiency and sustainability improving solutions and approaches for railway traction systems. In 2020, European studies predicted a large increase in passenger traffic and there is still a great potential to further optimise the energy efficiency and sustainability of rail transport [2].

In Amsterdam, various successful attempts have been made to make the use of metros more energy efficient and to decrease the related carbon emissions. This has been done by for example acquiring metros with more efficient motors, metros with regenerative braking capabilities and placing PV systems on station roofs (Figure 1.1) [3][4]. With the presence of new metros which are able to recover braking energy, also new solutions like substations with inverters and storage devices to recuperate braking energy have to be considered to increase efficiency and lower power consumption [5]. Together with the implementation of PV systems, this is a challenging task, but it also offers numerous advantages over the conventional traction systems.

Up until 2019, the energy consumption per travelled kilometre per passenger of the Amsterdam metro is reduced with 2% per year. The goal set by the GVB (responsible for the public transport in Amsterdam) is to become 35% more energy efficient in 2030 compared to 2013. Moreover, the goal is to offer emission free public transport in 2025 [3]. This is an ambitious goal and renewable energy sources and energy efficiency increasing solutions are therefore highly necessary.



Figure 1.1: 83 kWp PV system on roof of metro station Reigersbos [6]

Further, the municipality of Amsterdam has the goal to have an installed PV power capacity of 250 MW in 2022 and to reduce CO₂ emissions with 55% by 2030 compared to 1990 [7]. To reach this ambitious goal, no piece of land or roof suited for PV systems can be left unused. Therefore, the municipality of Amsterdam, but also other cities around the world, are increasingly interested in installing PV systems along metro tracks. Electrified metro networks have a great potential for PV systems, not only because metro networks consume a lot of energy, but also because there is a lot of unused land alongside the tracks. Also the PV systems can potentially be connected anywhere along the track, since there is always a feeder network available. For these reasons and more reasons that will be discussed in the remainder of the report, the focus of this report will be on connecting PV systems at the DC side of the metro traction network.

To exploit the advantages of connecting PV systems to the DC side of the metro traction network, in this report the associated challenges will be analysed and possible solutions will be discussed to come a step closer to a more sustainable way of using public transit. The goal of the study presented in this report is to accelerate the direct integration of PV systems on the metro traction network and to increase its sustainability. This report focuses on integrating PV systems on the metro network of Amsterdam, but applies to DC traction systems worldwide.

1.2 Previous studies

In the past, various studies have been done to explore the potential of connecting PV systems directly to the metro traction network. Already in 2011, the benefits of connecting PV systems to the DC side of traction networks are described, such as decreased transmission losses from the PV system to the consumer (the metro) [8].

In 2014 an interesting system design was proposed, including PV systems connected to the DC side of the traction network [9]. In this design an electric vehicle charging station is connected to the DC traction network, effectively creating a DC microgrid. The advantage of this design is that any surplus of braking energy or PV energy can be used to charge electric vehicles.

In 2018, a study was done on how PV systems could be indirectly integrated to the traction network by connecting them via super-capacitors to the traction system [10]. In the proposed approach, the PV systems charges the super-capacitors and the stored energy is then used to support the power supply during the acceleration of the metro. However, no direct connection of the PV system was discussed. Another study in 2018 introduced a hybrid traction power supply design, consisting of a bi-directional substation and a PV system connected at the DC side of the substation [11]. In this study, control methods for the converters are discussed in detail. Also the interface with the high voltage grid is included in this study. However, results were only given for time intervals of 2 seconds and mainly focused on voltage quality and harmonics. Also, the study focuses on the substation and the grid connection, but not on the traction network itself and the possible energy savings during a day were not discussed.

In 2018, the PV potential of the Amsterdam metro is explored, by calculating the available area to install PV systems including every piece of surface that can be used, like fields, embankments, spaces between tracks, sound barriers and even the sides of overpasses [1]. The available land is in the metro area and owned by the municipality of Amsterdam. This study shows that the total available surface for installing PV systems is 47991 m², the equivalent of 7 soccer fields. If this space is fully filled with 300 Wp P-type mono-crystalline PV modules from LG, an installed PV power of 4511 kWp can be achieved. However this study did not include the consequences of the challenges that will be discussed in Section 1.3 and only included the possible PV yield at the generation side.

Also in London, the PV potential for DC railways is investigated. A large project with multiple partners and founders was started to explore the potential of connecting PV systems directly to the DC traction network [12]. The researches recognised the potential of direct integration of PV systems on the DC traction network, as well as the challenges of doing this, which will be further explained in this thesis report. However to shorten the project timeline and to overcome the intermittency problem that will also be discussed in this thesis report, the initiators eventually decided to continue with PV systems connected to the AC side of the traction network [13].

In 2020, a team of researchers studied the potential of PV for the trackside of suburban elevated urban rail transit in Shanghai, which mainly uses a 1500V DC traction network [14]. This study was a continuation of the study that was already done in 2012 [15]. The researchers took the study one

step further and simulated the traction network with PV and storage using power system simulation software. From this study it became clear that the energy saved by injecting PV power can be more than the energy actually injected, due to the decreased ohmic losses in the traction network. This effect was even further exploited when using a storage system alongside the PV system. The researchers concluded their study stating that a connection of the PV system at the DC side of the traction system is superior to a connection at the AC side in terms of energy saving rate, traction power quality and safety improvement. However, the conclusions of the study were mainly based on a PV system working together with a storage system and did not include a detailed analysis of the mismatch effect of a PV system working alone. Also, simulations were done for only one metro, in a relatively small time interval of only maximal 100 seconds.

1.3 Problem statement

In this report the focus will be on connecting PV systems directly to DC side of the traction network of the Amsterdam Metro. Until now, there has been no known case of a PV system connected directly to the DC-side of a DC traction network in real life. There are still too many unknown factors and there is not yet a finished solution for the challenges that will be discussed in this report. The goal of the study presented in this report is to come one step closer to the actual implementation of a DC-side connected PV system. To do this, the studies on PV integration at the DC-side of the traction network will be taken a step further and the advantages/opportunities as well as the challenges will be analysed in more detail.

To connect a PV system at the DC-side, a power converter specifically designed for this purpose is required. Therefore, available solutions on the market will be explored, and different topologies for the total system will be discussed. Further, due to the intermittency of the load and the fact that the metro in Amsterdam is able to regenerate energy during braking, load matching is a challenge. The effect of the mismatch should be investigated in more detail in order to make a more reliable estimation for the PV yield in terms of financial savings. To solve the mismatch, additional solutions such as storage or bi-directional substations will be explored and the effects on the energy savings will be investigated in more detail. On top of that, voltage levels of the traction network should not rise beyond a critical level as a result of the energy injection of the PV system, or operation of additional equipment. Therefore it must be made sure that all proposed solutions will maintain or increase the voltage quality. Lastly, to gain better insight in the financial aspects of integrating PV systems directly on the metro traction network, a case study is required including an estimation of the return on investment, based on the actual PV yield, energy savings of additional equipment and costs of the required equipment and materials. The results discussed in this report will be used to make this case study more reliable.

1.4 The research objective

The main research objective that arises from the opportunities, challenges and research topics as described in Section 1.3 is:

How can the Amsterdam metro contribute to the acceleration of the energy transition by integrating PV systems directly on the traction network?

The emphasis in this research is on the word *how*. How can PV systems be connected directly to the traction network, what is the most optimal way of doing so and what are the challenges to overcome? To find the answer on the main research question, in this report, the following subquestions will be used to guide the study towards this answer:

1. What would be an optimal spot for a pilot and why?
 - (a) What would be the most efficient design of the PV system for the pilot location?
 - (b) What is the optimised kWp considering the metro network consumption profile if the system would be scaled up?
 - (c) How much yearly electrical yield is expected from the prospected PV systems?
2. How can the PV installations be directly integrated on the metro traction network?

- (a) What is the best conversion-stage design architecture?
 - (b) Can the proposed design satisfy the safety requirement of the metro network?
 - (c) What are the potential options in the electrical market for buying the equipment?
3. How can storage contribute to further improvement of the system?
- (a) Is using storage a necessity for this system? Or we can rely on the grid as the storage?
 - (b) How and how much storage can improve the current system?
 - (c) What technology and size for the storage is recommended? Higher energy density or higher power density or a combination of both?

Research subquestion 1 mainly focuses on the PV system itself, including its location, design and yield. Research subquestion 2 further explores the options to actually integrate this PV system on the metro traction network. Lastly, research subquestion 3 aims to find out the need for additional equipment to further improve the system like an energy storage system, but also the option to use the grid as "storage", using an inverter.

1.5 Thesis outline

This thesis report is build up step by step towards the point that enough information and data is collected to be able to answer the research questions that are listed in the previous section.

Chapter 2 starts by explaining how the current metro traction network in Amsterdam works. Next, the PV potential for the metro in Amsterdam as well as the criteria for the PV system are given, based on previous studies. Lastly the reasoning behind the choice for a pilot location is discussed in Chapter 2, which answers research subquestion 1.

In Chapter 3 different topologies that can be used for the integration of PV systems on the traction network are discussed, as well as their advantages and disadvantages, based on literature. The information in this chapter answers research subquestions 2, 2a, 2b and 2c.

In Chapter 4 it is explained how a model of the traction network and any connected system can help to answer the research questions. Also, the model that is used during this study is discussed, including an explanation of how the model is made and how simulations are done.

In Chapter 5 some control strategies are discussed to control the various systems that are modelled, such as the PV system, an inverter and an energy storage system. These control strategies are used to manage the power flow in the system such that it optimises the efficiency of the system, while maintaining the safety and reliability of the traction system.

Then in Chapter 6 the results are discussed which are obtained using the models discussed in Chapter 4 and the control strategies discussed in Chapter 5. In this chapter, the answers for research subquestions 3, 3a, 3b and 3c are discussed.

These results are then used in Chapter 7 to recommend a system, which is then studied in more detail. This answers research subquestions 1a, 1b and 1c. Also the economical feasibility of this system is assessed in Chapter 7.

Lastly, the conclusions of this study are given in Chapter 8. Also a discussion and some directions for future studies that may be interesting are given in Chapter 8.

2

The Amsterdam metro traction network and its PV potential

2.1 The Amsterdam metro traction network

The metro network of Amsterdam, as depicted in Figure 2.1, consists of 5 lines, with a total length of 52.2 km. 80% Of the metro tracks are above ground, which means a great potential for PV installations installed along the track [16].

The traction network of the Amsterdam metro is a DC network with a nominal voltage of 750 V, that uses a third rail to feed the metro and uses the railway track as a return path. The third rail is fed by substations, which are connected to the 10.5 kV grid. The substations use a three-phase transformer to step down the voltage and a 6-pulse or 12-pulse rectifier for AC to DC conversion. A schematic overview is given in Figure 2.2. The spacing between different substations is in the order of a few kilometres. The locations of the substations are shown in Figure A.1, included in Appendix A.

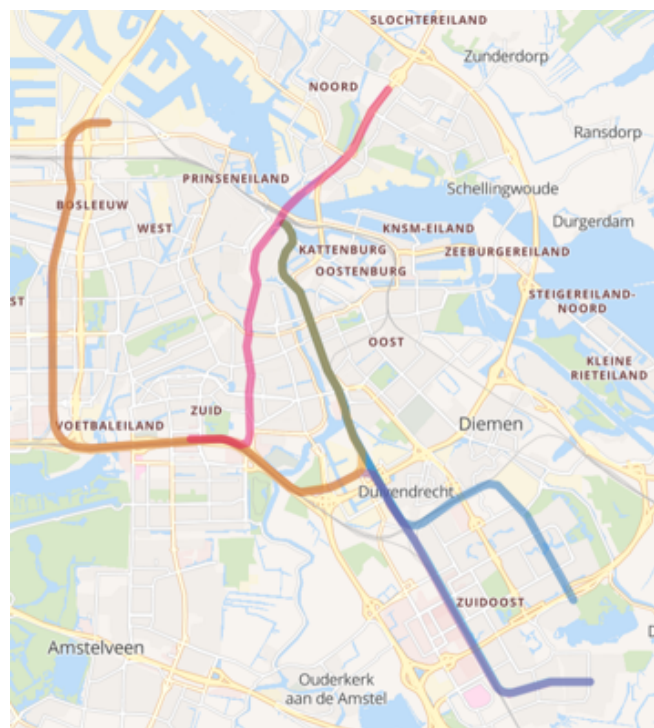


Figure 2.1: Metro network of Amsterdam [17]

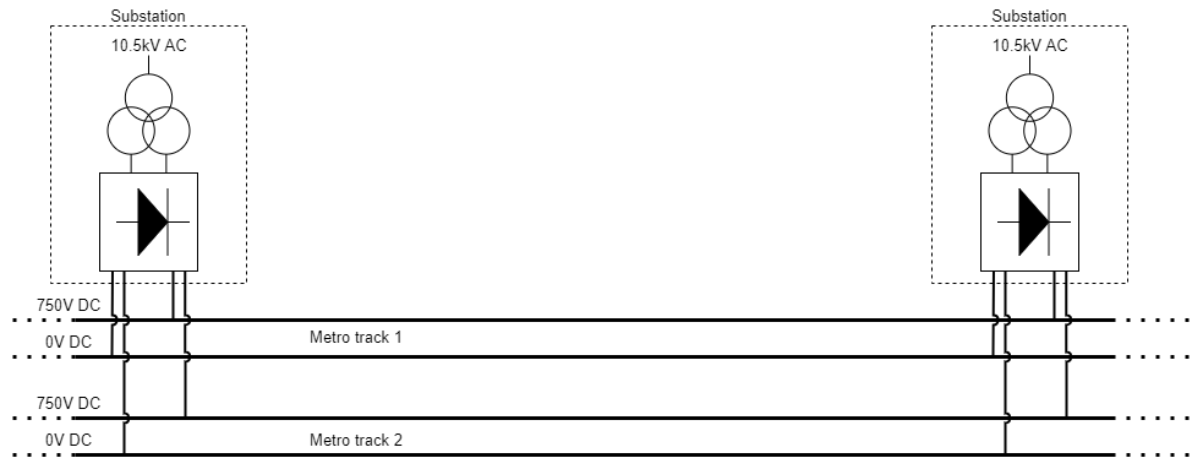


Figure 2.2: Schematic overview of metro traction network

The metro operation can be divided into three main modes: acceleration, coasting and braking. During the acceleration mode, the metro accelerates and consumes power from the third rail located next to the traction rails. In the coasting mode, the speed of the metro is nearly constant, and it consumes a negligible amount of power compared to the acceleration mode. In the braking mode, the metro decelerates [18]. It is important to know that an increasing number of metros in Amsterdam is able to recover its kinetic energy during braking, known as regenerative braking. The electric motors of these metros have the ability to act as generators [19]. This energy is fed back to the traction network and can be consumed by other metros nearby and/or can be fed to the auxiliary equipment in the braking metro like heating and lights. If no other consuming metros are nearby, the injected regenerative braking energy can cause voltage spikes. Therefore, the metros are equipped with a braking chopper or rheostat that is activated and dissipates power when the line voltage exceeds 900 V. However, as this dissipated power is completely wasted, it is desired to use these resistors as little as possible.

A typical load profile for the traction system of a M5-metro in Amsterdam is shown in Figure 2.3. This profile does not include the load of the auxiliary equipment of the metro. Here, the metro drives from station *Amsterdam RAI* to station *Amsterdam Zuid*. For this profile, measurement data of an actual driving metro is used [20]. Here, one can clearly see the power consumed during the acceleration at station *Amsterdam RAI*, some additional acceleration in between and the braking when the metro arrives at station *Amsterdam Zuid*.

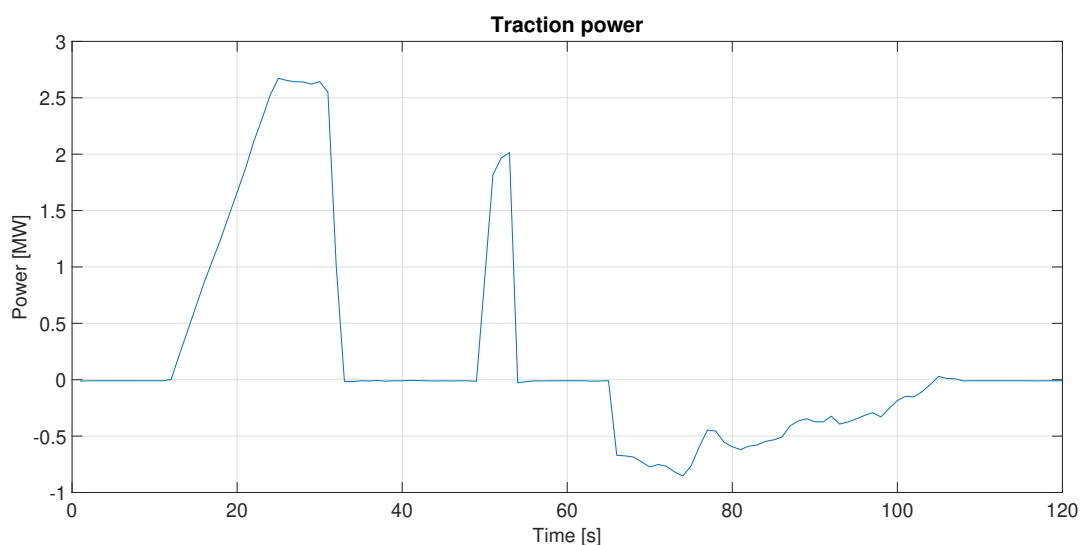


Figure 2.3: Power consumption of M5 metro Amsterdam

Further, the metro consumes power for auxiliary equipment like air-conditioning and lighting. In Figure 2.4, a Sankey diagram is depicted for a DC traction network, which clarifies the energy flows in the traction network. Also sources for several energy losses are shown. Here the "rectified" energy is the output of the substations. Note that for the metro traction network in Amsterdam, a third rail is used instead of a catenary. Because of the great variations in energy that is consumed (or regenerated)

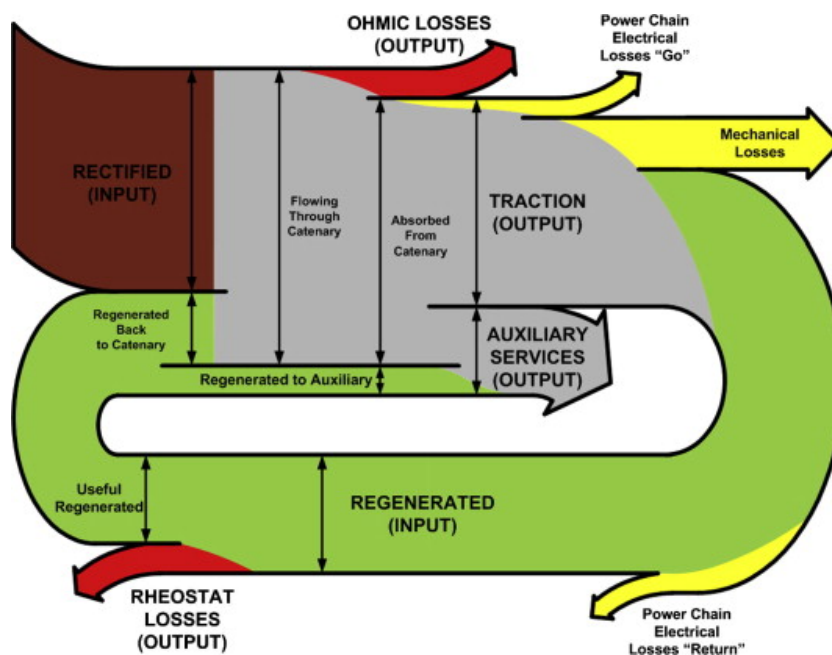


Figure 2.4: Energy flow diagram for DC traction network [21]

during the three operating modes of the metro, the third rail voltage also fluctuates a lot. This is also due to the resistance of the third rail and the traction network in general, which causes voltage drops. This can make the control of any connected systems like PV or storage more complex.

A PV system could either be connected to the AC side or the DC side of the traction network. PV systems have already widely been integrated to traction networks around the world using an AC side connection, also in Amsterdam. However, the next step is to consider the integration of a PV system at the DC side of the network. The reasons for this will be further explained in Section 3.1.2.

2.2 PV potential

As mentioned in Section 2.1, 80% of the Amsterdam metro lines are above ground. In 2018, a study has been done to determine suitable locations for PV systems around the metro track [1], to estimate the total available area to install PV systems. All the following information in this section comes from this study. For potential locations the following stakeholder criteria were used:

1. Maintenance:
 - A Obstruct the accessibility of machines as little as possible
 - B Obstruct the maintenance processes as little as possible
 - C The PV system must be low maintenance
2. View:
 - A The PV system must not obscure the metro driver's view
 - B The PV system must not contain any reflective objects that could cause glare for the metro driver
3. Safety:
 - A The constructional safety must be guaranteed so that no inadmissible safety risk arises
 - B The PV system is outside the profile of free space (see Figure B.1 in Appendix B)
 - C The solar panels should not obstruct escape routes and accessibility for emergency services in case of calamities. More specifically: every 12 solar panels, a space of 0.5 meters must be left empty that can serve as an escape route in the event of an emergency

4. Lifespan:
 - A Decrease the lifespan of the assets as little as possible
 - B The PV system has a lifespan of 25 years
5. Security: The PV system is protected against theft and vandalism
6. Functionality: The solar panels will hinder the function of the assets as little as possible. The assets are not dissected
7. Accessibility: The PV system does not impede the option of accessing the track with a machine
8. Availability: The PV system does not impede the possibility of infrastructural adjustments
9. Sustainability: Use the green area as little as possible for placing the PV system
10. Energy:
 - A Install as many solar panels as possible
 - B Catch as much solar irradiation as possible
11. Appearance: The PV system has a representative appearance
12. Design vision: The PV system will hinder the design vision of the surrounding objects as little as possible

Further, it is required that the PV system must:

1. have optimal efficiency
2. have a service life of ≥ 25 years in operation
3. be reliable and available at all times
4. have minimal impact on existing maintenance processes
5. not pose any danger to the operator, travellers and local residents
6. be sustainable
7. provide as few visual disturbances as possible

Using all these requirements and criteria, the available space to install PV systems is estimated to be 47991 m^2 , the equivalent of 7 soccer fields. This includes areas like fields, embankments, spaces between tracks, sound barriers and even the sides of overpasses. This available space is in the metro area and owned by the municipality of Amsterdam. If this space would be fully filled with 300 Wp mono-crystalline PV modules from LG, an installed PV power of 4511 kWp could be achieved.

2.3 The pilot location

To test the proper functioning of a PV system connected to the traction network, first a pilot location is chosen where a PV system can be tested before it is used at other locations. To determine a suitable pilot location, another study in 2020 by Movares is used to narrow down the options from the list obtained during the study in 2018 by A.A. Messaoudi [22]. Using all the requirements mentioned above, a list was compiled with all possible locations for a PV system around the metro track. From this list, the eight most promising locations for a pilot were picked and a more detailed study was performed by Movares on the following aspects to ensure the feasibility of a PV system:

- Underground infrastructure, like cables and pipes
- Flora and fauna
- Soil quality
- Archaeology
- Non-Burst Conventional Explosives (NGCE in dutch)
- Geotechnics:
 - Soil structure
 - Groundwater level
 - Geometry
 - Track load
- Carrying capacity and mounting options for artwork (for flyover Ganzenhoef)
- Arrangement and number of solar panels
- Power and connection to the network

The five most suitable pilot locations resulting from this study are listed below, with option 1 being the option with the least uncertainties and option 5 with most:

1. Location 15b, natural slope
2. Location 16a, natural slope
3. Location 21e, space between tracks
4. Location 15a, natural slope
5. Location 11b, ground level

From the 5 options, location 11b seems to be the best option, because of the following advantages:

- A lot of space
- PV panels can be installed using any orientation desired
- Good accessibility
- Flat terrain
- Few surrounding objects (also not planned [23]) that can block irradiation [24]
- Relatively easy to defend against vandalism
- Location can satisfy all requirements that are mentioned before

This location is next to station RAI in Amsterdam. The pilot location is shown in Figure 2.5 and 2.6. Note that, as stated in the Movares report, for this location it has to be investigated whether the local ecology is not harmed by the solar panels and the cadastral data has yet to be obtained. However looking at the cadastral data that is available on the internet, it appears that the plot at the pilot location is owned by the municipality of Amsterdam [23]. Further, there is some vegetation at this location that might limit the usable area, or that might have to be removed. The available area at the pilot location is about 10300 m^2 [23].



Figure 2.5: Pilot location next to station RAI, Amsterdam [25]



Figure 2.6: Pilot location next to station RAI, Amsterdam [25]

3

System Topology

When actually integrating a PV system on the metro traction network, there is some degree of freedom in the design of the total PV system. For example, the point of connection has to be chosen, the type of converter and potentially supplementary equipment like inverters and storage. In this chapter several possible topologies for the integration of PV and the optimisation of the energy efficiency of the system will be discussed, along with their advantages and disadvantages. The topologies can be summarised in two categories, DC-side connected and AC-side connected. A DC-side connection implicates a connection of the PV system directly to the third rail, or at the output of the rectifier in the power substation, albeit with the help of a power converter. An AC-side connection means that the PV system is connected to the grid, either directly to the 10.5 kV grid, or at the AC-side of the rectifier in the power substation. Further, the topologies can be further categorised by systems either with or without an electrical storage system.

Although more energy saving topologies and systems exist, this chapter gives an overview of the most promising topologies for the implementation of PV systems to the DC side of the traction network.

3.1 Topologies without storage

First the topologies without any form of storage are discussed in this section. These systems are most straightforward and minimise the investment costs for the total system.

3.1.1 PV system with grid connection

The most straightforward approach to connect a PV system to the traction network, is by connecting the PV system to the AC-side at the power substation by means of a DC/AC converter, as shown in Figure 3.1 [26]. In fact, this method of connecting PV systems to the traction network is already performed in several cities, including Amsterdam [4][13][27]. Although this thesis study focuses on DC-side connected PV systems, this topology is included for the sake of completeness.

DC/AC converters are widely available on the mass market and the technology for these converters is very mature. Also, besides powering the traction network, the PV system could power the AC loads at a metro station. Another advantage is that any surplus of generated PV power could be exported to the grid, meaning that the intermittency of the metro load would not cause any problems [13].

However, the downside of this topology is that the power that is generated by the PV system needs several conversion steps before it can be fed to the third rail of the metro network, leading to conversion losses. Also, the need for a grid connection is a problem when a PV system is to be installed at a location where no grid connection is available, or too expensive.

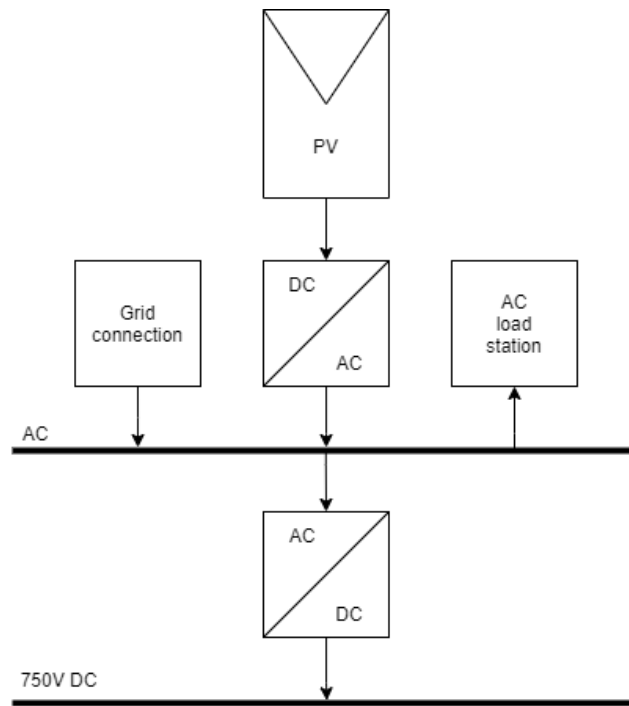


Figure 3.1: PV system connected at the AC-side of the traction network

3.1.2 Direct DC/DC connection

A promising way to connect PV systems to the traction network is by connecting it directly at the DC-side to the traction network, without a grid connection and outside the substation. This allows the PV system to be connected anywhere alongside the metro track. Not only does this allow the installation of PV systems where a grid connection is not possible or too expensive, but it could also be more efficient. This topology is shown in Figure 3.2a.

A PV array voltage output between 600 and 800 V DC is very common. This is very close to the nominal voltage of the metro traction network of Amsterdam. This means that only a small DC/DC conversion step is required to connect the PV system to the traction network. This is more efficient compared to an AC-side connection, where a DC to AC conversion is required to feed to PV power to the substation or grid, and another AC to DC conversion to feed the PV power to the traction network. A previous study suggests that supplying DC power directly to DC traction substations should yield 4 to 5% more useful electricity from a given PV system compared with a standard grid export model [12]. This also means that no harmonics are created by a DC to AC inversion. Also, transmission losses for a DC side connection are lower compared to an AC side connection of the PV system [8].

Moreover, experimental calculations done by Shen et al. suggest that during acceleration of the metro, the energy that is saved with the topology as shown in Figure 3.2a, is 1.2 more than is generated by the PV system [14][15]. This is mainly due to the fact that the PV system can increase the voltage of the traction network during acceleration and decrease the power loss in the traction network due to ohmic losses.

Another advantage is that a DC side connection can help to stabilise the voltage fluctuation of the traction network caused by the frequently switching operation modes of the metro [14][15]. G. Zhang et al. have proposed a DC/DC converter design at component level as well as a design for the control strategy for the converter to connect a PV system directly to a DC traction system [11]. X. Zhu et al. performed a comprehensive study on the stability of the DC traction network and the interaction between DC/DC converters and the substations when connecting PV systems [28].

However, there are some challenges related to this topology.

Both the load as the PV generation are very intermittent. This means that matching the generation with the load can be very difficult. If the load is too low, and/or the generation too high, the injection of PV power can cause the line voltage to rise beyond a critical level. On top of that, when the metro is

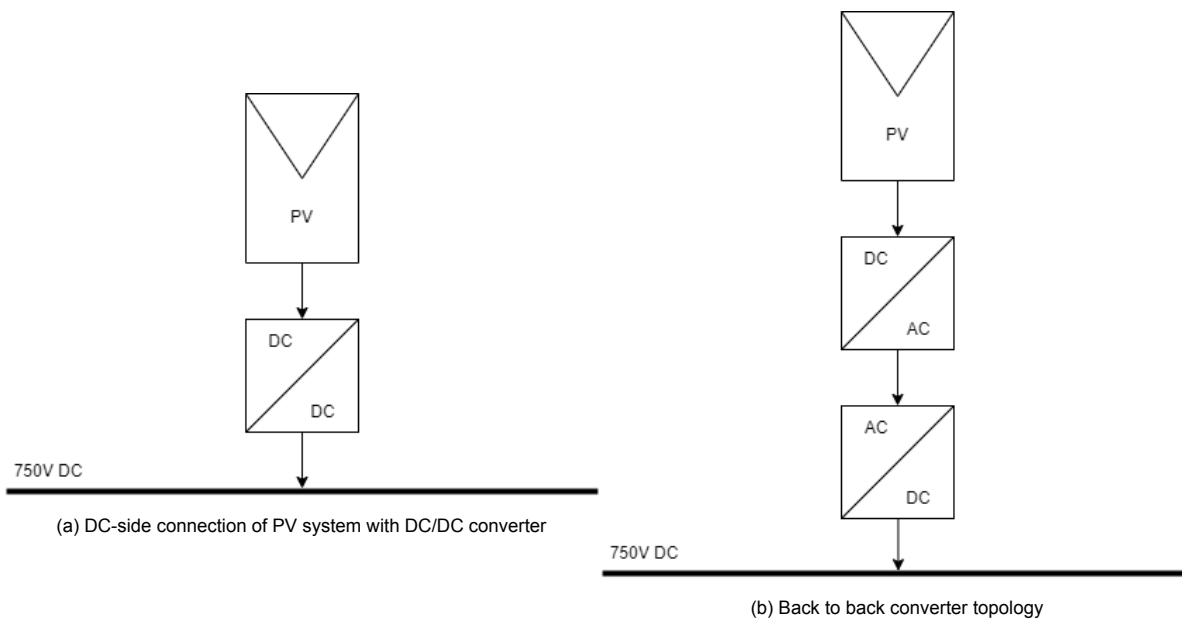


Figure 3.2: DC and DC/AC-AC/DC topologies

braking, it is delivering electrical power to the traction network as well, dropping the power demand of the traction system. Therefore the sizing of the PV system is very important. Also, it should be possible to disconnect the PV system, or to curtail the PV power output, to maintain a safe voltage level.

Although a direct DC/DC converter is hard to find, at the moment of writing a company claims to be able to make this converter with a power capacity of $200kW$ and an efficiency of 90%. Also multiple of these converters can operate in parallel to increase the power capacity. The specifications of this converter will be used as a reference for the models described in this report. Other companies like SMA and Siemens have indicated that they are considering manufacturing DC/DC converters for this application in the future, but are not able to supply this converter in the near future.

3.1.3 Back to back converter

Another way to connect the PV system at the DC-side of the traction network, is by using a grid forming DC to AC converter connected to a AC to DC converter or i.e. a rectifier. This is shown in Figure 3.2b. Although this topology may be less efficient than using a direct DC/DC conversion due to the extra conversion step and this may seem like a cumbersome topology, it may also be the key to finding the required components for a DC-side connection in the near future since both converters individually are widely available on the market and the technology used for these converters is very mature. However some adjustments may be necessary.

3.1.4 Inverter at substation

One way to solve the intermittency problem of the load and generation, is by installing a bi-directional AC/DC converter in the substation, or an inverter anti-parallel to the rectifier in the substations like shown in Figure 3.3 [5]. In this way, not only the surplus of PV energy can be exported to the grid, but also the surplus of braking energy. This would make it unnecessary to install any batteries. Also, this technology is already very mature and relatively easy to get on the market. Also, the efficiencies for such inverters are relatively high. Efficiencies of up to 98% are no exception. Different companies, like Siemens, Alstom, Meiden, Dynniq, ABB and Ingeteam are already able to supply these kind of equipment. Inverters of these companies have also been implemented in traction systems already, also in Rotterdam [29].

Inverters also have some advantages over storage, like a high efficiency due to fewer transformation losses, inverters need less space and they have lower safety constrains [30].

However, since the inverter must be placed in a substation, some PV power will be lost due to the ohmic losses in the network between the PV system and the inverter during export of PV power to the

grid. Also, power cost savings could be lower compared to energy storage systems, due to the fact that exported energy is sold for a lower price than it is imported. However this is not the case in Amsterdam. The use of inverters in DC traction system is already studied many times and in great detail [18][31][32]. Also algorithms to determine the optimal location and size of inverters have been studied [33].

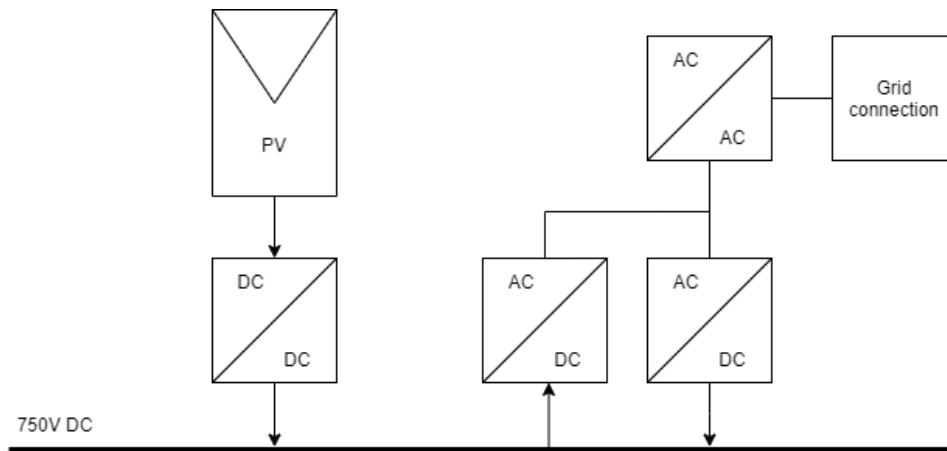


Figure 3.3: Inverter in substation

3.2 Topologies with storage

A combination of PV and an energy storage system (ESS) can be very useful for compensating voltage drops at weak points of the traction network [34]. Not only do voltage sags lead to higher ohmic losses, but it can also lead to damage to the electronic equipment in the metro [18]. Also, using an ESS allows the system to store the surplus of energy due to regenerative braking, or the generated PV energy, when no (other) metro is nearby to consume the generated energy. The stored energy can be fed into the traction network again when a metro nearby is accelerating and can compensate voltage drops [35]. This allows for peak shaving and peak shifting during voltage peaks [36]. This also prevents power from being wasted in the braking resistors of the metro [18]. In short, using an ESS solves the intermittency problem mentioned in Section 3.1.2.

Another advantage is that since the ESS does not require a connection to the AC grid, an ESS can be both installed inside the metro or along the metro track. In this report, only ESS along the track will be considered, since the equipment inside the metro is not to be changed.

3.2.1 PV system with super-capacitor

One way to implement an ESS is by using super-capacitors [10][37]. This system can be connected anywhere along the track using DC/DC converters. An overview of such a system is given in Figure 3.4. The high power density of the super-capacitors is especially useful for stabilising the grid voltage, since the grid voltage can vary a lot due to the large discontinuous power consumption of the metros. The super-capacitors are able to release or store the large amounts of energy quickly that is needed during acceleration or that is generated during braking, respectively [36]. This also increases the available peak power in the system [2]. Further, super-capacitors have a high energy efficiency of about 95%, a long lifetime and a long cycle life of more than 100000 cycles [18][30][38].

The proposed design is a modular design and can be distributed along the metro track. This does not only increase the system reliability, but can also decrease losses due to the resistance of the traction network. In Section 3.1.2, it is already noticed that using a direct DC connection can lead to energy saving of 1.2 times the energy that is generated by the PV system. The same study shows, that connecting an energy storage system (ESS) can also save another 6.45% of the power consumption of the metro by absorbing and releasing the braking energy of the metro [14][15]. Moreover, when the ESS and PV system are used together, the energy consumption is decreased by 2 times the PV energy yield. This is mainly due to the fact that the third rail voltage can be increased when power consumption is high, leading to less current through the third rail, hence less resistive losses. The topology used for these calculations is shown in Figure 3.5 [14].

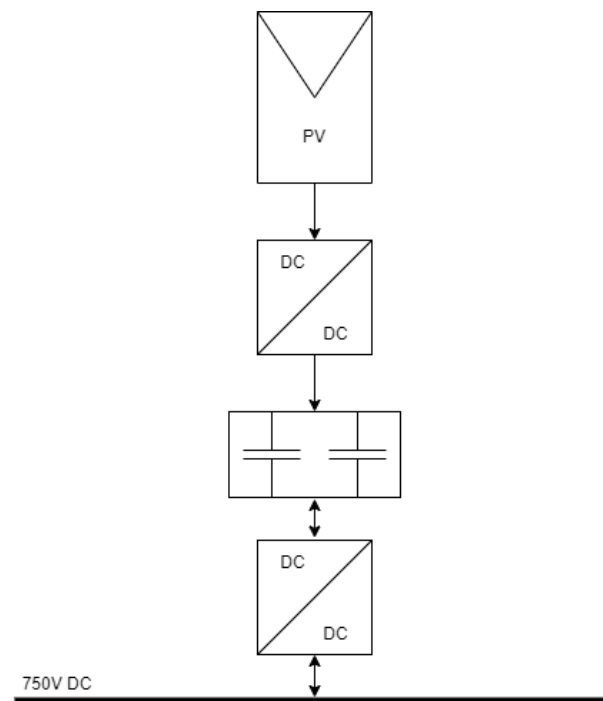


Figure 3.4: PV system with super-capacitors

However, super-capacitors are not able to efficiently store energy for longer periods [38]. Also, although super-capacitors are already used for railway applications, such a system in combination with PV does not seem to be available on the market yet. Nevertheless, the super-capacitors could be installed apart from the PV system in its vicinity. Various examples of super-capacitors integrated on traction systems already exist with equipment manufactured by well-known companies like ABB, Adetel, Bombardier, Meiden and Siemens [29].

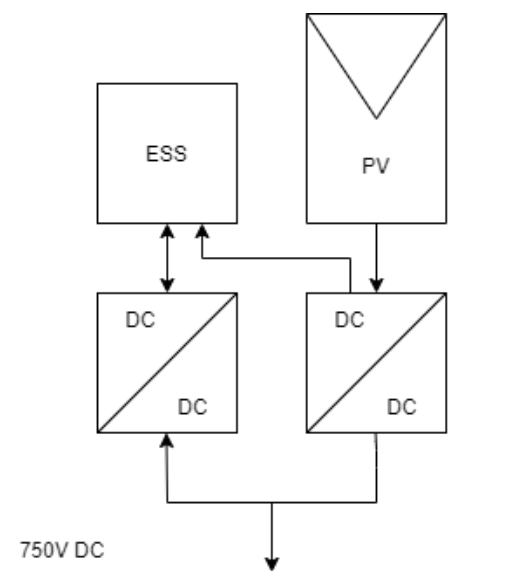


Figure 3.5: PV with ESS

3.2.2 Flywheels

Instead of super-capacitor, also flywheels could be used to store electrical energy. Flywheels can be considered as an electromechanical ESS that stores energy by converting the electrical energy to kinetic energy. Flywheels can have a high energy efficiency of about 95%, high power density (up to 5000 W/kg) and a high energy density (more than 50 Wh/kg). Further, they have a high cycling capacity (more than 20000 cycles), low environmental concerns and require little maintenance. However, flywheels have a high self-discharge current, are expensive and also very heavy [18][30][38]. Flywheels have already been implemented in traction systems with equipment manufactured by companies like Calnitex, Piller, Rosseta, Siemens and Urenco Power Technologies [29].

3.2.3 PV system with batteries

Also a combination of a direct DC/DC connection and energy storage with for example lithium-ion technology could be a good option for integrating PV systems. Li-ion batteries are more capable of storing the electrical energy for longer periods than super-capacitors [38]. This could be used to store energy during the day, when PV generation is high and the load is lower, to be released again during the peak hours in the morning and evening, when PV generation is low and the load is high.

Again, the storage can also be used to make more efficient use of the braking energy. Experiments with Li-ion batteries connected to the traction network have already resulted in energy savings of 4% of the total traction energy consumption [39]. Also the third rail voltage can be improved [40]. Further this system can act as voltage support when a fault occurs in a substation, since it could be able to operate alone [38][41].

However, due to the lower specific power of Li-ion batteries, it might be harder to handle the large currents during the acceleration and braking of the metro. Also, Li-ion batteries have a shorter lifetime and lower cycle life than super-capacitors [38]. Nevertheless, batteries are already integrated on traction system for energy saving purposes with components manufactured by for instance ABB, Hitachi and Kawasaki [29].

3.2.4 Hybrid storage

In the previous section, it is mentioned that, although super-capacitors have a high energy density and better cycle life, super-capacitors are not able to store energy for longer periods. Li-ion batteries on the contrary can, however they have a lower specific power and cycle life. To combine the best of both worlds, a hybrid energy storage system, with both super-capacitors and batteries can be used [42][43]. A case study for a Spanish railway line shows that a cost saving of 33.22% can be achieved by using renewable energy sources and a hybrid energy storage system [43].

3.2.5 Back to back converter with storage

The same solution as mentioned in Section 3.1.3 can be used in combination with a battery system, as shown in Figure 3.6. Standalone, grid forming DC/AC converters in combination with storage are already widely used for island operating PV systems. This could make it easier to find the required components on the market to connect the PV system, as well as the storage system to the DC-side of the traction network.

Although this may seem like a cumbersome topology, it also may accelerate the integration of PV systems and storage at the DC-side of the traction network in the near future, while DC/DC converters are difficult to acquire for this application.

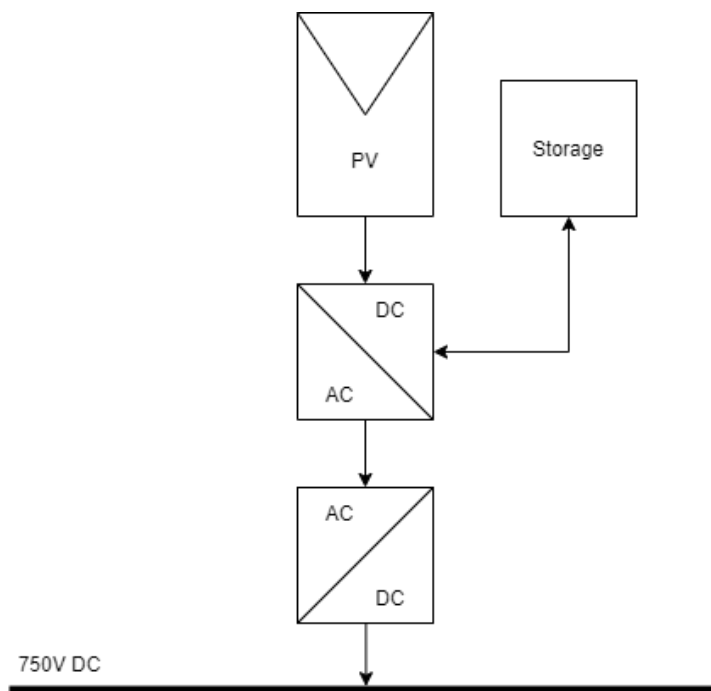


Figure 3.6: Back to back converter with storage

4

Traction Network Model

To study the effects and possibilities, as well as the challenges of injecting PV power into the traction network, a model of the traction network including a PV system is required. For this project, a model of the traction network in MATLAB and Simulink is created [44][45]. Also different PV systems are modelled together with storage systems or an inverter in one of the substations. These models can then be used to test various systems and to calculate the amount of energy that can be saved using them. Also the model helps to gain a better understanding of the behaviour of the metro traction network and of any additional connected systems. Also the model can be used to really show the impact and magnitude of challenges like the mismatch of load and generation.

4.1 The Traction Network

First, a model of the traction network is created. Because a model of the entire network would be too computational intensive, only the part where the PV system will be connected is considered. For the pilot location, a part of 5.64 km is modelled. This part is shown in Figure 4.1. Here, the orange markings represent the power substations and the green marking represents the point of connection for the PV system. This part consists of 4 substations, so 3 sections of rail between the substations and 4 passenger stations. The PV system at the pilot location is connected approximately in the middle of the part that is modelled. The part between two substations will hereafter be referred to as power section, or section. A simplified overview of the modelled traction network is depicted in Figure 4.2. The modelling of the various parts in this model will be discussed in the following sections.

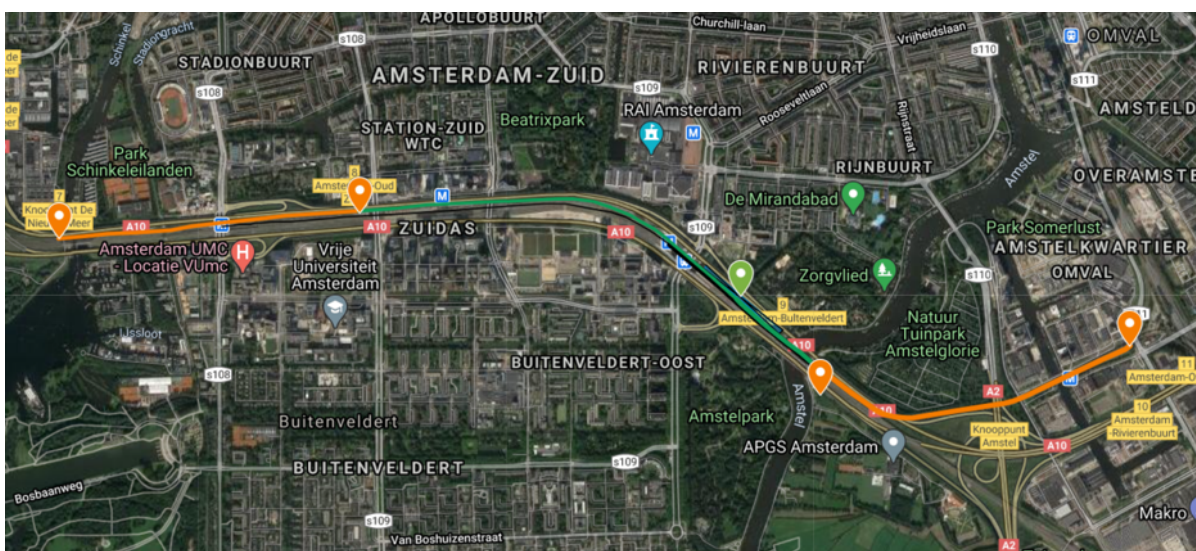


Figure 4.1: The modelled part of the traction network in Amsterdam [25]

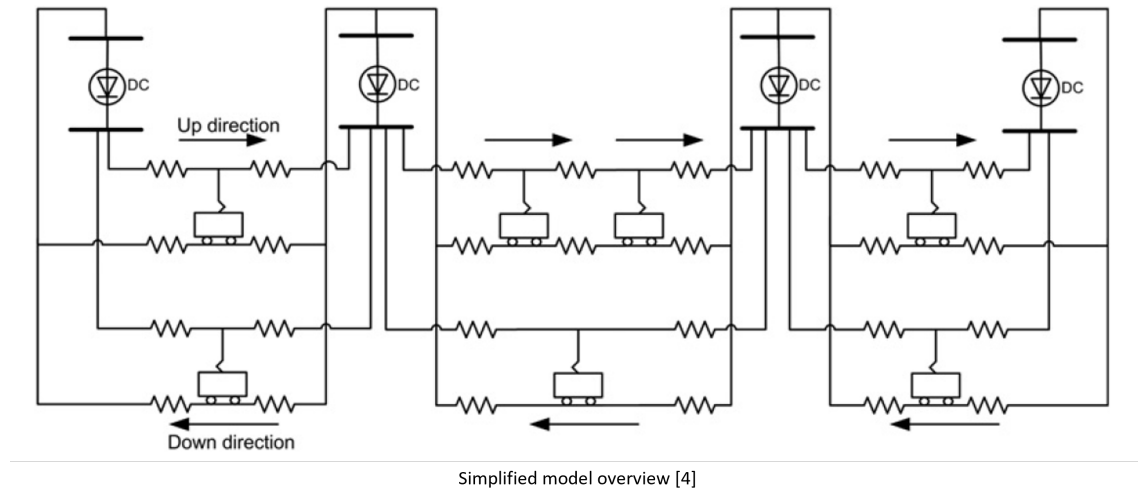


Figure 4.2: A simplified overview of the modelled traction network [46].

4.1.1 Substation

The DC traction network is powered by substations which are connected to the 10.5 kV grid. The voltage is stepped down using a three phase transformer. Then a 6-pulse or 12-pulse rectifier is used to create a DC voltage. The nominal voltage of the traction network is 750 V DC, however the actual voltage output of the substation depends on the load, due to the internal resistance of the substations. To simplify the model, the voltage output of the substation can be approximated as a straight line, as shown in Figure 4.3, where U_{d0} , U_N and I_N are the open circuit voltage, nominal voltage and nominal current of the substation [46][47][48]. Typical open circuit voltages, or zero-load voltages, are 820 or 870 V [49].

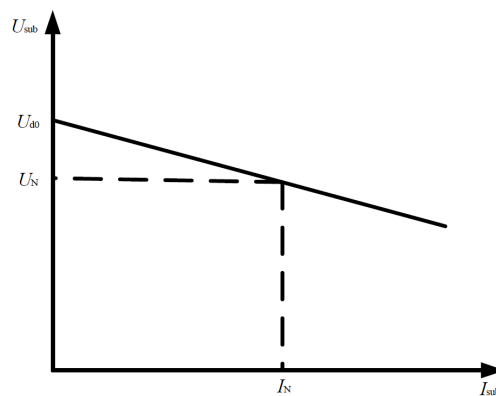


Figure 4.3: Rectifier unit external characteristic curve [47].

To model this behaviour the substation can be modelled as a constant voltage sources with an internal resistance [47]. To simulate the uni-directional behaviour of the substation, as well as the internal resistance of the substation, a constant voltage source in series with a diode with an internal resistance is used to model the substation [33][36][40][48]. This is shown in Figure 4.4. Here, R_{int} is the internal resistance of the substation and V_{0sub} is the zero-load voltage of the substation.

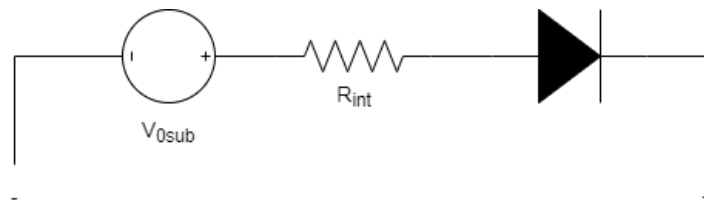


Figure 4.4: Substation model

To calculate the internal resistance equation 4.1 can be used [46], where $V_{OpenCircuit}$ and $I_{Nominal}$ are known from the Arcadis report shared by the municipality of Amsterdam [49] and $V_{nominal}$ is 750 V.

$$R_{Substation} = \frac{\Delta V}{\Delta I} = \frac{V_{OpenCircuit} - V_{nominal}}{I_{Nominal}} \quad (4.1)$$

For a substation with bi-directional properties, a different approach is used which will be explained in Section 4.3.

4.1.2 Metro

For the simulations done in this report, the characteristics of the M5 metro are used. This is the newest metro in Amsterdam and the old metros will be gradually replaced by this type. This metro is able to recover braking energy and supply this energy directly back to the traction network [49]. The M5 metro is depicted in Figure 4.6.

To model the metro power consumption, a controlled current source can be used [33][47]. The input of the current source is determined by the power consumption of the traction system of the metro and the power consumption of the auxiliary devices of the metro. The power consumption of the auxiliary devices is an estimated average from the M5 characteristics [49]. The traction power consumption profile is determined by measurements done on a real M5 metro, driving on the track that is modelled [20]. The timing of the power consumption profile is done using the timetable of the Amsterdam metro [50] and the position of the metro in the network. The resulting power profile is divided by the voltage over the metro. The resulting value is used to control the controlled current source [36][47]. A simplified overview of the metro model is depicted in Figure 4.5.

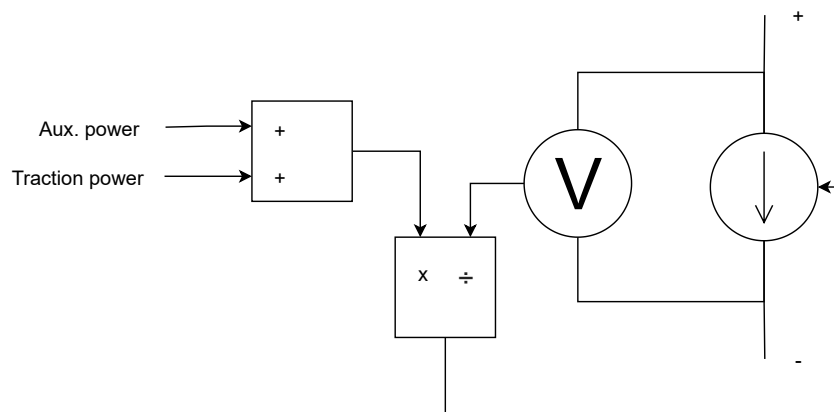


Figure 4.5: Metro model

Since the M5 metro is able to feed power to the traction network by regenerative braking, in real life the metro is also equipped with a braking chopper. The reason for this is that when no other load is nearby, the braking power that is being fed to the traction network results in a voltage spike. To stay within the voltage limits, the braking chopper can dissipate the superfluous power and convert it to heat. This is done when the third rail voltage exceeds 900 V, and the braking chopper will maintain the voltage safety [49].

This principle is included in this model by connecting a switch and a load parallel to the metro current

source to act as a braking chopper. This creates a path for the superfluous power and prevents excessive voltage spikes. However, in this model the braking chopper does not exactly maintain the voltage at 900 V, but allows the voltage to rise above 900 V. For the purpose of this study, it would add too much complexity to the dynamic behaviour of the system if the braking chopper would have to exactly mimic a real life braking chopper. But, since the braking chopper is only activated at voltage levels above the zero-load voltages of the substations, it does not influence the power consumption of the substations since the substation consumption is already zero at that point. Therefore it is safe to use this simple model of the braking chopper for this study. Nevertheless, voltage limits are respected by other systems like the PV system and the effect of the voltage spike and the braking chopper is taken into account when designing the control systems.



Figure 4.6: The M5 metro owned by the GVB [16]

4.1.3 Resistance

Since, together with the internal resistance of the substations, the resistance of the third rail and the return rail of the metro traction network are responsible for the voltage variations along the traction network, it is very important to model these resistances. Also, these resistances are an important source for energy losses in the traction network [21].

To model the resistance of the third rail and the return rail, resistors are modelled between every metro and the nearest substation (or PV system). This is also shown in Figure 4.2. During the simulation, for every timestep the distance between the metros and the nearest substation (or PV system) is calculated. This distance can then be multiplied with the resistance per unit length of the third rail and return rail [49] to compute the value of the resistances of the third rail and the return rail [40]. A schematic of this method is depicted in Figure 4.7.

In Simulink, the resistances can be modelled by a variable voltage source. The value of the voltage source is computed by multiplying the measured "resistor" current with the resistance value computed earlier [47][51]. This is a useful method, because the controlled voltage source allows for a variable control of the resistor. Simulink also has the option to model a variable resistor as a current source, however using this component results in great instability in this model and is therefore not used.

Another way to simulate the third rail and return resistance, is by using a constant resistor and by repeating the Simulink model for every time step and changing the value of the resistances accordingly. Although this method has the highest computation time, it is also the most stable method compared to a resistor as a current source or voltage source when simulating more than 4 resistors. Since for this part of the traction network 24 variable resistors are modelled, this last method is used.

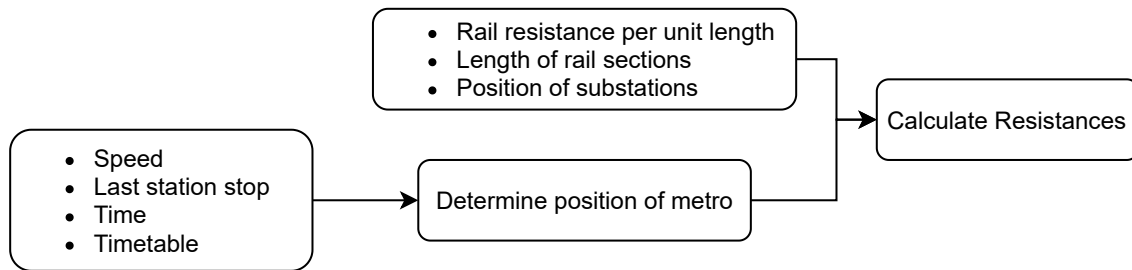


Figure 4.7: Computation of network resistances

4.2 The PV system

The PV system that is modelled for this project consists of a DC/DC converter, PV modules and possibly a storage system, depending on the topology that is being simulated. The PV system can be modelled by a controlled current source. The input of the current source is determined by a power flow control algorithm, which will be further discussed in Chapter 5. This output power is then divided by the traction network voltage to compute the appropriate current for the controlled current source. In case of a PV system without storage, the control algorithm redirects the output power of the PV model directly to the the controlled current source connected to the traction network, provided that the voltage of the traction network is within limits. A simplified overview of this is given in Figure 4.8.

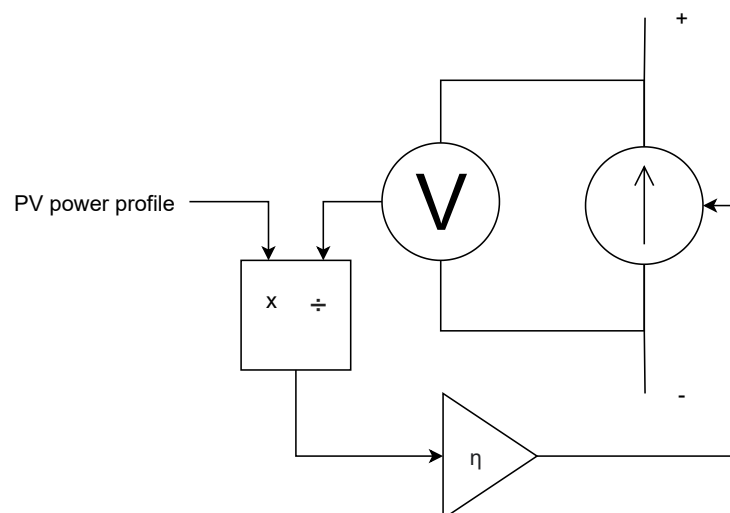


Figure 4.8: PV system model

The PV power output profile of the PV model is created by simulations using PVsyst [52]. Various configurations and sizes have been modelled. The PV power generated at the DC side of the PV array, the so-called *array virtual power at maximum power point*, is used as the input for the PV model. This includes for example ohmic losses in the PV array, temperature losses and mismatch losses of the modules and strings. It does not include efficiency losses of the converter, in this case a DC/DC converter. The converter losses are included by multiplying the PV output with an efficiency factor η , as shown in Figure 4.8.

4.3 Inverter at substation

To model an inverter at the substation a similar approach as for the PV system can be used. A controlled current source is connected anti-parallel to a substation, as shown in Figure 4.9. Here, on the left the model of the conventional substation is shown as described in Section 4.1.1 and on the right the simplified model for the inverter is shown. For this project the substation closest to the PV system is

chosen. The current source is controlled by the algorithm that will be discussed in Section 5.2. In this way, the amount of inverted power can be controlled. The power output of the inverter is measured and multiplied with the inverter efficiency to account for conversion losses. The downside of this model is that the control and the power flow management are based on the voltage of the traction network at the point of connection of the inverter, which is a problem when the voltage is very volatile. This is the case when only three sections are simulated, without the buffer effect of other sections.

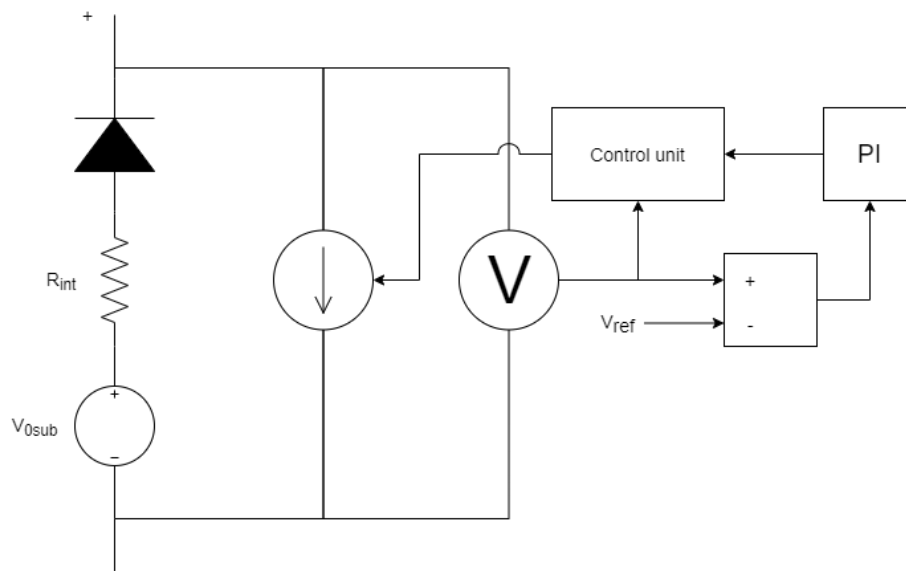


Figure 4.9: Inverter model as current source

Another way to model the inverter at the substation, is by using the scheme as shown in Figure 4.10. To model the fact that the inverter enables a bidirectional power flow in the substation, an IGBT switch is connected anti-parallel to the substation rectifier [33]. The IGBT can be enabled when there is a surplus of power in the traction network. The control will be further described in Section 5.2. The advantage of this model is that it is easy to control and the performance of the inverter is not deteriorated when the voltage is more volatile. The disadvantage is that the exact power flow is hard to control. The power flow can be controlled by a PWM control controlling the IGBT switch. This can be used to limit the power flow to respect the maximum power limit of the inverter. Also, the effect of the maximum power rating of the inverter can be computed by post-processing the simulation results.

4.4 The ESS system

To model an ESS together with PV, the PV system model from Section 4.2 is extended. A simplified overview of this model is shown in Figure 4.11. Again, a controlled current source is used to simulate the interaction between the PV system, the ESS and the traction network. The control unit controls the power flows between the PV system, the ESS and the traction network. A PI controller is used to compute the amount of energy that can be extracted from the traction network and stored in the ESS, based on the traction network voltage. A second PI controller is used to compute the amount of power that can be supplied to the traction network from the ESS. Also, the control unit redirects the PV power to either the ESS or the traction network. The exact control strategy of this control unit will be discussed in Chapter 5. Also, an efficiency factor is included in the model to simulate the conversion losses.

Using this model, different storage systems and topologies can be modelled by adjusting the ESS settings in Simulink and by changing the control of the control unit. The performance of the PV system can be monitored, and the battery model in Simulink can be used to read the state of charge of the battery and consequently find out what is an appropriate storage system size. Further, using this model, the required power capacity can be determined and the effect of this system on the energy savings in the traction network.

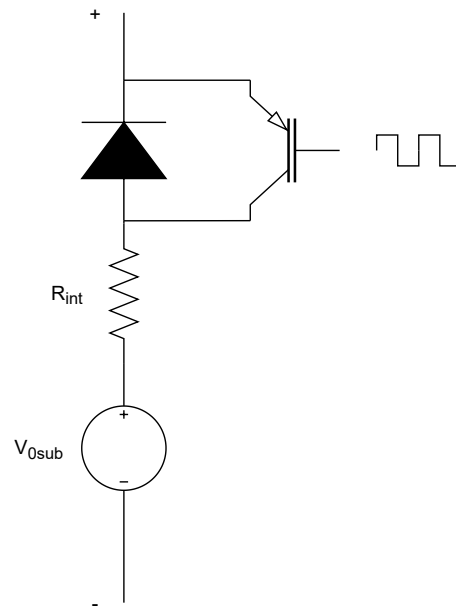


Figure 4.10: Inverter model as IGBT

4.5 Model outputs

To determine the effectiveness and efficiency of the topology that is being simulated, some performance parameters are calculated.

First of all, the reduction of energy consumption of the substation is calculated. This is done by comparing the simulation results with the results of a reference simulation of the traction network without any inverter, storage system or PV system. All further input data remains the same.

Secondly, the third rail voltage is measured and compared with the reference simulation, to judge the effect on the quality and safety of the third rail voltage. Also, the effect on the ohmic losses in the third rail and return rail can be studied. Lastly, the amount of energy that can be supplied by the PV system to the traction network, as well as the amount that can be recuperated and exported to the grid by an inverter can be computed.

The results from the simulations using the aforementioned models are discussed in Chapter 6.

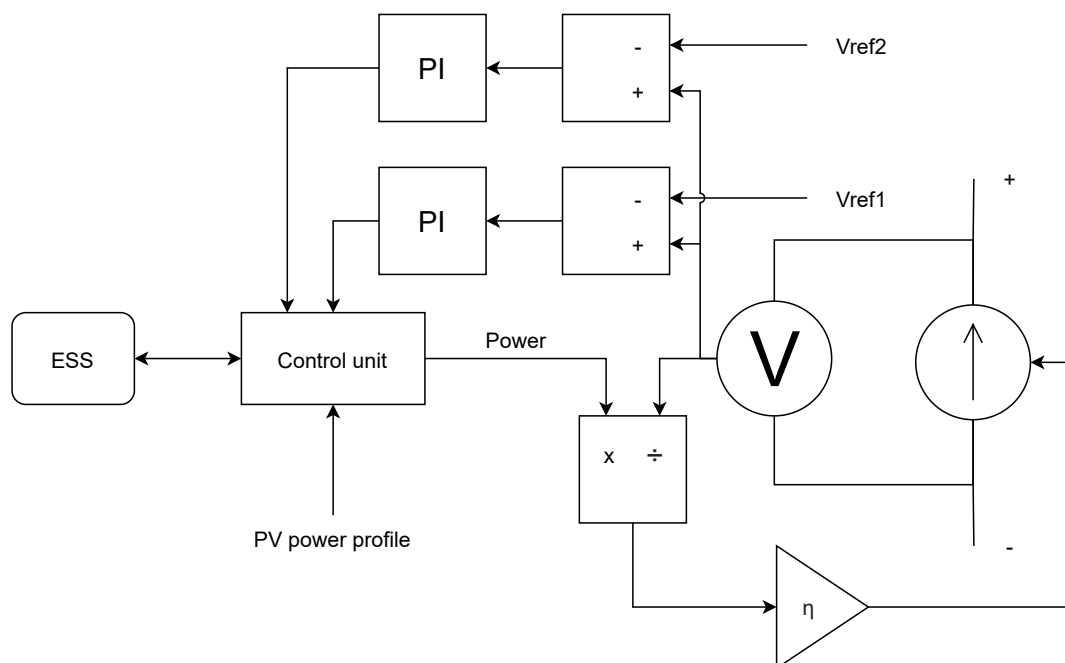


Figure 4.11: PV and ESS model

5

Power Flow Management

To make sure that every system like the PV system or energy recuperation system does exactly what it is supposed to do on the right moment, some power flow management strategies should be thought of to implement in the Simulink models. The first objective of the control system is to direct the power flows in such a manner, that the power usage is managed in the most efficient way, yielding the most energy savings. Secondly, the control system should maintain a stable voltage on the third rail and should make sure that the voltage is within the boundaries. Lastly, in case of an energy storage system (ESS), the control system must guarantee optimal operating conditions that prolongs the operating life of the ESS.

In this chapter, the power flow management strategy for every system will be discussed, including a graphical representation of the control strategies in action.

5.1 PV system control

The main challenges while operating the PV system, are to prevent an excessive voltage rise during cruising or deceleration of the metros, to compensate voltage drop during the acceleration of the metro and matching the PV output with the load. One way to manage this, is to control the PV system using a Multi Agent System (MAS), with communication between the load, the renewable energy source and the ESS, if any [53]. This communication enables the control system of the PV system to accurately predict the power demand. However, the changes in the metros that would be required for this method are beyond the scope of this project, since the metros themselves are not to be changed at this point. The PV system can also be controlled using the voltage at the Point of Connection (POC) of the PV system to the traction network (V_{POC}), which is an indication of the demanded power. Also the State of Charge (SOC) of the ESS, if an ESS is used, can be used as an input for the control system [15][40][41].

Binary PV power output

The proposed control strategy for a PV system without storage connected to the traction network is rather straightforward. The main goal is to connect and disconnected (or set its output to 0 W) the PV system such that the voltage of the traction network remains stable to ensure a safe operation of the PV system. This is called power curtailment [54]. The power output of the PV system to the traction network must be controlled such that it does not result in excessive voltage peaks. As braking resistors dissipate power when the network voltage exceeds 900 V, the PV system is disconnected, or curtailed, before the traction network voltage reaches 900 V, so for example at 895 V. This prevents the braking resistors from being overloaded and dissipating more power than necessary. The PV system is reconnected again when the voltage has reached a safe, lower level, for example 845 V. This voltage level is chosen such that the voltage level is below the zero load voltage of the substations, indicating that there is a demand for power again. The main reason for this is to prevent the PV system from oscillating around the disconnection voltage level. An overview of this control strategy is shown in Figure 5.1.

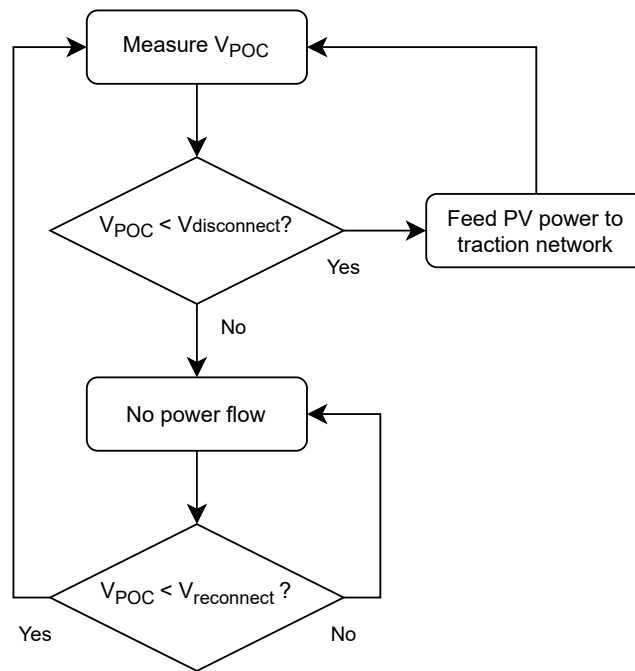


Figure 5.1: Control scheme for PV

Here $V_{reconnect}$ and $V_{disconnect}$ are the voltages at which the PV system is reconnected or disconnected, respectively. When V_{POC} is less than $V_{disconnect}$, the PV system supplies power to the traction network at its maximum power point (MPP). When V_{POC} exceeds $V_{disconnect}$, the PV system is disconnected.

As said, the PV system is reconnected again at a lower voltage level than it was disconnected. This is done because the disconnection of the PV system, when the voltage at PoC exceeds $V_{disconnect}$, can result in a voltage decrease below $V_{disconnect}$. However, the PV system can not yet be reconnected, because at that moment the PV power input would again result in a voltage increase beyond $V_{disconnect}$. Instead, the control system waits until V_{POC} is at a level where it can be guaranteed the re-connection of the PV system will not result in a voltage increase beyond $V_{disconnect}$. In this way, hysteresis is prevented. In the simulations done in this report $V_{reconnect}$ and $V_{disconnect}$ are fixed values, optimised for the PV system and the scenario that is being simulated. In real life however, it would be better to make $V_{reconnect}$ a variable value, depending on the amount of power that is generated by the PV system. This in order to prevent the control system from waiting too long or too short with reconnecting the PV system, resulting in lost PV power or oscillations, respectively. This would further optimise the control. However, for the simulated PV systems the impact of the fixed values on the power output of the PV system is relatively low and therefore it is safe to keep the voltage levels fixed.

The reason that the PV power output control is called binary, is because the PV system is either "on" (operating at maximum power point) or "off" (zero power output). Figure 5.2 shows the response of the PV system when using this control method. Here, during a time interval 5 minutes, at 7:15 am on a weekday, the amount of PV power supplied to the traction network and the voltage at the point of connection are depicted. One can see, for example between 7:16 and 7:17, that when the voltage rises above 895 V ($V_{disconnect}$, shown as a horizontal red line), because of regenerative braking in this case, the PV power output becomes 0. The PV systems starts supplying power again when the voltage reaches $V_{reconnect}$ (shown as a horizontal red line), which in this case was set at 845 V. Therefore the PV system control functions as desired, and respects the voltage limits.

Variable PV power output

Although the aforementioned approach is straightforward and effective, there is one downside. There are only two options, either the PV system supplies power at its MPP, or it does not supply power at all due to the power curtailment. However, in some situations, when the load is less than the PV generation, but not 0, the PV system could supply a portion of its maximum power production without supplying too much and exceeding the maximum voltage level. This is a well known problem in residential areas with a high density of PV systems. To fight this problem, a droop control can be implemented using the

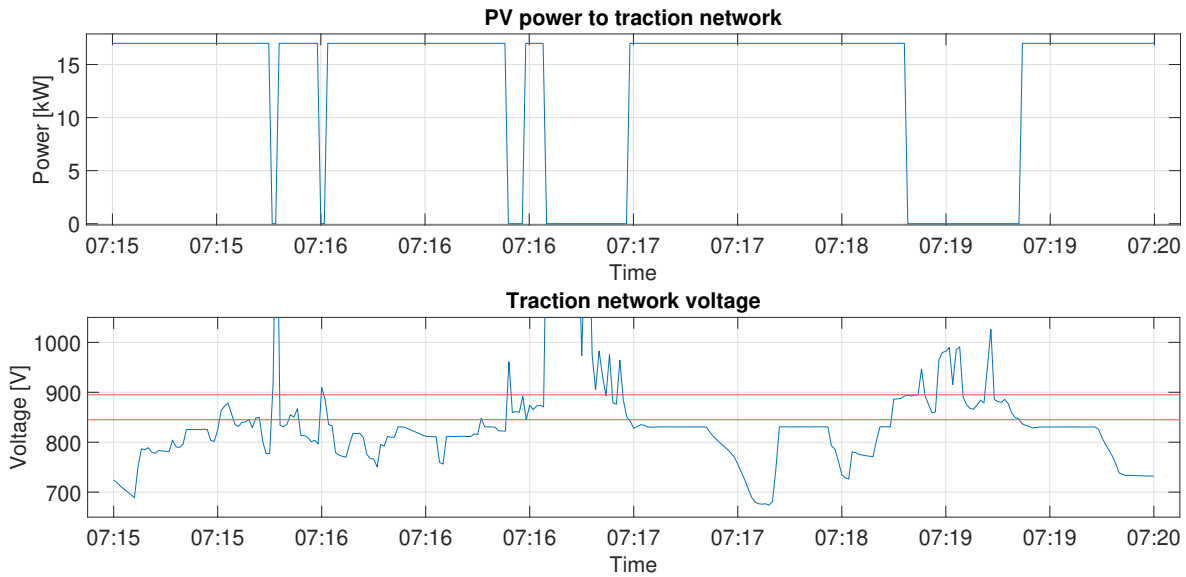


Figure 5.2: PV power output response

grid voltage (or in this case the traction network voltage) as a reference to control the power output of the PV system [54][55].

Therefore a second model and control strategy is made to demonstrate what would be the effect when the power output of the PV system depends on the voltage of the traction network (which is an indicator for the power balance). The PV power output is then variable, in terms of the amount of PV power output as a fraction of the maximum PV power output. The control for this model is very similar to the control mentioned earlier, but instead of always supplying power at the MPP of the PV system when connected, the power output of the PV system can be controlled by a PI controller. The PI controller tries to keep the voltage level of the traction network at the point of connection at a preset level, for example 870V, and adjusts the PV power output accordingly. In this way, as the voltage approaches $V_{disconnect}$, the PV power output is decreased, to prevent the disconnection of the PV system. Therefore, instead of a total power curtailment or i.e. 0 W PV power output, the PV system can still supply a portion of its maximal power production to the traction network. For voltage levels below a certain preset level (V_{low}), the maximal PV power is supplied to the grid. A schematic overview of this control strategy is shown in Figure 5.3. Figure 5.4 shows the power supplied to the traction network of a PV system simulated with the binary output control strategy on the top and the power output for a PV system with a variable power output using PI control at the bottom. The resulting power profile in the bottom graph shows that now PV power is supplied to the network at moments that there was no power supplied before, for example between 13:08 and 13:09. In total, more power is supplied to the traction network during the time window that is shown in Figure 5.4. However, one can see that also for some moments the PV system from the bottom graph supplies less power to the traction network, for example at 13:06. This is because when network voltage is rising, the PV power output is decreased to prevent power curtailment, which in this case happened too soon. This illustrates the challenge of finding the balance between on the one hand maximum PV power output and on the other hand maintaining a safe and stable network voltage. In Chapter 6, the potential of this control strategy will be further discussed.

5.2 Inverter control

When adding an inverter model to the traction network model, as described in the first half of Section 4.3, the same control strategy as explained in Section 5.1 can be used for the PV system, however, the value of $V_{reconnect}$ in the PV control might have to be changed to prevent any hysteresis between the inverter, PV system and the braking resistors.

For the inverter, a similar control strategy as for the PV system is used, but the other way around. When

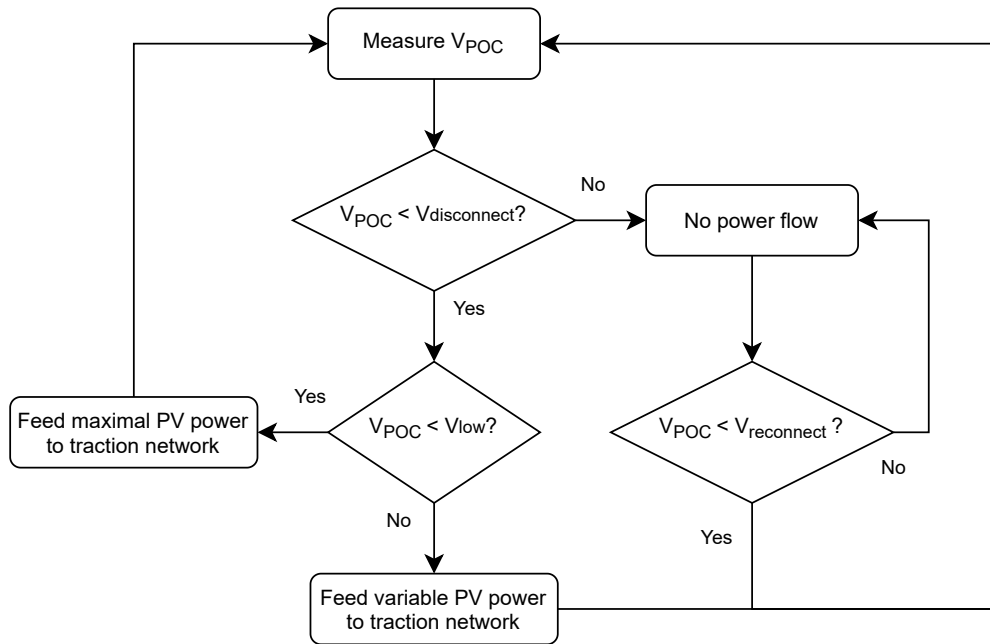


Figure 5.3: Control scheme for PV with variable output

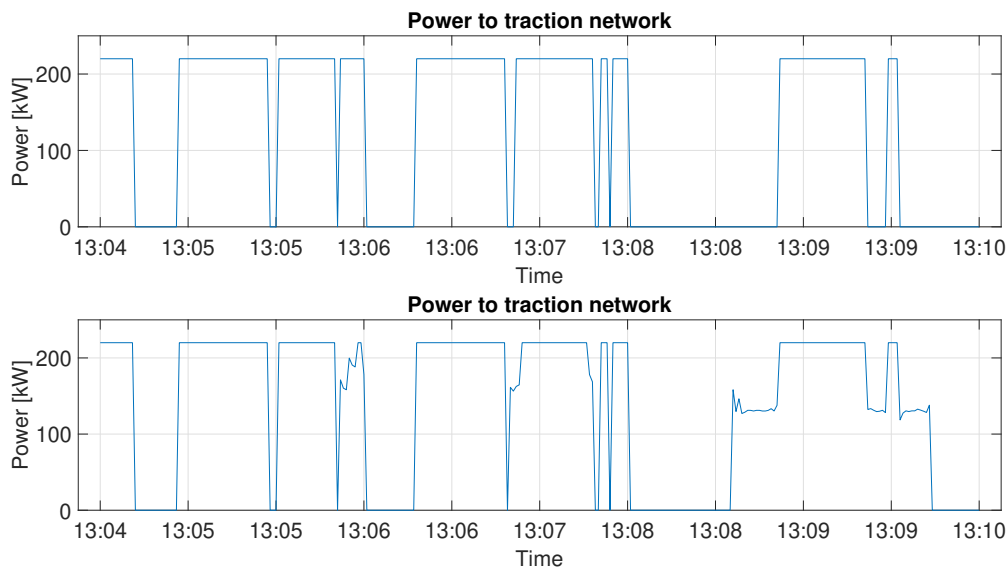


Figure 5.4: PV power output response with PI control

the voltage at the point of connection of the inverter (V_{POC}) is below V_{invert} , the inverter is disabled. When V_{POC} exceeds V_{invert} , the inverter starts exporting power to the utility grid. The amount of power that is exported to the utility grid is related to the difference between V_{stop} and V_{POC} , or in other words the degree in which the voltage limit (V_{invert}) is exceeded. This difference goes to the input of a PI controller and the output of the PI controller determines the amount of power that is inverted, or exported. The amount of power that can be exported is limited by the power capacity of the inverter.

When the inverter is enabled, it exports power to the utility grid until V_{POC} has decreased to a safe voltage level again, at V_{stop} . This is again to prevent any hysteresis as explained in Section 5.1.

It is advisable to choose V_{invert} such that it is well below 900 V, but above the zero load voltage of the power substation. This is to make sure that the inverter is enabled well before the voltage exceeds 900 V, but does not export any power which is coming from other substations, creating a power loop. As

said, for the latter it is important to make sure that V_{stop} is above the zero load voltage of the substations near the inverter. This fact can result in an operation window of only 30 V for some locations. However, it is possible to increase the maximum voltage level to up to 1000 V [32], but that is not within the scope of this project. For now, a maximum voltage level of 900 V is used. During the exportation of power, also a signal can be send to the power supply of the traction network inside the substation and optionally to substations nearby to disable the power supply, to prevent power loops. In this case, only a signal is send to the power supply inside the same substation as where the inverter is placed. An overview of the control strategy for the inverter is depicted in Figure 5.5.

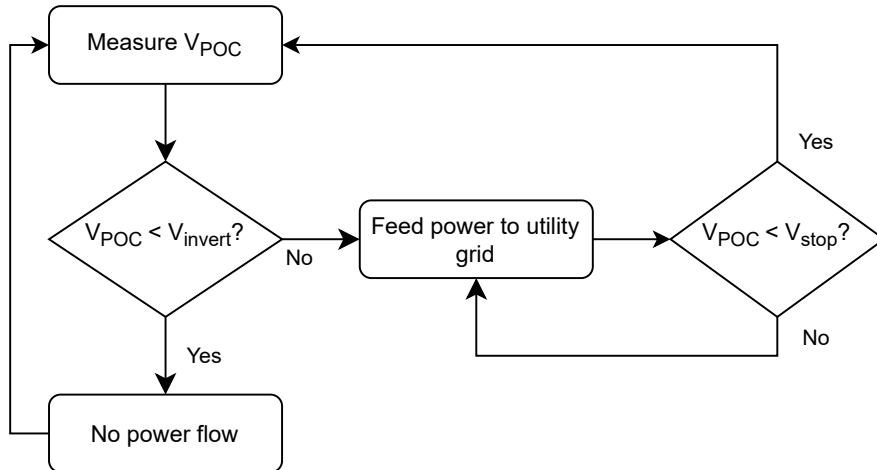


Figure 5.5: Control scheme for inverter

For the inverter model described in the second half of Section 4.3, a different control method is used. For this model, the control unit must simply enable the IGBT switch when the network voltage exceeds V_{invert} and disable the IGBT when the network voltage is below V_{invert} . Optionally, the power flow can be controlled using a PWM signal to control the IGBT, to simulate the maximum power rating of the inverter. Alternatively, the resulting power profile from the simulations of the inverter can be post-processed to compute a power profile that respects the power limits of the inverter.

5.3 PV with storage control

The control scheme for a PV system together with an ESS is a bit more involved. In this case, a PV system and an ESS is modelled, with the ability to store PV energy, but also braking energy from the traction network. In this case these two functions are intertwined, but an ESS connected apart from the PV system could fulfil the same tasks. Figure 5.6 shows an overview of the control scheme of this system.

Again, the control algorithm checks V_{POC} , but this time also the state of charge (SOC) is checked. Note that although the measurement of V_{POC} and SOC is only mentioned in the starting state of the diagram shown in Figure 5.6, these parameters are measured in every state of the diagram. Based on these parameters the control algorithm can make its decisions [15][40][41].

The following parameters are used in this control algorithm:

- V_{POC} : the traction network voltage at the point of connection
- SOC : the state of charge of the ESS
- SOC_{th} : below this SOC level, for example 70%, the ESS only supplies power when V_{poc} is very low
- V_{high} : maximum allowable voltage, for example 895 V, above this voltage the PV system is turned off and the ESS absorbs energy from the traction network
- V_{high1} : below this voltage not only the PV system, but also the ESS starts supplying power to the traction network, for example 800 V

- V_{low} : below this voltage, for example 730 V, the PV system as well as the ESS supplies power to the traction network at full capacity
- V_{low1} : when the ESS is supplying power to the traction network, the control algorithm waits until the voltage level is high enough again, above V_{low1} , for example 750 V

Basically the control algorithm has 3 main goals: supply PV power to traction network during medium voltage levels, store energy when the traction network voltage is high, and inject stored energy to the traction network when the network voltage is very low. Also, the control algorithm makes sure that maximum power limits are respected, the battery is not overcharged nor discharged too deep, to prevent any damage.

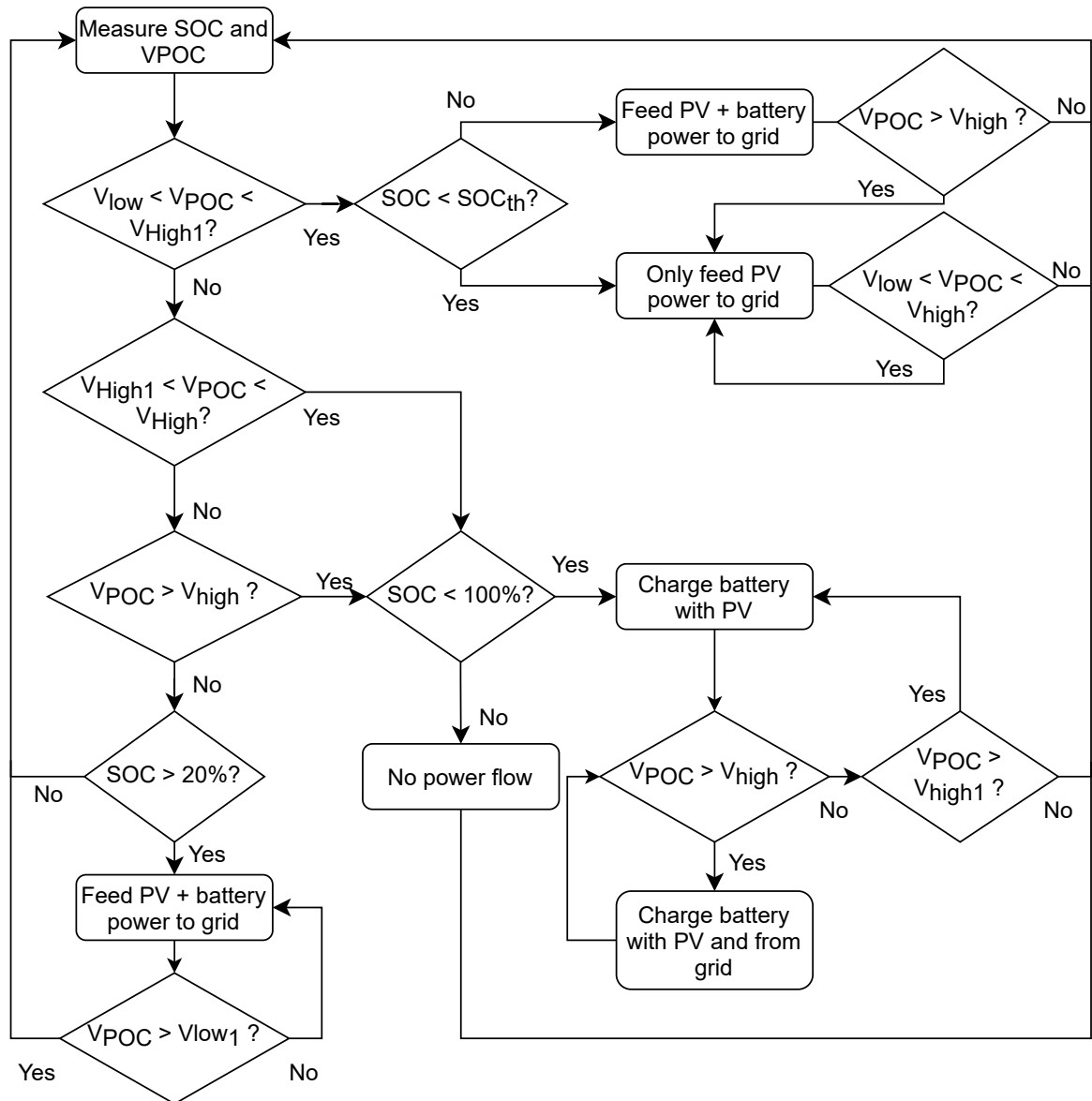


Figure 5.6: Control scheme for PV & an ESS

6

Results

In this chapter the results are discussed from the simulations, using the models discussed in Chapter 4. The power flow management strategies as discussed in Chapter 5 are used for these simulations. To include every event during a day, such as rush hours, quiet hours, high irradiation, night and so on, simulations are done for one entire day (24h). Discrete time steps of 1 second are used, to accurately simulate the dynamic behaviour of an accelerating and braking metro. Although it would be interesting to simulate the traction network for a year as well, the long computation time of the simulation does not allow this during the duration of this thesis project. Nevertheless, simulating different scenarios during a day can give sufficient insight for the system operating for a year. Here, the train plans for a regular weekday are used [50]. In the train plans for the weekend slightly less stops are included, but the results will be similar.

6.1 Conventional operation of traction network

First the traction network without any PV system, storage system or inverter is simulated to create a reference for all the other simulations. In this way, the consumption can be compared and thus the energy savings can be determined. In addition, the ohmic losses in the traction network are monitored to study the effect of different systems on the ohmic losses. Also, the voltage at the point of connection of the PV system or other systems is measured to compare the quality and safety of the voltage when any additional equipment is connected.

The conventional traction network is simulated for two scenarios.

The first scenario is that any power generated or consumed, in the three power sections that are modelled around the pilot location, can come from or go to sections adjacent to the three modelled sections, which is also the case in real life. To simulate this, at the end of the modelled sections a load is connected that represents the average load of the adjacent sections. This load represents the average load that would have been fed by the outer substations if additional sections would have been included in the model. To estimate this power consumption, the consumption profile of the modelled sections are used together with the train plans and the characteristics of the adjacent sections. This also simulates a buffer effect of the other sections, meaning that a part of the surplus power can go to these sections. In the second scenario, it is assumed that almost no power can come from or go to sections adjacent to the three modelled sections. In this scenario, it is thus simulated that all power that is generated does not leave the three modelled sections. This is an important scenario to simulate, because when more PV systems will be connected to the metro traction network in the future, any superfluous PV power can not flow, or less, to the adjacent power sections where PV systems are connected as well. Also, it is undesirable to supply PV power to a load far away, because then more power will be lost due to ohmic losses. By simulating this scenario, PV systems and other equipment can be specifically designed for the consumption in the three sections around the point of connection.

Figure 6.1 shows the energy consumption in the three modelled power sections during a weekday. One can see that the peak consumption occurs during rush hours and there is no consumption be-

tween 01:00 and 06:00 since no metro is operational at that time. From this graph, it may seem that matching the load with the generated PV energy would be a straightforward task, however Figure 6.2 shows otherwise. In Figure 6.2 the power consumption of the substation is depicted from 07:00 until 07:15. For better visibility a time interval of 15 minutes is depicted, but others times of the day show similar profiles. Here one can clearly see the intermittent nature of the power consumption of the metros. During acceleration, the metro demands about 40 times more power than during cruising. At some points, the power consumption in the network peaks at 7 MW. This happens when two metros accelerate at the same time. When no metro is present in the three sections, the load demand is 0. Also, during braking, the amount of regenerated power can often cover the complete power demand at that moment, resulting in 0 power demand from the substations.

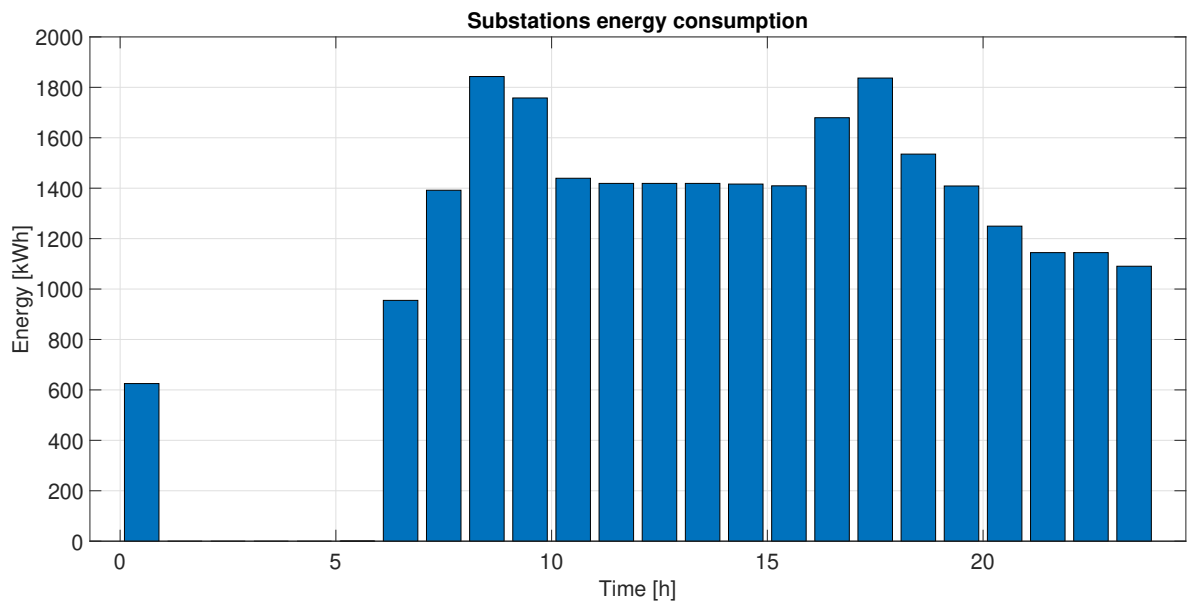


Figure 6.1: Energy consumption of substations

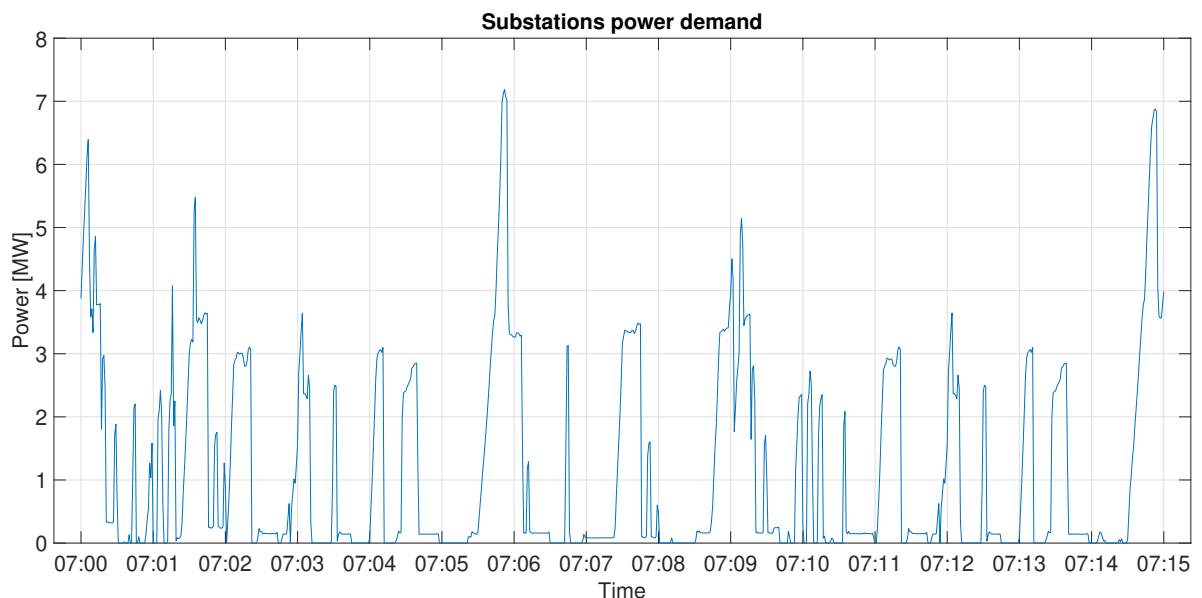


Figure 6.2: Power consumption of substations

Figure 6.3 show the difference in power consumption when the metros would not have been able to recover braking energy. The blue line represents the power consumption of the substations when

metros are able to recover braking energy, the orange line shows what would be the power consumption when the regenerative braking ability is disabled. In this part of the metro network, about 28% of the energy that is consumed for the traction of the metro, is regenerated during braking. Needless to say, the power consumption decreases when regenerative braking is enabled. In fact, the power consumption decreases with 12.5%. However, this consumption could have been decreased even more. In Figure 6.3, one can see that part of the regenerative braking occurs at times were the load is very low. For example at 07:05, the load is only about 155 kW, while the power that can be supplied by regenerative braking is in the order of megawatts. The surplus of power is dissipated in the braking resistors of the metro and converted to heat, hence wasted. This power could however be recuperated using an inverter in a substation, as will be discussed in Section 6.3. Also, this regenerated braking energy could be temporarily stored, which will be further discussed in Section 6.4. Another solution is timetable optimisation, to time the acceleration of one metro during the braking of another metro [19][56]. However this is not within the scope of this thesis project.

Another problem is that, because of the regenerative braking, at some points there is zero load and therefore a PV system would not be able to supply power to the traction network without wasting the PV energy in the braking resistors. In Section 6.2, this problem is discussed in more detail. Solutions for this problem could for example be an inverter in the substations or an ESS as well.

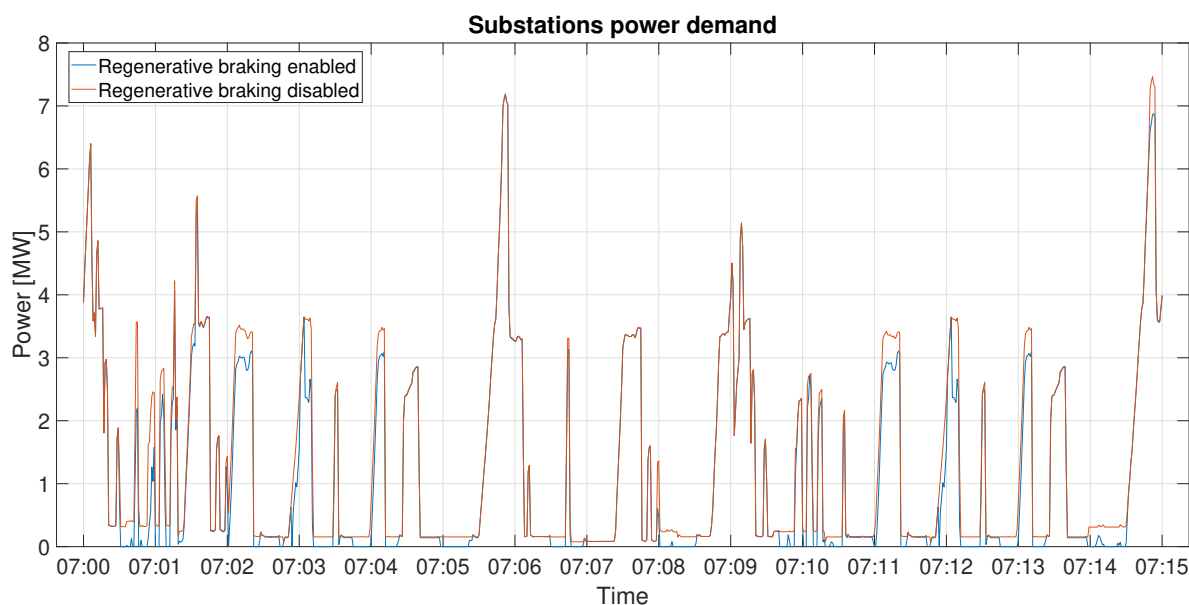


Figure 6.3: Power consumption of substations with and without regenerative braking

Since the resistance in the third rail and the return rail result in a significant amount of energy losses in the traction network, the ohmic losses in the traction network are computed as well [21]. Since previous studies show that PV systems and storage can have a positive effect on the ohmic losses, it is interesting to use these results to study the effect of PV systems and storage on the ohmic losses in the traction network [14][15].

Figure 6.4 shows the ohmic losses for the same system and time interval as Figure 6.2. The ohmic losses range from almost 0% up to almost 30% of the total consumption of the substations, when the metros are cruising or accelerating, respectively. During acceleration of the metros the ohmic losses are at the highest point, as can be seen in Figure 6.4. The reason that the ohmic losses are so high during acceleration lies in the quadratic relationship between the ohmic losses and the current in the traction network, as shown by Equation 6.1. On top of that, the network voltage drops during acceleration due to the internal resistances of the substation transformers. Due to this voltage drop, a higher current is required to supply the same amount of power to the metro. Naturally, the position of the metro also influences the ohmic losses due to the different distances between the substations and the metro and thus the network losses.

$$P_{ohmicloss} = I^2 \times R_{network} \quad (6.1)$$

In total, 11.21% of the total energy supplied by the substations during a day is lost due to the ohmic losses. This amount could be lowered by for instance installing more substations, replacing the substation transformers with more efficient transformers with also lower internal resistances, increasing the network voltage or by replacing the rails with better conducting materials. But also PV and storage can contribute to the lowering of ohmic losses, as will be discussed in Section 6.2 and 6.4. In Appendix C, the power consumption and the ohmic losses for an entire day are shown in Figure C.1.

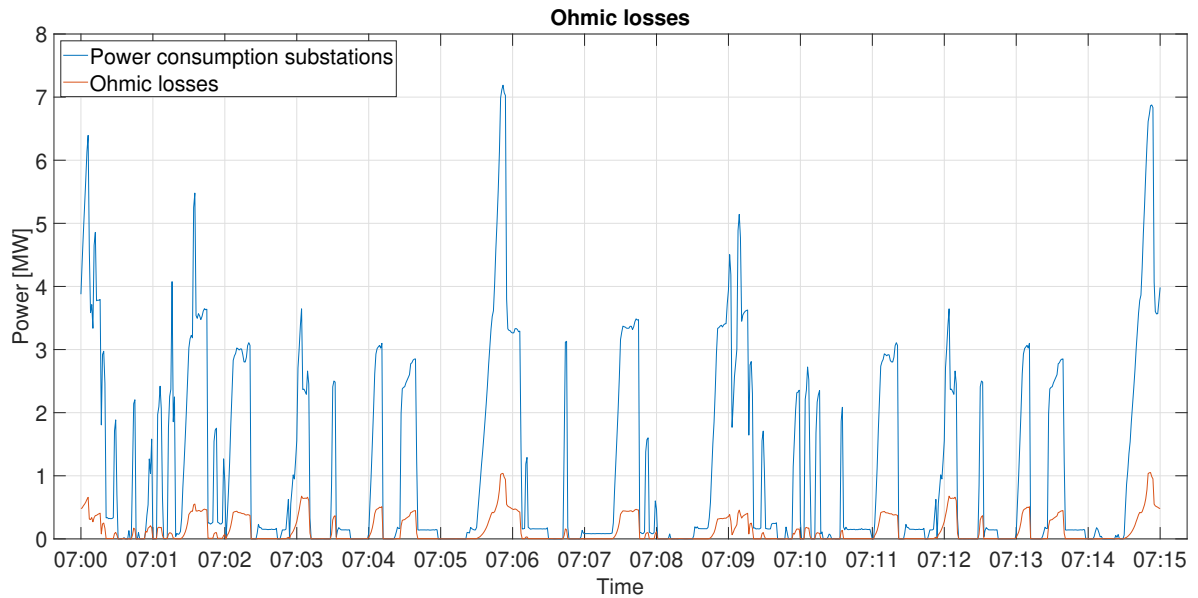


Figure 6.4: Power consumption of substations compared to ohmic losses

6.2 Traction network with PV

Now that the results for the conventional traction network are known, the next step is to investigate the effect of connecting a PV system to the traction network. In this chapter, the results for a PV system connected to the traction network at the pilot location will be discussed.

To simulate this connection, various PV power output profiles are created using PVsyst [52]. This is a simulation program that can accurately simulate PV systems, including meteorological influences at the pilot location, loss mechanisms and accurate results for the energy yield. For these simulations, south facing PV systems are considered, as well as PV systems with an east-west configuration with different tilt angles. For the south facing system the optimal tilt angle for the pilot location is used, which is 40°. Different PV system sizes are simulated with size steps of around 200 kW_p, because for these simulations the specifications of the DC/DC converter as described in Section 3.1.2 are used for the simulations. This DC/DC converter has a maximum power limit of 200 kW, but multiple of these converters can work in parallel. To give an idea of how much this is in comparison with the power consumption of in the traction network, the average energy generation of PV system of about 10000 kW_p would cover the entire energy consumption of the modelled traction network during a day. The PV power profile obtained with the PVsyst simulations is from the DC output of the PV array. For the daily profile, the yearly average is used. Mutual shading losses caused between PV modules are not considered in this section. In the model, the PV system is connected at the pilot location as discussed in Section 2.3.

In Section 6.2.1 and 6.2.2, the effects of the PV system when there is a normal consumption/low generation in the adjacent power sections, as well as when there is a low consumption/high generation in the adjacent power sections, respectively, are discussed. This is done to account for the fact that in the future more PV systems may be connected in the adjacent sections of the traction network. This will be further explained in Section 6.2.2.

6.2.1 Normal power consumption in adjacent power sections

In this section, the results from the simulations of a PV system connected at the pilot location are discussed, with the assumption that a part of the superfluous power can flow to the power sections adjacent to the three sections that are modelled around the pilot location. This simulates the fact that there may be no, or not enough consumption in the section of the point of connection (PoC) to consume the PV power, but there is always a consumer in the network further away. For the simulations, the model as discussed in Section 4.2 and the control strategy as discussed in Section 5.1 are used.

South facing PV systems

The results for the simulations with different PV systems facing south with a tilt of 40° are shown in Table 6.1. The first column shows the size of the PV system in terms of installed power. The second column shows the average energy yield per day, at the DC side of the PV array. The third and fourth column shows how much of the energy that is produced by the PV system operating at maximum power point (MPP) can actually be supplied to the traction network. For this experiment, it is assumed that the efficiency of the DC/DC converter between the PV system and the traction network is 100%.

Table 6.1: Results south facing PV systems

System Size	Yield/Day	To Network	To Network	Energy Saving	Energy Saving [%/Yield]	Energy Saving [%/Supplied]
202 kW _p	561 kWh	465 kWh	83.0%	483 kWh	86.1%	103.9%
405 kW _p	1118 kWh	915 kWh	81.8%	942 kWh	84.3%	103.0%
597 kW _p	1647 kWh	1338 kWh	81.2%	1420 kWh	86.4%	106.3%
799 kW _p	2209 kWh	1777 kWh	80.4%	1890kWh	85.6%	106.5%

The fourth column is a good indication of the mismatch between the PV generation and the load. Although the biggest PV system from this table produces 6.3% of the total energy demand in the traction network, the PV systems are only able to supply up to 83% of the generated energy to the traction network. This illustrates how complex it is to match the load profile of the traction network with the PV generation profile. Figure 6.5 shows this problem in more detail. Here the power consumption of the substations is depicted together with the amount of PV power supplied to the traction network, during

a 5 minute time interval. For this figure, the results for the 597 kWp south facing PV system is used. In this figure one can see that the delivered PV power drops to zero when the load is less than the MPP of the PV system. This is a problem, because during these moments the potential PV power production is wasted. For this particular PV system, 18.8% of the PV energy that could have been supplied to the traction system is wasted due to the power mismatch.

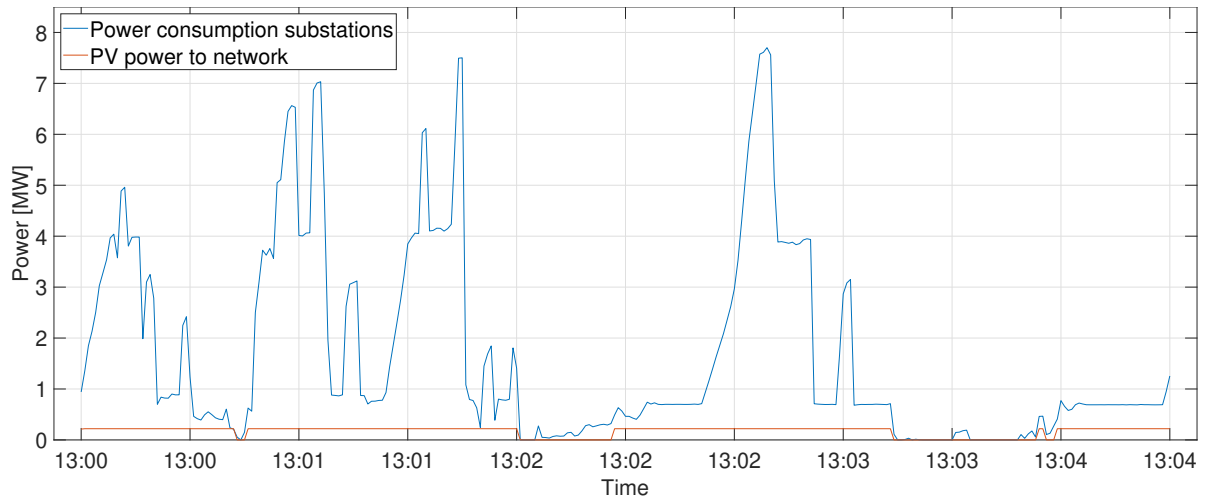


Figure 6.5: Power consumption of substations compared to PV power supplied to traction network

Column six of Table 6.1 shows how much the energy consumption of the substations is decreased, as a percentage of the normal energy yield of the PV system. Interestingly, this percentage is higher than the percentage of PV energy supplied to the traction network. The seventh column, showing the energy savings as a percentage of the amount of supplied PV energy to the traction network, confirms this fact. In other words, more energy is saved than supplied to the network by the PV system. This can be explained by the fact that the voltage between two substations is increased and consequently the ohmic losses are decreased [14].

Figure 6.6 shows the voltage and ohmic losses for a traction system with and without a 597 kWp south facing PV system connected, during a 10 minutes time interval. The upper graph shows the traction network voltage at the point where the PV systems is connected, or would have been connected. A threshold voltage level of 895 V is indicated by the horizontal red line. Above this voltage, the PV system power output is curtailed, to prevent a further increase of the voltage. One can see, that for the case with a PV system connected, indicated by the orange line, the voltage is indeed increased, as long as the voltage is below 895 V . Above 895 V , the voltage remains the same as in the case without PV, as it should be. Not only does this confirm a correct behaviour of the PV system, it also shows that the PV system is able to slightly increase the voltage level of the traction system.

In the bottom graph of Figure 6.6, the ohmic losses for the same time interval are depicted. Here, one can see that the ohmic losses during acceleration of the metros (the peaks in the graph) are slightly decreased, when a PV system is connected. However, the ohmic losses are not always decreased when a PV system is connected. In fact, during some periods of relatively low power demands, the ohmic losses are actually higher. This is because during those periods, the PV power has to be transported to metros further away, whereas when a substation nearby would have delivered the same power, the ohmic losses would have been lower due to the shorter distance. Nevertheless, with this PV system, during an entire day, the total ohmic losses are decreased with 1.5%.

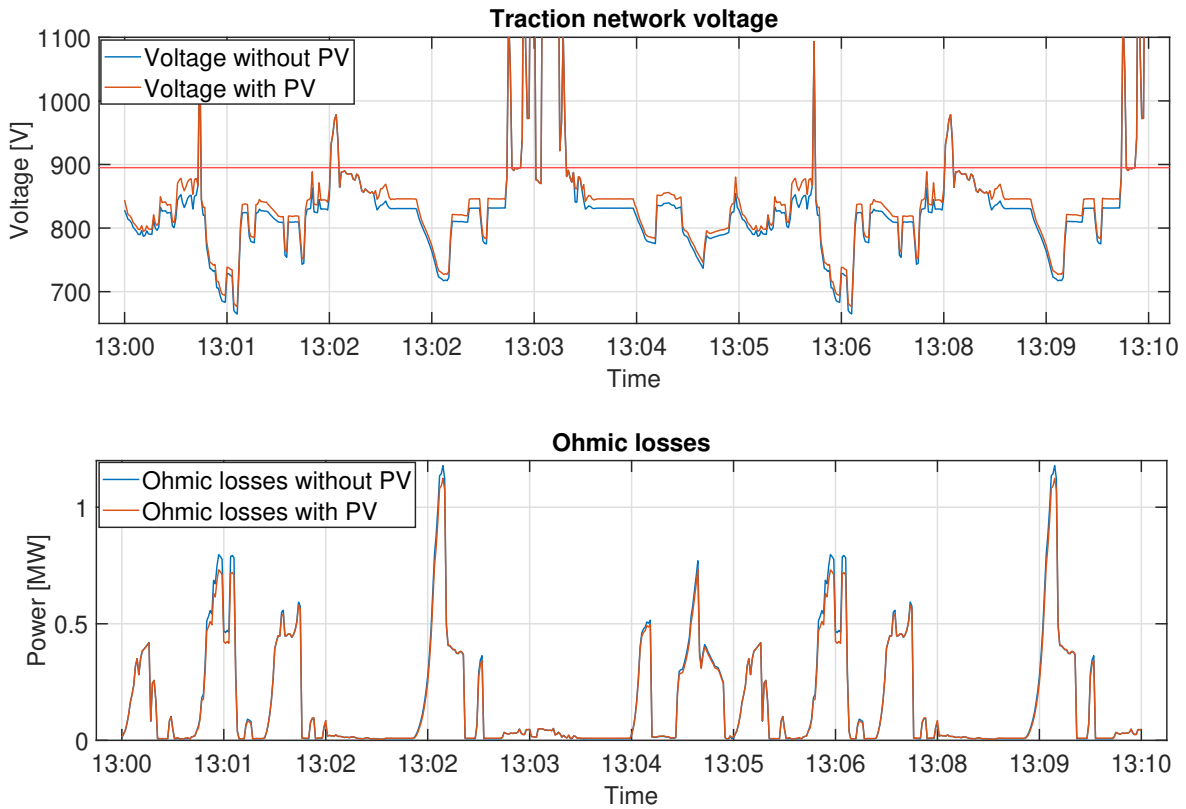
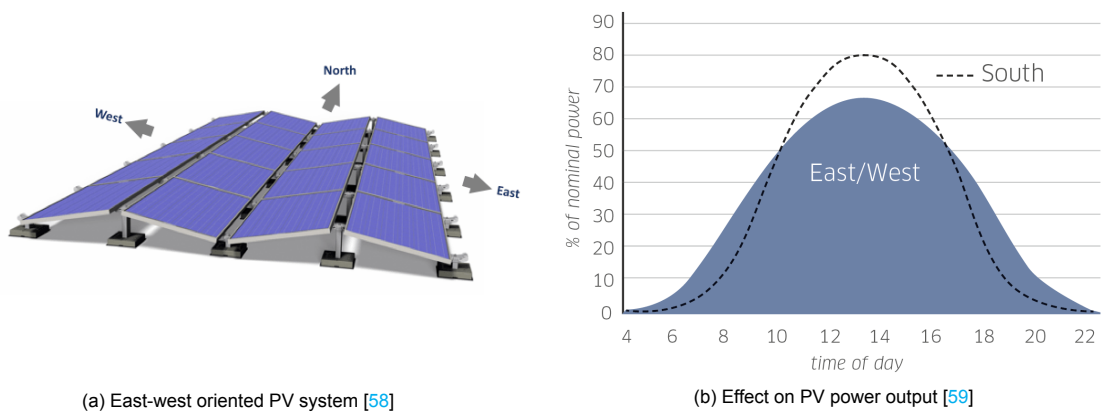


Figure 6.6: Voltage and ohmic losses after PV connection

East-west oriented PV systems

As shown in Table 6.1, the PV generation only matches the load up to 83%. In an attempt to increase this percentage, different PV systems with an east-west configuration, like shown in Figure 6.7a, are simulated. Using an east-west configuration, the power output of the PV system can be spread more evenly during the day, like shown in Figure 6.7b. The peak PV power output is decreased, but during the metro rush hours the PV power output is increased, which is beneficial for the power matching [57].



(a) East-west oriented PV system [58]

(b) Effect on PV power output [59]

Figure 6.7: East-west configuration for PV systems

Table 6.2 shows some results for different PV system sizes and different east-west configurations. Column one shows the installed power for each PV system and column two shows the tilt angle of the east-west oriented PV modules. Column five shows the percentage of generated PV energy that could

be delivered to the traction network. Comparing these results with Table 6.1, one can see that these percentages are slightly increased. Therefore, using east-west configured PV systems will increase the power match. However, the total PV energy generation is decreased, because the east-west configuration is less optimal in terms of total energy yield, as can be seen in column three of Table 6.2. Due to this in total less PV energy is delivered to the traction network, as can be seen in column four. Therefore, in this situation it is not recommended to use east-west oriented PV systems instead of south facing PV systems.

Table 6.2: Results east-west oriented PV systems

System Size	Tilt Angle	Yield/Day	To Network	To Network
202 kWp	20°	475 kWh	395 kWh	83.1%
202 kWp	35°	456 kWh	379 kWh	83.2%
597 kWp	20°	1402 kWh	1145 kWh	81.7%
597 kWp	35°	1344 kWh	1103 kWh	82.0%

6.2.2 Low power consumption in adjacent network

In this section, again different connected PV systems are considered, but with the assumption that (almost) no superfluous power from the PV system can flow to power sections of the traction network adjacent to the 3 sections that are modelled around the pilot location. This is to account for the fact that in the future additional PV systems may be connected to the sections adjacent to the sections that are considered for the pilot. Therefore, in the following simulations, the power exchange only happens in 3 sections (so including 4 power substations in total). This also allows for a design specifically scaled for the power consumption in the area around the pilot location. This prevents an oversized PV system where generated power has to be transported along larger distances, resulting in more wasted PV power due to ohmic losses. It is for this reason better to design the PV system specifically for the power consumption at the location where it is installed and have more PV systems distributed along the traction network, instead of one big PV system.

South facing PV systems

Table 6.3 shows the results for south facing PV systems connected to the traction network, with the power consumption of only three sections. What immediately stands out from this table is the lower percentage of PV energy that could be delivered to the traction network. Figure 6.8 visualises this problem by comparing the power consumption of the substations without a PV system connected, with the PV power that is supplied to a traction network by a 597 kWp south facing PV system. Here, one can clearly see that during high irradiation (which is the case for the time interval shown in the figure), almost 50% of the time the PV system is not able to supply power to the traction network. All in all, the results show that a solution is needed to solve the mismatch problem.

Table 6.3: Results south facing PV systems

System Size	Yield/Day	To Network	To Network	Energy Saving	Energy Saving [%/Yield]	Energy Saving [%/Supplied]
202 kWp	561 kWh	347 kWh	61.9%	355 kWh	63.3%	102.3%
405 kWp	1118 kWh	654 kWh	58.5%	701 kWh	62.7%	107.2%
597 kWp	1647 kWh	889 kWh	54.0%	974 kWh	59.2%	109.6%
799 kWp	2209 kWh	1138 kWh	51.5%	1333 kWh	60.3%	117.1%

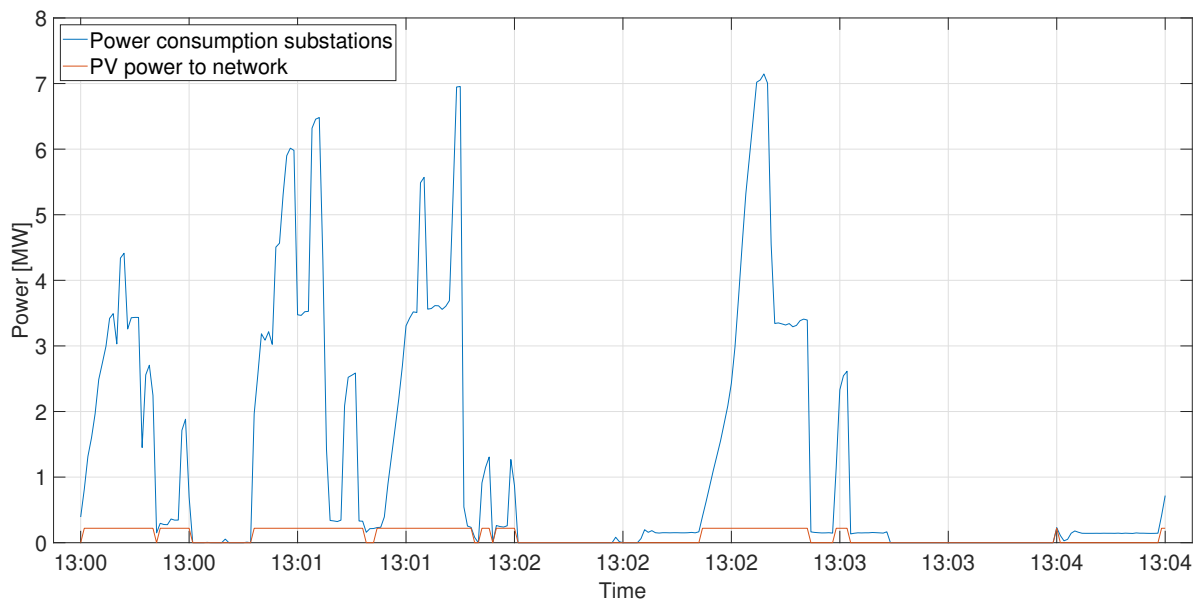


Figure 6.8: Power consumption of substations compared to PV power supplied to traction network

Although the mismatch between load and generation is in this case rather high, the effect on the decrease of ohmic losses is slightly better than for the case discussed in Section 6.2.1. Comparing Table 6.1 and 6.3, one can see that the saved energy as a percentage of the (supplied) PV power is higher in Table 6.3. This is because in the scenario discussed in this section, no PV power is supplied to power section further away and therefore less PV power is lost due to the ohmic losses for higher distance power transportation. But still, the energy savings are lower due to the power mismatch.

Another interesting result is that the energy savings as a percentage of the supplied PV energy strongly increases while the power match percentage decreases and the PV system size increases. This is because although larger PV systems are more often curtailed, when they are supplying energy most of the time this is during the acceleration of the metro, because then there is enough power demand. As shown in Figure 6.6, during this stage, the energy saving effects related to decreased ohmic losses are the highest.

East-west oriented PV systems

Again, in an attempt to improve the match between power consumption and PV generation, PV systems with an east-west orientation, like discussed in Section 6.2.1, are simulated to study the effect on the power match and the effect on the total saved energy. Table 6.4 shows the results for some east-west oriented PV systems. In this table one can see that the power match is slightly improved by using east-west oriented PV systems. However, the total PV energy generation is decreased, because the east-west configuration is less optimal in terms of total energy yield. Due to this in total less PV energy is delivered to the traction network. Therefore, in this situation it is again not recommended to use east-west oriented PV systems instead of south facing PV systems, just like for the case discussed in Section 6.2.1.

Table 6.4: Results east-west oriented PV systems

System Size	Tilt Angle	Yield/Day	To Network	To Network
202 kWp	20°	475 kWh	294 kWh	61.9%
202 kWp	35°	456 kWh	283 kWh	62.0%
597 kWp	20°	1402 kWh	784 kWh	55.9%
597 kWp	35°	1344 kWh	769 kWh	57.2%

6.2.3 Decreased consumption

Due to the corona pandemic, in 2020 the amount of travellers using public transit significantly decreased. The amount of travellers using the metro in Amsterdam almost halved [3]. Public transport

companies therefore changed their timetables accordingly. This inspired to include the effect on the output of the PV system in the scenario that the amount of metro rides during a day is halved. This gives insight in the effects on the energy efficiency of such a decision, but also shows how a traction system would perform in areas where the frequency of metro rides is lower. In this section the results for this scenario will be briefly discussed.

Table 6.5 shows some results for this scenario, for different PV system sizes and different PV module orientations. For the simulations, half of the metro rides in the train plan are omitted. During the simulations, no power transfer between the three power sections around the pilot location and the rest of the network occurs, like discussed in Section 6.2.2. In column 2 of the table the configuration of the PV systems is shown, including the tilt angle and the orientation, where S indicates south faced and EW indicates east-west orientation.

Table 6.5: Results for halved power consumption

System Size	Configuration	Yield/Day	To Network	To Network
202 kWp	S, 40°	561 kWh	53.0%	297 kWh
202 kWp	EW, 20°	475 kWh	53.6%	254 kWh
202 kWp	EW, 35°	456 kWh	54.0%	246 kWh
597 kWp	S, 40°	1647 kWh	30.4%	501 kWh
597 kWp	EW, 20°	1402 kWh	39.0%	546 kWh
597 kWp	EW, 35°	1344 kWh	41.8%	561 kWh

Two main conclusions can be drawn from these results. The first is that the halving of the power consumption drastically worsens the power match between load and generation. The second conclusion is that for the larger PV system of 597 kWp, it pays off to use an east-west orientated setup of the PV modules. Column 5 of Table 6.5 shows that while the potential energy yield for the east-west configured PV systems is lower, the amount of energy that is supplied to the traction network is higher due to the better power match.

6.2.4 Variable PV output

Another solution for the mismatch of the PV generation and the load, is to use a variable power output for the PV system, as discussed in Section 5.1. In this way, it can be prevented that the PV power output is curtailed during low load or high PV generation.

Figure 6.9 shows the amount of PV power supplied to the traction network for a 597 kWp south facing PV system, with either a binary PV power output control or variable PV power output control. Both control strategies are explained in Section 5.1. Also, the power consumption of the substations, in the scenario that no PV system is connected to the traction network, is shown to compare the PV power generation with the load. A zoomed-in version of Figure 6.9 is shown in Figure 6.10 for a better visualisation of the amount of PV power that is supplied to the traction network. Here, one can clearly see that the PV system with variable PV power output control is able to supply more power to the traction network, by following the power demand and adjusting the PV system output accordingly. In this way, the PV system is able to supply 22.1% more energy to the traction network during a day, which is a significant increase.

The effect for different PV system sizes is shown in Table 6.6. In this table, the amount of PV energy that can be delivered to the traction network as a percentage of the maximum PV energy generation during a day for that particular PV system is shown, for the two different control methods. For these calculations, the same PV systems and settings are used as described in Section 6.2.2. Clearly, the variable PV output control is a very promising method for increasing the amount of PV energy that can be supplied to the traction network. However, implementing this control accurately can be challenging. Since the only reference for the control is the traction network voltage, it is hard to estimate the amount of PV power that can be supplied to the traction network, without increasing the network voltage too much. Therefore for the results in the other parts of this report, the binary PV power output control is used. Nevertheless, this method is worth serious consideration and further research.

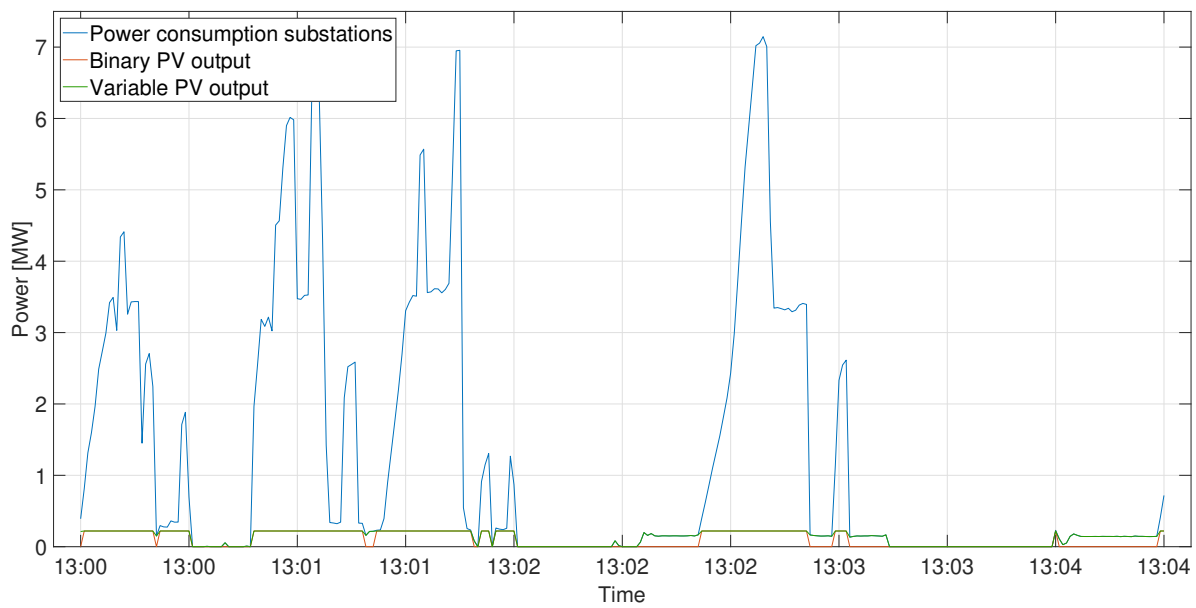


Figure 6.9: Power consumption of substations compared to PV power supplied to traction network

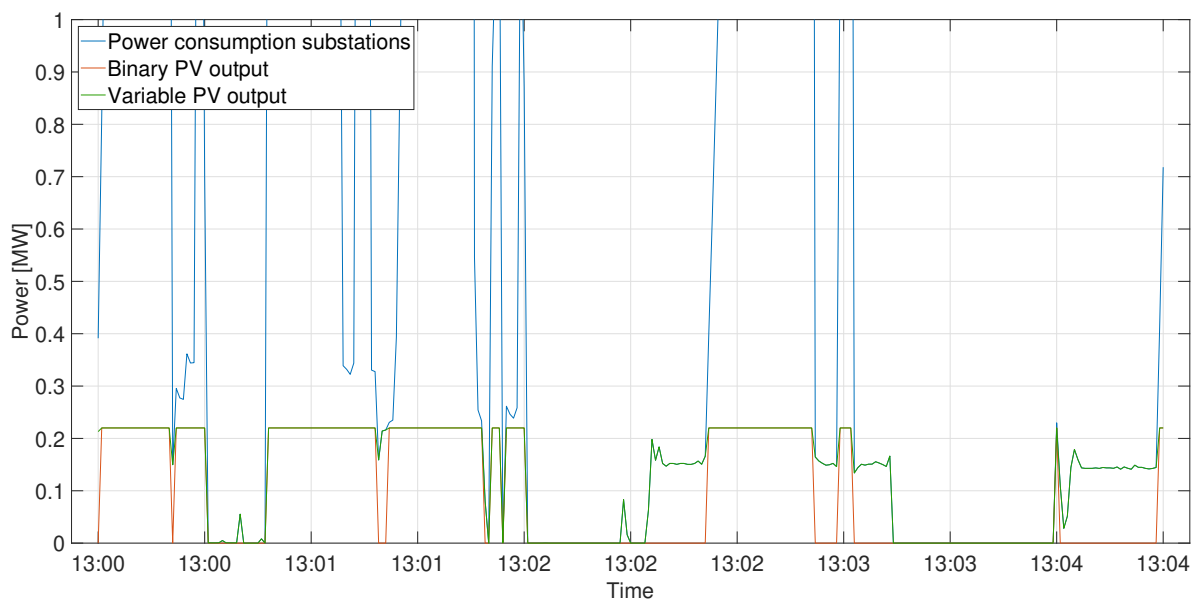


Figure 6.10: Power consumption of substations compared to PV power supplied to traction network

Table 6.6: Results for different south facing PV systems

System Size	Yield/Day	To Network Binary Output	To Network Variable Output
202 kWp	561 kWh	61.9%	70.3%
405 kWp	1118 kWh	58.5%	69.3%
597 kWp	1647 kWh	54.0%	65.9%

Although using the variable PV output power control method is a good way to increase the amount of PV power that can be supplied to the traction network, still the maximum amount that can be delivered for the three different PV system sizes is only 70.3%. Hence still almost 30% of PV energy is lost due

to the power mismatch. In the following sections, other options to prevent this waste of PV energy will be discussed.

6.3 Traction network with inverter

As discussed in Section 3.1.4, an inverter in a substation can be used to recuperate any surplus of energy, either generated by the PV system or because of the regenerative braking. The inverter will feed the surplus of energy back to the grid to save electricity costs and to allow for a useful destination of the energy. For the simulation results discussed in this section, an inverter model is used in the substation that is closest to the PV system, as discussed in Section 4.3, to minimise ohmic losses between the PV system and the inverter. For the following results, the INGEBER inverter with a maximum power capacity of 1.5 MW is used as a reference [60], also shown in Figure 6.11. However some numbers for different power capacities are given as well. The conversion efficiencies are assumed to be 100%.



Figure 6.11: 1.5 MW INGEBER inverter [60]

6.3.1 Inverter without PV

Figure 6.12 shows the amount of braking energy that can be recuperated using the 1.5 MW inverter, during a regular weekday, assuming no power exchange between the three power sections around the pilot location and the rest of the traction network. During the simulation no PV system is connected to the traction network. For the 1.5 MW inverter, a total of 2294 kWh can be recuperated, which is 8.9% of the total energy consumption and 35% of the total regenerated braking energy. This is energy that would otherwise have been wasted in the braking resistors of the metros. Therefore, it can be concluded that even without a PV system connected to the traction network it might already be profitable to install an inverter to recuperate braking energy.

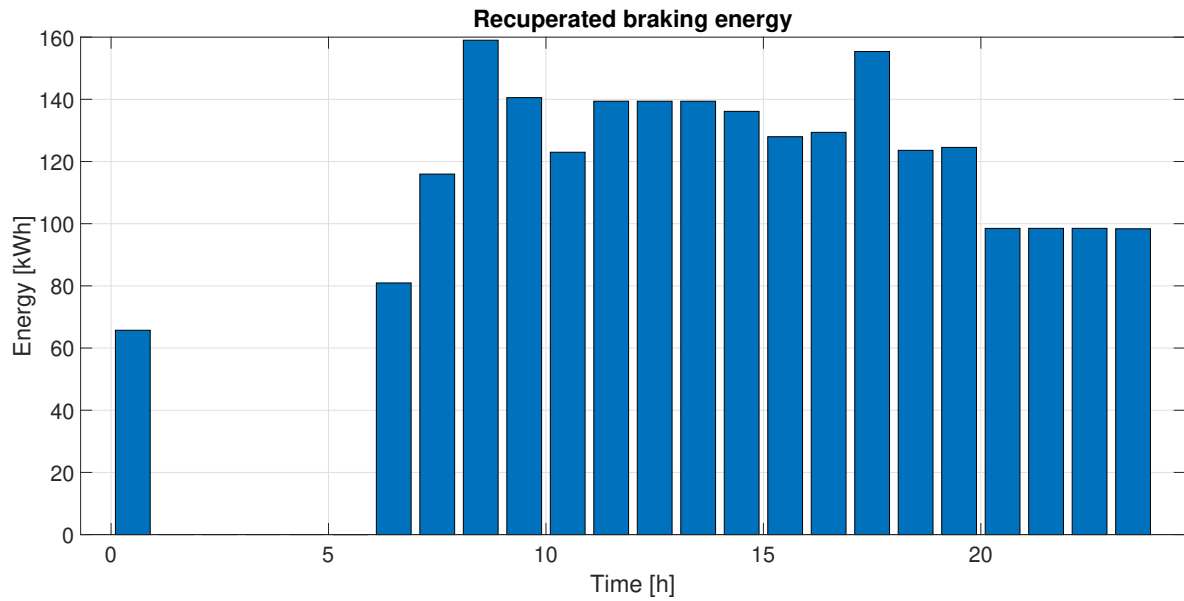


Figure 6.12: Braking energy recuperated by the inverter during a weekday

To show the operating principle of the inverter, Figure 6.13 depicts both the power consumption of the substations and the amount of inverted power, during a 15 minutes interval from 07:15 until 07:30. Here one can clearly see that where the power consumption is zero, the inverter is operating. At these moments a metro is braking and thus producing electrical energy using regenerative braking. At these moments the amount of generated power is more than the power demand and therefore there is a surplus. This surplus is recuperated by the inverter and fed to the 10.5 kV grid, shown by the orange line in the figure.

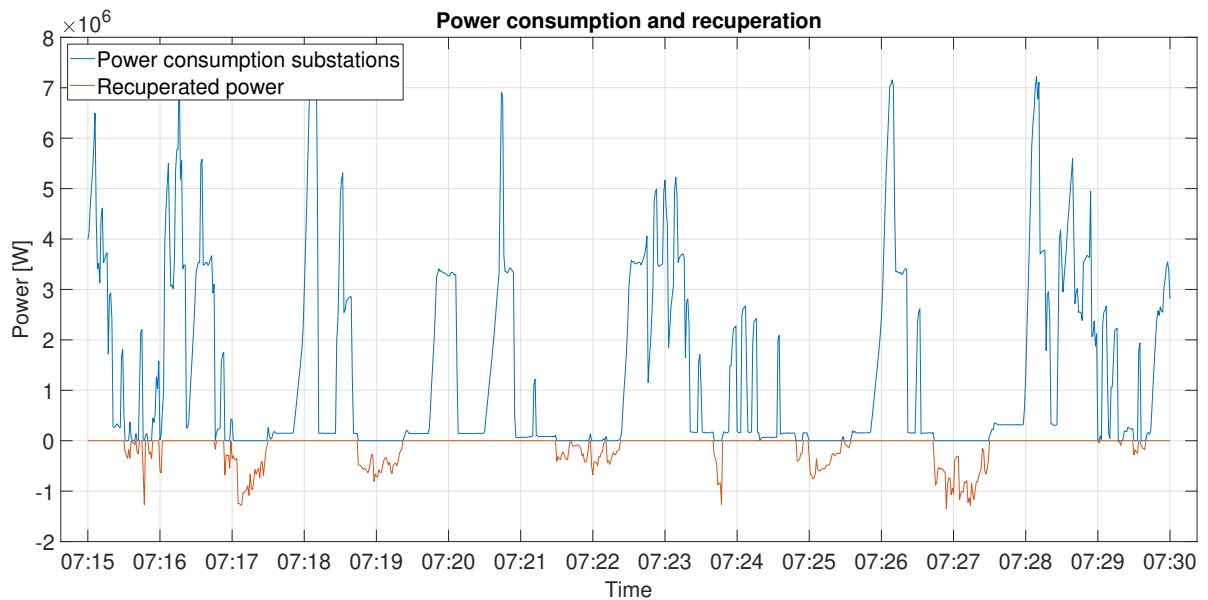


Figure 6.13: Power consumption substations vs recuperated power by inverter

The power flow in the inverter is in this case limited to 1.5 MW. However, also inverters with a smaller maximum power rating are available on the market, for instance the ERS750 inverter produced by ABB, with a maximal power rating of 1.15 MW [61]. If the amount of surplus power is higher than the maximum power rating of the inverter, some energy will be lost. Therefore, for lower power ratings, the potential amount of recuperated energy will be lower. Figure 6.14 shows the relation between the

maximum power rating of an inverter in *MW* and the potential amount of energy that can be recuperated in *kWh*. As can be seen in this figure, the total amount of energy that can be recuperated during a day almost saturates at 1.5 *MW*. Table 6.7 show a comparison between the amount of energy that can be recuperated by the 1.5 *MW* inverter and the 1.15 *MW* inverter during a day. Interestingly, decreasing the maximum power rating of the inverter with 23.3% only results in a decrease of recuperated energy of 1.74%. Therefore, in this case it might be more economical to choose a smaller inverter than the 1.5 *MW* inverter.

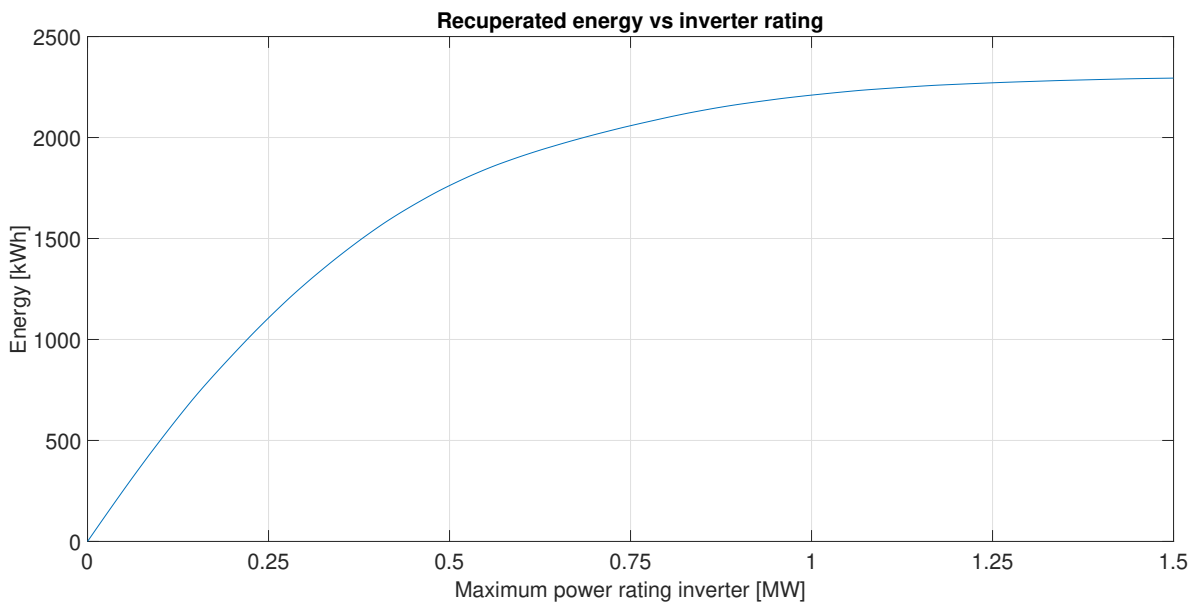


Figure 6.14: Relation between potential recuperated energy and maximum power rating of the inverter

Table 6.7: Comparison potential recuperated energy for different inverters

	1.5 MW inverter	1.15 MW inverter
Recuperated Energy [kWh]	2294	2254

When braking energy is able to flow to power section adjacent to the three sections discussed in this section, an even smaller inverter can be used. Figure 6.15 again shows the relation between the maximum power rating of an inverter in *MW* and the potential amount of energy that can be recuperated in *kWh*, but now for the case that part of the braking energy is able to flow to power sections adjacent to the three section discussed in this section. In this figure one can clearly that less braking energy has to be recuperated from the traction network and that a smaller inverter can be used.

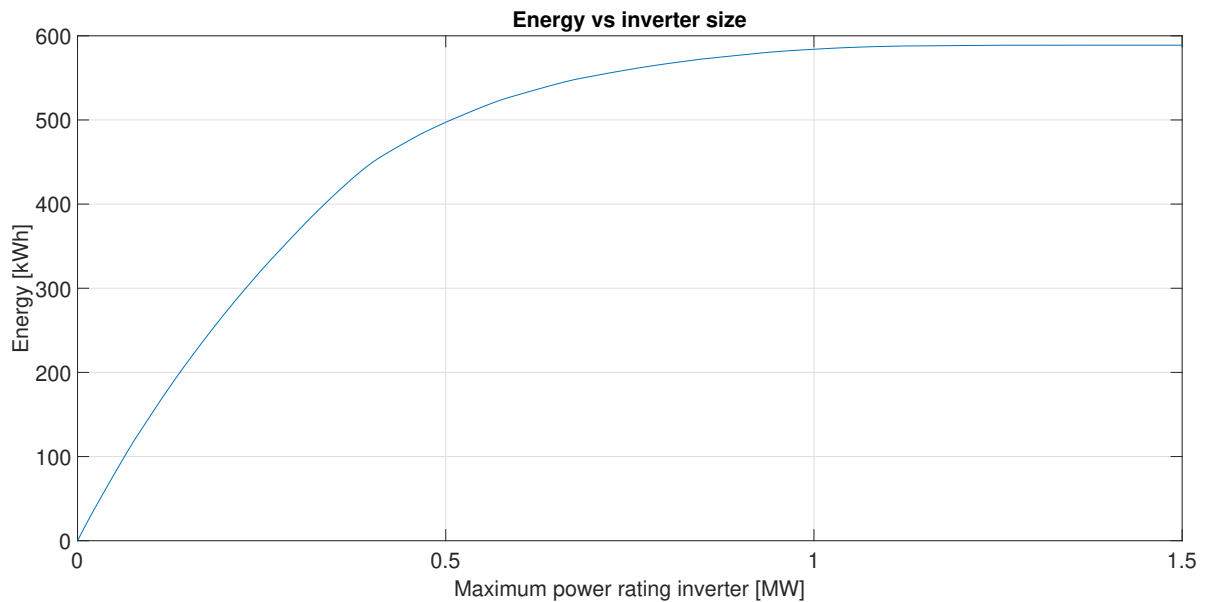


Figure 6.15: Relation between potential recuperated energy and maximum power rating of the inverter

6.3.2 PV + Inverter

Now that the results for a traction system with a PV system connected and with an inverter connected are discussed, it is time to study the results for a traction system with both a PV system as well as an inverter connected.

Just like in Section 6.2, in this section the results for the traction network with an inverter and PV system connected are discussed, when there is a normal consumption/low generation in the adjacent power sections, as well as when there is a low consumption/high generation in the adjacent power sections, respectively.

High consumption in adjacent network

First the results are given in the scenario that part of the surplus power is able to flow to the rest of the network. For the simulations, a model of a 1.5 MW inverter is used. Table 6.8 shows an overview of these results. What immediately stands out from this table is the drastic increase of PV power that could be supplied to the traction network. Therefore, combining PV systems with an inverter is a good solution for solving the power mismatch between the load and generation. Column 7 of the table shows the total energy saving, which is a combination of the decreased energy consumption in the traction network and the amount of recuperated energy.

Table 6.8: Results for different south facing PV systems and inverter

PV System Size	Yield/Day	To Network	To Network	Energy Saving	Recuperated Energy	Total energy Saving
202 kWp	561 kWh	534 kWh	95.2%	492 kWh	641 kWh	1133 kWh
405 kWp	1118 kWh	915 kWh	97.6%	1034 kWh	704 kWh	1738 kWh
597 kWp	1647 kWh	1338 kWh	94.1%	1508 kWh	732 kWh	2240 kWh

In Figure 6.16 the amount of energy that can be recuperated versus the maximum power rating of the inverter is shown again. In this graph, the amount of energy that can be recuperated for PV systems with different sizes connected to the traction network are shown. This graph can be used to determine what would be an appropriate inverter for this scenario. Clearly, in this case an inverter with a lower power rating could have been used than the 1.5 MW inverter used in the simulations discussed in this section, which would have been more cost-effective.

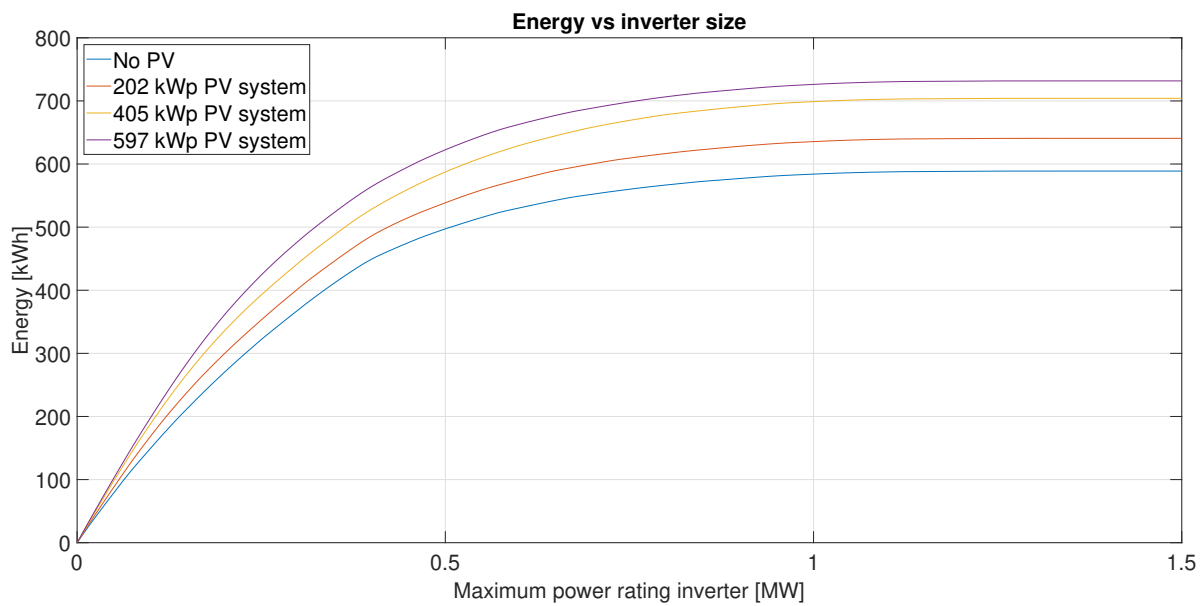


Figure 6.16: Relation between potential recuperated energy and maximum power rating of the inverter

Low consumption in adjacent network

Now, the results for the scenario when there is no power exchange between the three power sections around the pilot location and the rest of the network are discussed. The results are shown in Table 6.9. In this scenario, again, the amount of PV energy that could be supplied to the traction network is significantly increased. However still approximately 15% of the PV energy is lost due to power mismatch. Again, in Figure 6.17 the amount of energy that can be recuperated versus the maximum power rating of the inverter is shown. Like discussed in Section 6.3.1, the maximum power rating of the inverter could have been decreased to 1.15 MW while losing only little recuperated energy compared to the decrease in maximum power rating.

Table 6.9: Results for different south facing PV systems and inverter

PV System Size	Yield/Day	To Network	To Network	Energy Saving	Recuperated Energy	Total energy Saving
202 kWp	561 kWh	477 kWh	85.1%	422 kWh	2399 kWh	2821 kWh
405 kWp	1118 kWh	933 kWh	83.4%	799 kWh	2506 kWh	3305 kWh
597 kWp	1647 kWh	1390 kWh	84.4%	1129 kWh	2663 kWh	3792 kWh

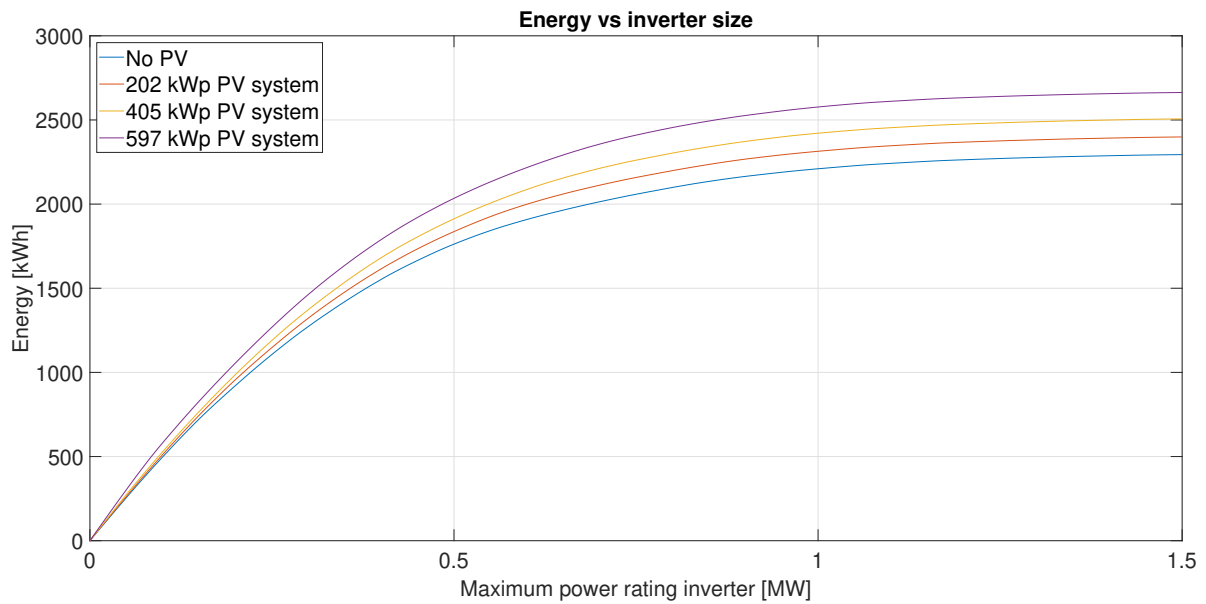


Figure 6.17: Relation between potential recuperated energy and maximum power rating of the inverter

6.4 Storage

In this section the results for a traction system with an energy storage system (ESS) connected is discussed. For the results discussed in this section, simulations are done using the model shown in Chapter 4 and the control strategy discussed in Chapter 5. No conversion losses are considered in the simulations. The simulations that will be discussed are done to show what ESS could potentially do to the energy efficiency of the traction network in Amsterdam. Due to time limitations during the thesis project, only few simulations could be done. Therefore, this chapter only briefly discusses the results and potential of ESS. However, considering the positive effects of ESS, as will be explained, the usage of ESS deserves more research.

6.4.1 ESS without PV

First, the potential for ESS connected to the traction network without PV will be discussed. For the simulations, the ESS will be connected at the pilot location. The model and control strategy as discussed in Chapter 4 and 5, respectively, are used for the simulations.

Figure 6.18 shows the positive effect of an ESS on the voltage of the traction network during a time interval of 10 minutes. In this Figure, one can clearly see that above 900 V, the voltage is reduced by absorbing (braking) energy from the traction network, which is stored in the ESS. Below 900 V, the voltage is increased by releasing this energy again. Due to this voltage increase, the ohmic losses in the network are decreased.

Figure 6.19 shows the state of charge for the same ESS during a day. Here one can see, that the ESS is mostly discharged during rush hours and charged again during more quiet hours of the day. Between 01:00 and 06:00 AM, the SOC is constant because at that moment no metros are operational. By storing and releasing the braking energy, in this simulation, the total energy consumption of the traction network during a day was decreased with 2.45%. This proves the energy saving effect that ESS can have for a traction network. For this simulation, a 90 kWh battery was used which was able to store energy for a longer time period, as can be seen in Figure 6.19.

To estimate a proper size for ESS in the traction network, the power profile of the modelled traction network is used. From this profile, a time interval with the largest amount of braking energy for the longest amount of time was selected as a reference, to make sure that no braking energy is lost for every moment of the day. From this calculation it is estimated that an ESS of 13 kWh would be sufficient. This includes an extra 20% to prevent a too deep discharge of the ESS. Also, it is assumed that the stored energy is released right after the metros have stop braking, to be able to store energy again

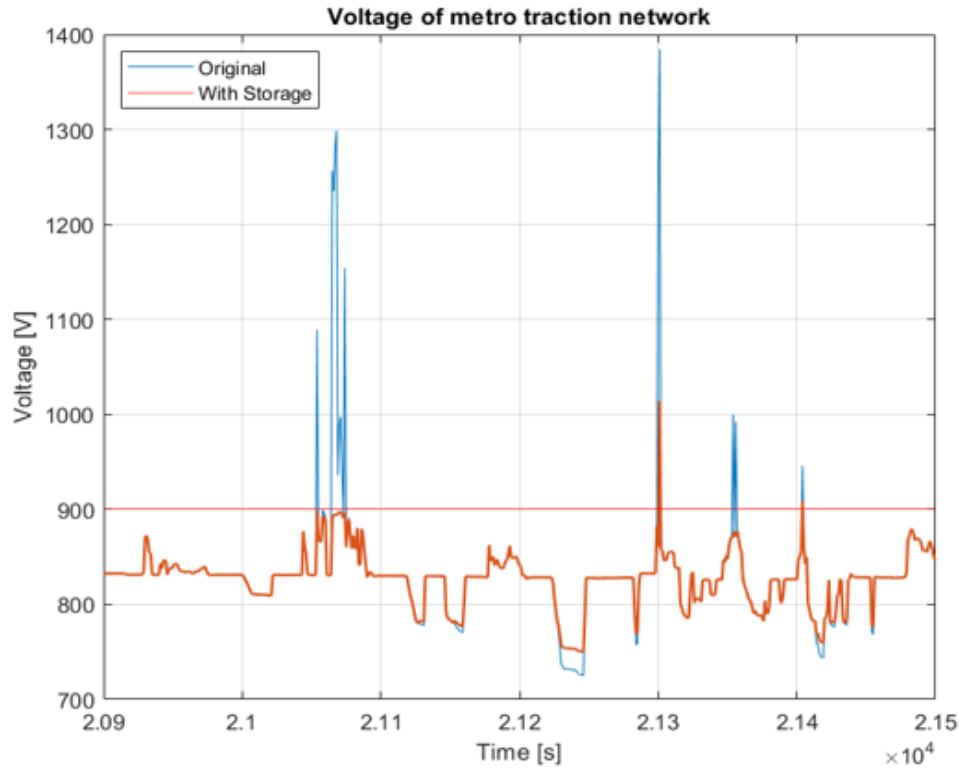


Figure 6.18: Traction network voltage with ESS

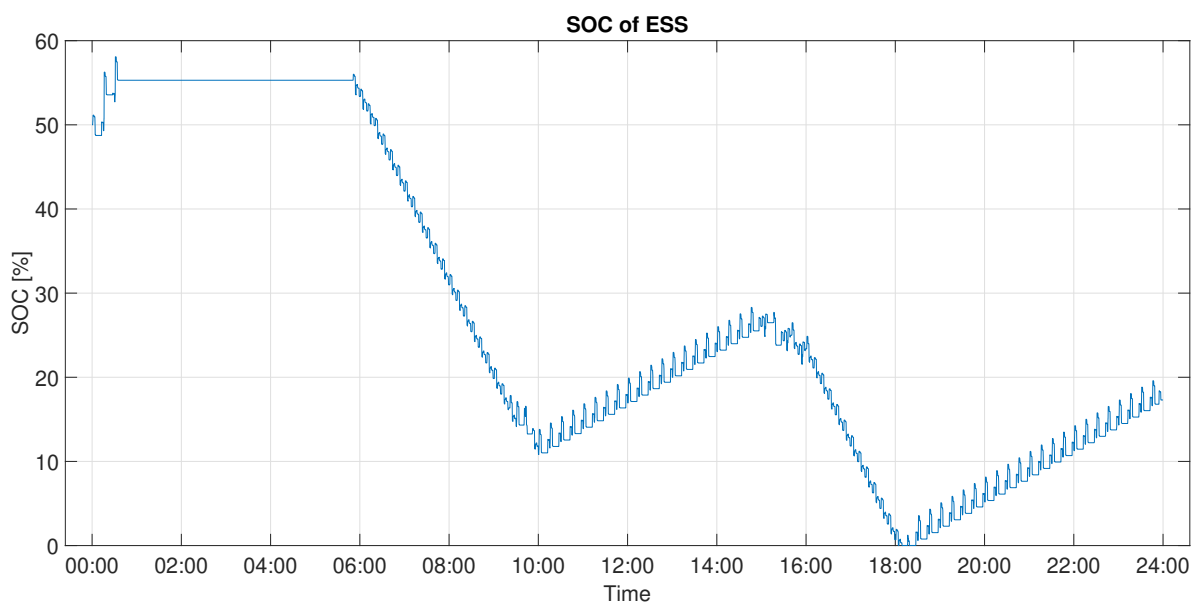


Figure 6.19: State of charge of the ESS during a day

when metros are braking again. The maximum power that had to be handled by the ESS is around 1.6 MW.

6.4.2 ESS with PV

In this section, a proper size for the ESS will be estimated again, but now for a traction network including a PV system as well. To make sure no braking energy is lost, as well as no PV energy, the ESS size

has to be increased. For this calculation, the power profile of the traction network is used again, as well as the power generation profile of a PV system, for instance for a 597 *kW_p* PV system. The estimated required ESS size is in this case 16 kWh, including an extra 20% again. This is sufficient to store braking energy as well as PV energy during high solar irradiation. Again, it is assumed that the stored energy is released again right after it is stored, during high power demand. In other words, the ESS size calculation is done for short term storage. The maximum power that had to be handled when a 597 *kW_p* PV system was connected, was around 1.8 *MW*. Considering this high power flow, ESS with super-capacitor technology is recommended, because of the high power density of this technology. Also because of the many discharge cycles, as shown in Figure 6.19, super-capacitors are recommended because this technology has a higher cycle life, as discussed in Chapter 3.

7

Case Study

Although it is very interesting to study the technical opportunities to make the metro traction network more sustainable, it is important to look at the financial aspects as well. In the end, any system will only be really implemented if a positive business case goes along with it. Therefore, in this chapter, a system is advised and a case study is done for this system to discover whether the proposed system is economically feasible. The choice for the proposed system is made based on the results discussed in Chapter 6.

7.1 The PV system

Choosing the right PV system size is a difficult trade-off between the desire to make the traction network more sustainable, while also being realistic about the efficiency and performance of the PV system. The results in Chapter 6 show that for every increase of the PV system size, more energy is lost due to power mismatch. Considering this fact, as well as the fact that there is no experience with PV systems connected to the DC side of a metro traction network, it is recommended that the pilot starts with a PV system that is not too large. At the same time, when using the 200 kW DC/DC converter, it would not be cost-effective to use a too small PV system and only use a small part of the DC/DC converter power capacity. Therefore, based on the aforementioned considerations and the results discussed in this report, a PV system is recommended with a size of 200 kW_p of installed power. The advised orientation of the PV system is towards the south, since from the results in Chapter 6 it could be concluded that east-west configured PV systems of 200 kW_p would not increase the amount of PV energy supplied to the traction network.

For this case study, a 300 W_p poly-crystalline PV module manufactured by Canadian Solar Inc. will be used, which is shown in Figure 7.1a [62]. This is a PV module that has a good availability on the European market with a competitive price [63]. Although poly-crystalline PV modules have a lower efficiency compared to mono-crystalline PV modules, poly-crystalline PV modules have been chosen, because the lower price per W_p. This parameter is more important than the efficiency, because the land that will be used for the PV system is already owned by the municipality of Amsterdam and therefore the extra land that is required due to the lower efficiency is not a problem. Moreover, for this PV system size plenty of land is available at the pilot location.

The PV modules will be oriented to the south, for maximum energy yield. Because of the abundance of space, the PV module rows, or sheds will be spaced 5 meters from each other to minimise mutual shading losses caused by the PV modules. For this setup, the most optimum tilt of the PV module in terms of energy yield is 33°. This setup of the PV system is shown in Figure 7.1b. The ground coverage ratio of the PV system is 33.5%. The space needed for the PV system, including the space between the PV sheds, is approximately 3300 m². This is about a third of the land that is available at the pilot location. This leaves room for additional PV systems in the future, when more experimental results are available, the density of metro traffic and the traction network energy consumption has grown or when additional solutions like storage have been installed.

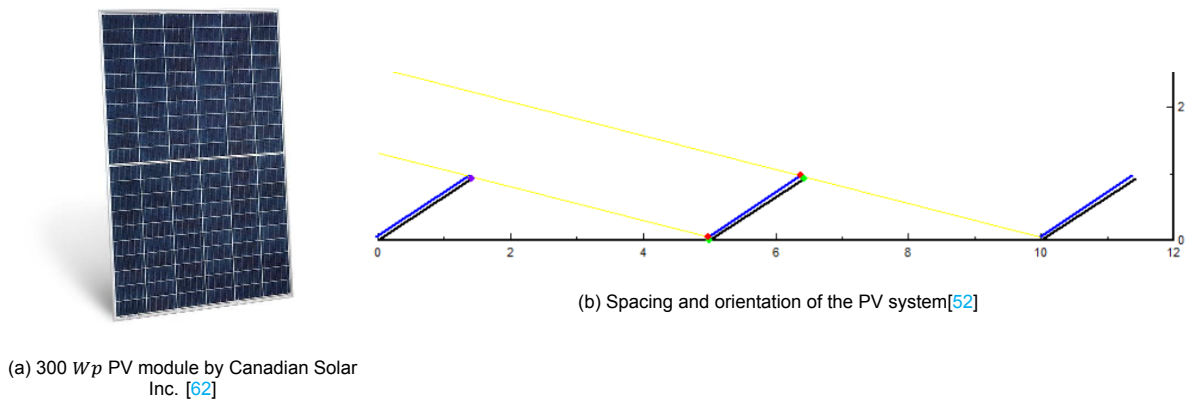


Figure 7.1: The chosen PV module and setup

To account for the shading losses caused by surrounding obstacles like buildings, the skyline profile is analysed using LiDAR data from the AHN database, which has an elevation map of the Netherlands, including objects like buildings, which is publicly available on the internet [24]. This data is then processed to obtain the skyline profile for the pilot location [64]. The resulting profile is shown in Figure 7.2. Here one can see that the skyline is relatively clear of obstacles. The profile is used in the simulations with PVsyst to account for the shading losses.

The main results from the PVsyst simulation are shown in Appendix D. The effective energy at the output of the PV array is used to determine the PV profile used in the simulations of the traction network with the PV system. The PV generation profiles for different seasons have been simulated to account for seasonal influences.

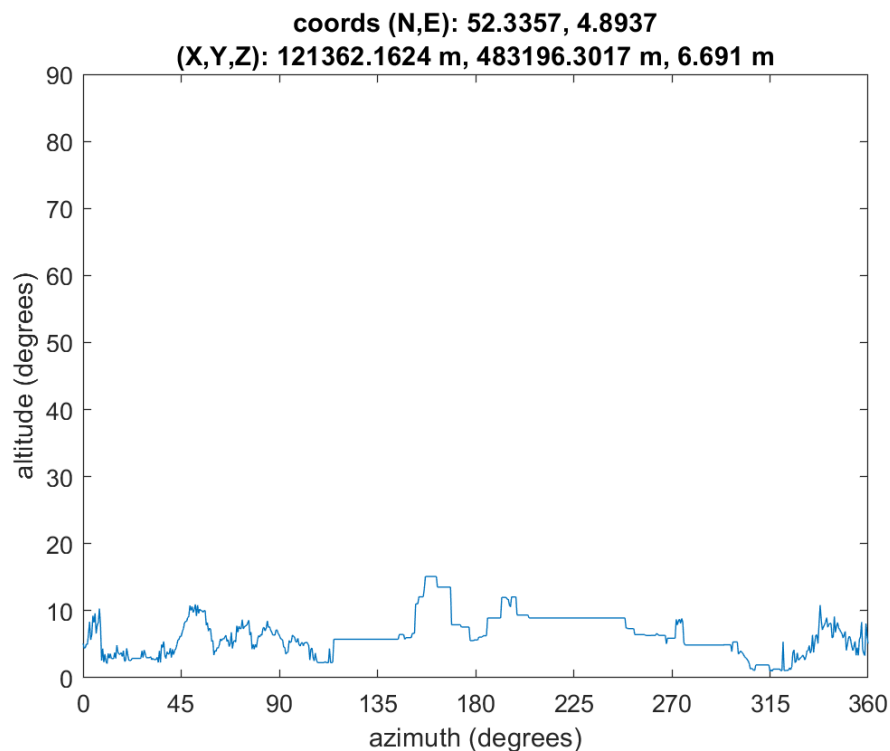


Figure 7.2: Horizon profile of pilot location

7.2 Additional equipment

To connect the PV system to the metro traction network, a DC/DC converter is required. For this case study, the 200 kW DC/DC converter manufactured by Elektroline (a company specialised in compo-

nents for traction systems) is used as a reference for the model[65]. This company claimed that the DC/DC converter has a conversion efficiency of 90%. The conversion losses related to this efficiency are included in the simulations.

Further, to partially solve the mismatch problem between PV generation and the load, an inverter is included in the model to minimise the mismatch losses by recuperating the surplus of PV energy. Moreover, as discussed in Section 6.3, the inverter proved to be an interesting option to recuperate the surplus of braking energy. Based on the results in Section 6.3, an inverter with a maximum power rating of 1.15 MW is chosen. Although some energy will be lost due to the power limit of the inverter, it is not cost effective to choose an inverter with a higher power rating, since the inverter power rating would have to be increased significantly to recuperate only a small amount of extra energy.

The inverter that is chosen for the case study is the ERS 750 IGBT inverter manufactured by ABB [61]. This inverter has an efficiency of 97.5%. The inverter is shown in Figure 7.3a. Because the inverter can be connected anti-parallel to the rectifier unit in the substation, this device is very suitable for expansion of the existing substations, instead of having to replace the entire rectifier unit. This is shown in Figure 7.3b. The costs of required components for the installation of the systems are included in the cost calculations.

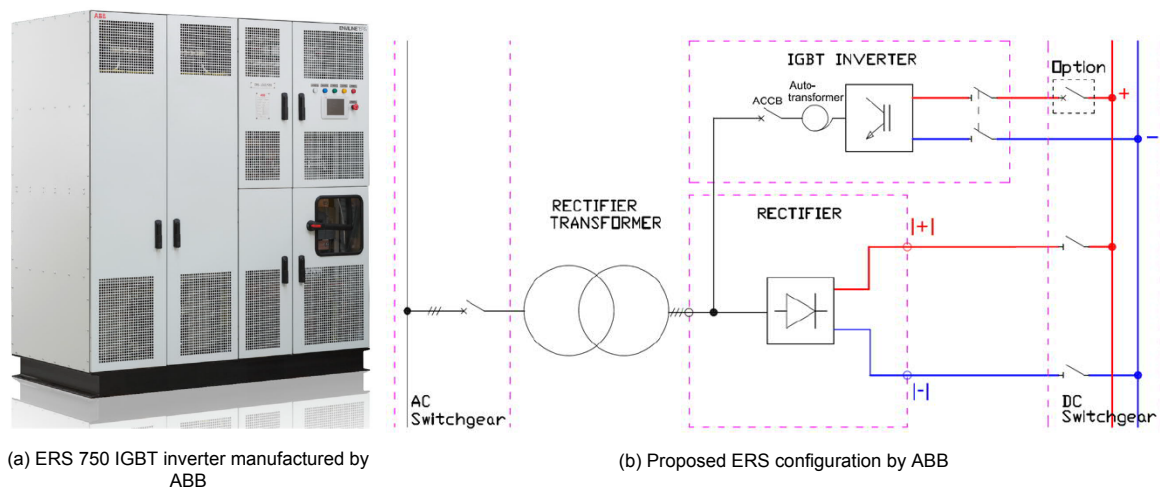


Figure 7.3: ERS inverter and proposed implementation by ABB [61]

7.3 Results

For this case study, three different systems will be simulated. The study focuses on the pilot location discussed in Section 2.3. First the traction network with only an inverter connected in a substation will be simulated. Secondly, the traction network with only a PV system connected will be simulated. Lastly, the a combination of the two is simulated.

The simulations are done with the assumption that there is almost no power exchange between the three power sections around the pilot location and the sections adjacent to these sections, further away. The results for the three different systems are shown in Table 7.1. In this table, the energy savings using the different systems for an entire year are shown. To calculate these energy savings, the traction network with PV system is simulated for different seasons, to include the seasonal effects on the PV yield. The PV yield shown in Table 7.1 is the total amount of PV energy that is supplied to the traction network during a year. The energy saving is the total reduction of energy consumption in the traction network. The total energy savings column is the sum of the energy consumption reduction in the traction network and the amount of recuperated energy. This sum is used to calculate the profits of the systems. Note that these are the energy savings for the first year. In the following years the PV yield will be slightly lower due to the degradation of the PV modules.

Table 7.1: Energy savings of the different systems for a year

System	PV yield	Energy Saving	Recuperated Energy	Total Energy Saving
Only PV	105 MWh	123 MWh	0 MWh	123 MWh
Only Inverter	0 MWh	0 MWh	780 MWh	780 MWh
PV + Inverter	134 MWh	93 MWh	829 MWh	922 MWh

7.4 Economical evaluation

In this section, an estimation for the profits and return of investment is made. To calculate the return of investment of the systems discussed in this chapter, first the costs of the different components required for the system have to be estimated. Also additional costs like insurance have to be considered.

First, the costs for the PV system are estimated. Because the DC/DC converter required for the PV system is not yet available on the market, the price is estimated by using the costs of 200 kW DC/AC solar inverters [66][67]. Using this information, the price is estimated to be €9,000.-. For the PV modules, a price of €84.- per module is used [63]. This results in a total price of €56,028.- for the PV modules. Others costs, like cabling, switches, mounting (including labour) etc. are estimated to be 26,000.- [68]. The price of the ABB inverter is €220,000.-.

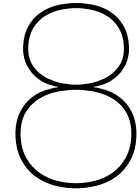
Other costs are cleaning and maintenance of the PV system (€770/year), insurance (0.21% of total investment) and monitoring costs (€100/year). Further, a degradation of the PV system of 0.5% per year is included in the profit calculations. For the profit calculations, an energy price of €0.078 per kWh is used. This information is given by the metro and tram department of the municipality of Amsterdam. All mentioned prices are without VAT.

The results are shown in Table 7.2. The second column of the table shows after how much time the investment is earned back. As can be seen, the payback time for the PV system without inverter is very long. This because of the high mismatch losses of the PV system operating without an inverter. For the systems with inverter, the payback time can be significantly reduced. The third column of the table shows the return of investment after 15 years, assuming that no components have been replaced in this period. As can be seen, the installation of the inverter result in a significant increase of the return of investment. In Appendix E, the costs and profit for the three different systems during 15 years is shown in Figures E.1, E.2 and E.3.

Summarising, the integration of PV systems is only financially attractive if it is combined with an inverter.

Table 7.2: Return of investment

System	Payback Time	ROI
Only PV	11 years	130%
Only Inverter	4 years	403%
PV + Inverter	5 years	321%



Conclusions

8.1 Conclusion

In this report, a comprehensive insight is given for the performance of PV systems connected to the DC-side of a metro traction network. As became clear in Chapter 6, it is a serious challenge to match the PV generation with the load of the traction network. Because of the intermittency of the load and the regenerated braking energy, the PV power output is curtailed for a significant amount of time. However, using an inverter or ESS, the performance of the PV system was improved.

Also the additional energy saving effect related to the decreased ohmic losses in the traction network where studied in more detail. In addition, for the proposed systems it was proven that the voltage level of the traction network could be increased to decrease ohmic losses, without increasing the voltage too much.

In Chapter 2, the choice for a suitable pilot location is explained. Different considerations and criteria for the pilot location were given to make sure that the pilot location is suitable for the installation of PV systems. In Chapter 7, a PV system design is proposed, based on the results that are obtained during the thesis project. The results were used to reach the most optimal performance of the PV system in term of the amount of PV energy that could be supplied to the traction network, while having a cost-effective system. Also, the expected energy yield is given for the prospected PV system, as well as an economical evaluation. This answers research subquestion 1 from Chapter 1.

In Chapter 3, different topologies where discussed to connect the PV system to the traction network, including additional options like an inverter and an ESS. Also, potential manufacturers for the required equipment were discussed. In this chapter also the advantages and disadvantages of the different topologies were given. Further, in Chapter 5, control strategies where proposed for the optimal operation of different systems, while satisfying the safety requirements for the traction network. Lastly, the effectiveness, efficiency and safety of the different systems were analysed in Chapter 6. This answers research subquestion 2 from Chapter 1.

The potential for storage is discussed in Chapter 3 and 6. Also, an estimation was given for the ESS size that is required to prevent any energy losses and a recommendation for the technology was given. Further, the potential for using the grid as the "storage", by using an inverter was analysed in Chapter 6. This answers research subquestion 3 from Chapter 1.

The entire report aims to answer the main research question, *How can the Amsterdam metro contribute to the acceleration of the energy transition by integrating PV systems directly on the traction network?*. Different options for the integration of PV systems where given in this report, which partly answers this question. In Chapter 7, a concrete example of how a PV system could be integrated on the traction network was given, including an analysis of the potential energy yield and return of investment.

From the study that is presented in this report, it can be concluded that the integration of PV systems on the traction network is very interesting and promising, but it should also be noted that the integration can be challenging. If the sustainability ambitions in Amsterdam are to be reached using the integration of PV systems at the DC side of the traction network, additional devices like inverters and/or ESS are required.

8.2 Discussion

For the simulation discussed in this report, the data for the Amsterdam metro network is used, for a specific pilot location. Although this study focuses on the traction network of Amsterdam, the conclusions in this report could be used for other DC traction systems as well. However, one should keep in mind that the differences between the traction network of Amsterdam and other networks, like the substation voltages, location of the substations, resistances of the network, type of metro that is used, frequency of metro stops, frequency of metro rides (train plan), environmental data, irradiation blocking objects etc. will all influence the results discussed in this report.

As discussed in Section 4.1.2, the power consumption of the auxiliary equipment on board of the M5 metro is an estimated average, based on the characteristics of the M5 metro [49]. However, in real life, this power load is not constant and is influenced by for example seasonal and weather influences like the ambient temperature, humidity and the amount of light during a day. These factors have a strong influence on loads like air-conditioning and ventilation. A recent study on the power consumption of trolley busses show a strong relation between ambient temperature and the power consumption of auxiliary loads [69]. Also this study suggest a method to model this load using input data like relative humidity, air temperature and solar irradiance. Although this study focuses on trolley busses, similar conclusions can be drawn for metros. Modelling the auxiliary loads using this data as an input can further increase the accuracy of the simulations discussed in this report.

In Chapter 6 it is explained that two different scenarios are simulated with respect to the power sections of the traction network that are adjacent to the three power sections that are modelled in detail around the pilot location. In the first scenario it is simulated that power can come from or go to sections adjacent to the three sections that are modelled in detail and in the second scenario the power can *not* come from or go to sections adjacent to the three sections that are modelled in detail. However, it would of course be more accurate if the adjacent sections would have been modelled in detail, instead of connecting an average load to simulate adjacent sections, or connecting no load at all. Commercially available simulation software for traction systems could be used for this purpose. Nevertheless, the modelling of more sections is not done in this study because it adds too much computation time to the simulations in Simulink. Also in literature where the power flows of DC traction networks are studied, often at most three power sections are modelled, which still results in accurate conclusions. However, it should be kept in mind that the load of the rest of the network does influence the simulation results. It should also be noted that the aforementioned influences also effect the results for the economical evaluation in Chapter 7. Due to the fact that no superfluous power flows to sections further away in the network, the amount of energy that is recuperated could be overestimated.

8.3 Future work

In Section 6.2.4, the results for a variable PV power output control method are discussed. It is shown that this method is a promising way of increasing the amount of PV power that can be supplied to the traction network. However, the implementation of this control method has some challenges and requires more research to accurately match the PV power output with the load. Nevertheless, it is worth doing this since the power matching can be improved significantly, as proved in Section 6.2.4.

In Chapter 6, the potential for an ESS in the traction network is discussed. Due to time limitations, the potential energy saving could not be analysed in great detail and only few results could be given. For future research it is recommended to further study the potential energy savings using ESS in the traction network of Amsterdam.

Although different options are discussed to improve the performance of PV systems connected to the

traction network, it is recommended that more research is done on other solutions, like for example timetable optimisation. Also, a further optimisation of the control strategies proposed in Chapter 5 could be done. Further, more research on the hardware design and control software for the DC/DC converter between the PV system and the traction network could be done, since this is a new type of converter which is not mature and available on the market yet for traction network applications.

Lastly, in continuation of the research done in this thesis project, the next step is to actually implement the proposed system at the pilot location. By doing this, experimental results could be obtained, which will give further insight of the performance of DC-side connected PV systems and potentially additional devices like inverters or ESS. The implementation of the PV system may also encourage other cities to also integrate PV systems on their traction systems, which will improve the sustainability of public transit worldwide.

References

- [1] A. A. Messaoudi, “Zonnepanelen naast metrospoor,” De Haagse Hogeschool, 2018.
- [2] W. Günselmann, “Technologies for increased energy efficiency in railway systems,” in *2005 European Conference on Power Electronics and Applications*, 2005, 10 pp.–P.10. DOI: [10.1109/EPE.2005.219712](https://doi.org/10.1109/EPE.2005.219712).
- [3] GVB, “Jaarverslag gvb holding nv 2020,” GVB Holding NV, 2020.
- [4] —, “Jaarverslag gvb holding nv 2019,” GVB Holding NV, 2019.
- [5] M. Popescu and A. Bitoleanu, “A review of the energy efficiency improvement in dc railway systems,” *Energies*, vol. 12, no. 6, 2019, ISSN: 1996-1073. DOI: [10.3390/en12061092](https://doi.org/10.3390/en12061092). [Online]. Available: <https://www.mdpi.com/1996-1073/12/6/1092>.
- [6] Zonnefabriek, *Amsterdams metrostation bedekt met zonnepanelen*. [Online]. Available: <https://www.zonnefabriek.nl/nieuws/reigersbos-metro-zonnepanelen/> (visited on 06/28/2021).
- [7] Municipality of Amsterdam, *Sustainability policy*. [Online]. Available: <https://www.amsterdam.nl/bestuur-organisatie/volg-beleid/duurzaamheid/> (visited on 06/21/2021).
- [8] H. Hayashiya, H. Yoshizumi, T. Suzuki, T. Furukawa, T. Kondoh, M. Kitano, T. Aoki, T. Ishii, N. Kurosawa, and T. Miyagawa, “Necessity and possibility of smart grid technology application on railway power supply system,” in *Proceedings of the 2011 14th European Conference on Power Electronics and Applications*, 2011, pp. 1–10.
- [9] M. Meng, Y. Yuan, M. Guo, L. Jiang, J. Liu, D. Hu, H. Cong, and D. Hao, “A novel dc microgrid based on photovoltaic and traction power supply system,” in *2014 IEEE Conference and Expo Transportation Electrification Asia-Pacific (ITEC Asia-Pacific)*, 2014, pp. 1–4. DOI: [10.1109/ITEC-AP.2014.6941272](https://doi.org/10.1109/ITEC-AP.2014.6941272).
- [10] F. Ciccarelli, L. Pio Di Noia, and R. Rizzo, “Integration of photovoltaic plants and supercapacitors in tramway power systems,” 2018.
- [11] G. Zhang, Z. Tian, H. Du, and Z. Liu, “A novel hybrid dc traction power supply system integrating pv and reversible converters,” *Energies*, vol. 11, no. 7, 2018, ISSN: 1996-1073. DOI: [10.3390/en11071661](https://doi.org/10.3390/en11071661).
- [12] L. Murray and N. Bottrell, “Riding sunbeams - powering our railways with solar pv,” Imperial College London, 10:10 Climate Action, Innovate UK, Community Energy South, TPS, 2017.
- [13] —, “Riding sunbeams - before dawn,” Imperial College London, 10:10 Climate Action, Innovate UK, Community Energy South, TPS, 2019.
- [14] X. J. Shen, H. Wei, and L. Wei, “Study of trackside photovoltaic power integration into the traction power system of suburban elevated urban rail transit line,” *Applied Energy*, vol. 260, p. 114 177, 2020, ISSN: 0306-2619. DOI: <https://doi.org/10.1016/j.apenergy.2019.114177>.
- [15] X. J. Shen, Y. Zhang, and S. Chen, “Investigation of grid-connected photovoltaic generation system applied for urban rail transit energy-savings,” in *2012 IEEE Industry Applications Society Annual Meeting*, 2012, pp. 1–4. DOI: [10.1109/IAS.2012.6373995](https://doi.org/10.1109/IAS.2012.6373995).
- [16] GVB, *Metro in cijfers*. [Online]. Available: <https://over.gvb.nl/ov-in-amsterdam/feiten-en-cijfers/metro-in-cijfers/> (visited on 04/21/2021).
- [17] —, *Metro lijnen amsterdam*. [Online]. Available: <https://reisinfo.gvb.nl/nl/lijnen?metro&show> (visited on 04/21/2021).
- [18] M. Khodaparastan, A. A. Mohamed, and W. Brandauer, “Recuperation of regenerative braking energy in electric rail transit systems,” *IEEE Transactions on Intelligent Transportation Systems*, vol. 20, no. 8, pp. 2831–2847, 2019. DOI: [10.1109/TITS.2018.2886809](https://doi.org/10.1109/TITS.2018.2886809).

- [19] I. E. Demirci and H. B. Celikoglu, "Timetable optimization for utilization of regenerative braking energy: A single line case over istanbul metro network," in *2018 21st International Conference on Intelligent Transportation Systems (ITSC)*, 2018, pp. 2309–2314. DOI: [10.1109/ITSC.2018.8569553](https://doi.org/10.1109/ITSC.2018.8569553).
- [20] H. Hoeksma, "Gvb analyse meetresultaten m5," RailwaySafe BV, 2018.
- [21] Á. J. López-López, R. R. Pecharromán, A. Fernández-Cardador, and A. P. Cucala, "Assessment of energy-saving techniques in direct-current-electrified mass transit systems," *Transportation Research Part C: Emerging Technologies*, vol. 38, pp. 85–100, 2014, ISSN: 0968-090X. DOI: <https://doi.org/10.1016/j.trc.2013.10.011>.
- [22] S. Keetels, "Rapportage zonnepanelen langs het spoor / proj.nr. mn000779," Movares, 2020.
- [23] Municipality of Amsterdam, *Gemeente amsterdam, data en informatie*. [Online]. Available: <https://data.amsterdam.nl/data/brk/object/NL.KAD.OnroerendeZaak.11720507170000/> (visited on 07/06/2021).
- [24] *Algemeen hoogtebestand nederland*. [Online]. Available: <https://www.ahn.nl/>.
- [25] Google, *Amsterdam-south*. [Online]. Available: https://www.google.com/maps/d/edit?mid=1u_IreYCb97Bn6xMxez3yyX_TzEs5lroZ&ll=52.33581438284303%2C4.870006879101538&z=14 (visited on 04/06/2021).
- [26] R. Faranda and S. Leva, "Energetic sustainable development of railway stations," 2007.
- [27] H. Hayashiya, S. Kikuchi, K. Matsuura, M. Hino, M. Tojo, T. Kato, M. Ando, T. Oikawa, M. Kamata, and H. Munakata, "Possibility of energy saving by introducing energy conversion and energy storage technologies in traction power supply system," in *2013 15th European Conference on Power Electronics and Applications (EPE)*, 2013, pp. 1–8. DOI: [10.1109/EPE.2013.6631780](https://doi.org/10.1109/EPE.2013.6631780).
- [28] X. Zhu, H. Hu, H. Tao, and Z. He, "Stability analysis of pv plant-tied mvdc railway electrification system," *IEEE Transactions on Transportation Electrification*, vol. 5, no. 1, pp. 311–323, 2019. DOI: [10.1109/TTE.2019.2900857](https://doi.org/10.1109/TTE.2019.2900857).
- [29] F. Meishner and D. U. Sauer, "Wayside energy recovery systems in dc urban railway grids," *eTransportation*, vol. 1, p. 100 001, 2019, ISSN: 2590-1168. DOI: <https://doi.org/10.1016/j.etrans.2019.04.001>.
- [30] A. González-Gil, R. Palacin, and P. Batty, "Sustainable urban rail systems: Strategies and technologies for optimal management of regenerative braking energy," *Energy Conversion and Management*, vol. 75, pp. 374–388, 2013, ISSN: 0196-8904. DOI: <https://doi.org/10.1016/j.enconman.2013.06.039>.
- [31] M. Khodaparastan and A. Mohamed, "Modeling and simulation of a reversible substation for recuperation of regenerative braking energy in rail transit systems," in *2019 IEEE Transportation Electrification Conference and Expo (ITEC)*, 2019, pp. 1–5. DOI: [10.1109/ITEC.2019.8790530](https://doi.org/10.1109/ITEC.2019.8790530).
- [32] W. de Jager, M. Huizer, and E. K. H. van der Pols, "Implementation of an active regeneration unit in a traction substation," in *2014 16th European Conference on Power Electronics and Applications*, 2014, pp. 1–9. DOI: [10.1109/EPE.2014.6911054](https://doi.org/10.1109/EPE.2014.6911054).
- [33] S. A. Hosseini-pour and M. R. a. Zolghadri, "Effectiveness and optimal placement of bidirectional substations for regenerative braking energy recovery in electrical network of metro system," *International Journal of Railway Research*, vol. 6, no. 2, 2019. DOI: [10.22068/IJRARE.6.2.43](https://doi.org/10.22068/IJRARE.6.2.43).
- [34] D. Iannuzzi, E. Pagano, and P. Tricoli, "The use of energy storage systems for supporting the voltage needs of urban and suburban railway contact lines," *Energies*, vol. 6, pp. 1802–1820, Apr. 2013. DOI: [10.3390/en6041802](https://doi.org/10.3390/en6041802).
- [35] M. Khodaparastan and A. Mohamed, "A study on super capacitor wayside connection for energy recuperation in electric rail systems," in *2017 IEEE Power Energy Society General Meeting*, 2017, pp. 1–5. DOI: [10.1109/PESGM.2017.8273915](https://doi.org/10.1109/PESGM.2017.8273915).
- [36] A. Ebrahimian, A. Dastfan, S. Ahmadi, and H. Khaligh, "Metro train line voltage control: Using average modeling bidirectional dc-dc converter," in *2018 9th Annual Power Electronics, Drives Systems and Technologies Conference (PEDSTC)*, 2018, pp. 7–13. DOI: [10.1109/PEDSTC.2018.8343763](https://doi.org/10.1109/PEDSTC.2018.8343763).

- [37] L. Sparavigna, "Control algorithms for the optimization of energy storage systems management in urban transport systems," 2018.
- [38] X. Liu and K. Li, "Energy storage devices in electrified railway systems: A review," *Transportation Safety and Environment*, vol. 2, no. 3, pp. 183–201, Jul. 2020, ISSN: 2631-4428. DOI: [10.1093/tse/tdaa016](https://doi.org/10.1093/tse/tdaa016).
- [39] H. Hayashiya, D. Hara, M. Tojo, K. Watanabe, M. Hino, T. Suzuki, H. Okamoto, H. Takahashi, T. Kato, and M. Teshima, "Lithium-ion battery installation in traction power supply system for regenerative energy utilization: Initial report of effect evaluation after half a year operation," in *2014 16th International Power Electronics and Motion Control Conference and Exposition*, 2014, pp. 119–124. DOI: [10.1109/EPEPEMC.2014.6980621](https://doi.org/10.1109/EPEPEMC.2014.6980621).
- [40] V. Calderaro, V. Galdi, G. Graber, A. Piccolo, A. Capasso, R. Lamedica, and A. Ruvio, "Energy management of auxiliary battery substation supporting high-speed train on 3 kv dc systems," in *2015 International Conference on Renewable Energy Research and Applications (ICRERA)*, 2015, pp. 1224–1229. DOI: [10.1109/ICRERA.2015.7418603](https://doi.org/10.1109/ICRERA.2015.7418603).
- [41] S. Aatif, X. Yang, H. Hu, S. K. Maharjan, and Z. He, "Integration of pv and battery storage for catenary voltage regulation and stray current mitigation in mvdc railways," *Journal of Modern Power Systems and Clean Energy*, pp. 1–11, 2020. DOI: [10.35833/MPCE.2019.000155](https://doi.org/10.35833/MPCE.2019.000155).
- [42] S. de la Torre, A. J. Sánchez-Racero, J. A. Aguado, M. Reyes, and O. Martínez, "Optimal sizing of energy storage for regenerative braking in electric railway systems," *IEEE Transactions on Power Systems*, vol. 30, no. 3, pp. 1492–1500, 2015. DOI: [10.1109/TPWRS.2014.2340911](https://doi.org/10.1109/TPWRS.2014.2340911).
- [43] J. A. Aguado, A. J. Sánchez Racero, and S. de la Torre, "Optimal operation of electric railways with renewable energy and electric storage systems," *IEEE Transactions on Smart Grid*, vol. 9, no. 2, pp. 993–1001, 2018. DOI: [10.1109/TSG.2016.2574200](https://doi.org/10.1109/TSG.2016.2574200).
- [44] MathWorks, *Matlab*, version R2020a.
- [45] —, *Simulink*, version R2020a.
- [46] Z. Tian, M. Chen, P. Weston, S. Hillmanssen, N. Zhao, C. Roberts, and L. Chen, "Energy evaluation of the power network of a dc railway system with regenerating trains," *IET Electrical Systems in Transportation*, vol. 6, Oct. 2015. DOI: [10.1049/iet-est.2015.0025](https://doi.org/10.1049/iet-est.2015.0025).
- [47] F. Mao, Z. Mao, and K. Yu, "The modeling and simulation of dc traction power supply network for urban rail transit based on simulink," *Journal of Physics: Conference Series*, vol. 1087, p. 042 058, Sep. 2018. DOI: [10.1088/1742-6596/1087/4/042058](https://doi.org/10.1088/1742-6596/1087/4/042058).
- [48] H. Xia, H. Chen, Z. Yang, F. Lin, and B. Wang, "Optimal energy management, location and size for stationary energy storage system in a metro line based on genetic algorithm," *Energies*, vol. 8, pp. 11 618–11 640, Oct. 2015. DOI: [10.3390/en81011618](https://doi.org/10.3390/en81011618).
- [49] J. Meester, "Analyse tractie-energievoorziening bij inzet m5 - uitgangspunten," Arcadis, 2015.
- [50] GVB, *Subway amsterdam timetable*. [Online]. Available: <https://reisinformatie.gvb.nl/en/lijnen> (visited on 06/11/2021).
- [51] M. Khodaparastan, O. Dutta, M. Saleh, and A. A. Mohamed, "Modeling and simulation of dc electric rail transit systems with wayside energy storage," *IEEE Transactions on Vehicular Technology*, vol. 68, no. 3, pp. 2218–2228, 2019. DOI: [10.1109/TVT.2019.2895026](https://doi.org/10.1109/TVT.2019.2895026).
- [52] PVsyst SA, *Pvsyst*, version 7.1.8 (rev. 20607).
- [53] S. Boudoudouh and M. Maaroufi, "Renewable energy sources integration and control in railway microgrid," *IEEE Transactions on Industry Applications*, vol. 55, no. 2, pp. 2045–2052, 2019. DOI: [10.1109/TIA.2018.2878143](https://doi.org/10.1109/TIA.2018.2878143).
- [54] K. De Brabandere, A. Woyte, R. Belmans, and J. Nijs, "Prevention of inverter voltage tripping in high density pv grids," *19th EU-PVSEC, Paris*, 2004.
- [55] T. Alquthami, R. S. Kumar, and A. Al Shaikh, "Mitigation of voltage rise due to high solar pv penetration in saudi distribution network," *Electrical Engineering*, pp. 1–10, 2020.

- [56] S. Yang, F. Liao, J. Wu, H. J. Timmermans, H. Sun, and Z. Gao, "A bi-objective timetable optimization model incorporating energy allocation and passenger assignment in an energy-regenerative metro system," *Transportation Research Part B: Methodological*, vol. 133, pp. 85–113, 2020, ISSN: 0191-2615. DOI: <https://doi.org/10.1016/j.trb.2020.01.001>.
- [57] E. Tröster and J.-D. Schmidt, "Evaluating the impact of pv module orientation on grid operation," in *Proceedings of the 2nd International Workshop on Integration of Solar Power into Power Systems, Lisbon, Portugal, 2012*.
- [58] T. J. Taylor, *Solar power is now competitive*. [Online]. Available: <https://blog.gaf.com/solar-power-is-now-competitive/> (visited on 07/02/2021).
- [59] BELECTRIC Solar Battery GmbH, *Peg solar power plant, revolution in utility-scale pv power*. [Online]. Available: <https://belectric.com/solarplants/peg/> (visited on 07/02/2021).
- [60] Ingeteam, *Ingeber: Converter for energy recovery*. [Online]. Available: https://www.ingeteam.com/en-us/sectors/railways/p15_59_601/ingeber.aspx (visited on 06/28/2021).
- [61] ABB Sp. z o.o., *Brochure enviline ers, energy recuperation system for dc rail transportation*. [Online]. Available: <https://library.e.abb.com/public/348174e8288f4093a3eca60b7d05d4a2/Enviline%20ERS%20EN.pdf> (visited on 06/28/2021).
- [62] *Kupower high efficiency poly module cs3k-300 (1500v)*, V5.61_EN, Canadian Solar Inc., 2020.
- [63] Eborx Solar Systems, *Pvshop.eu by eborx solar systems*. [Online]. Available: <https://pvshop.eu/canadiansolar> (visited on 07/06/2021).
- [64] M. Keijzer, "A multi-surface reflected irradiance model for pyranometer corrections and pv yield calculations in complex urban geometries," 2019.
- [65] *Elektroline inc.* [Online]. Available: <https://www.elektroline.cz/homepage.php>.
- [66] *Eeurope-solarshop*. [Online]. Available: <http://www.europe-solarshop.com/> (visited on 07/06/2021).
- [67] *Europe-solarstore*. [Online]. Available: <https://www.europe-solarstore.com/> (visited on 07/06/2021).
- [68] F. Baumgartner, "5 - photovoltaic (pv) balance of system components: Basics, performance," in *The Performance of Photovoltaic (PV) Systems*, N. Pearsall, Ed., Woodhead Publishing, 2017, pp. 135–181, ISBN: 978-1-78242-336-2. DOI: <https://doi.org/10.1016/B978-1-78242-336-2.00005-7>.
- [69] A. Saffirio, "Investigation of the potential of pv in trolleygrids: Study of the effect of key performance indicators on the integration of photovoltaic (pv) systems in trolleygrids-arnhem and gdynia case studies," 2021.

Appendix A

Power substations metro traction network Amsterdam

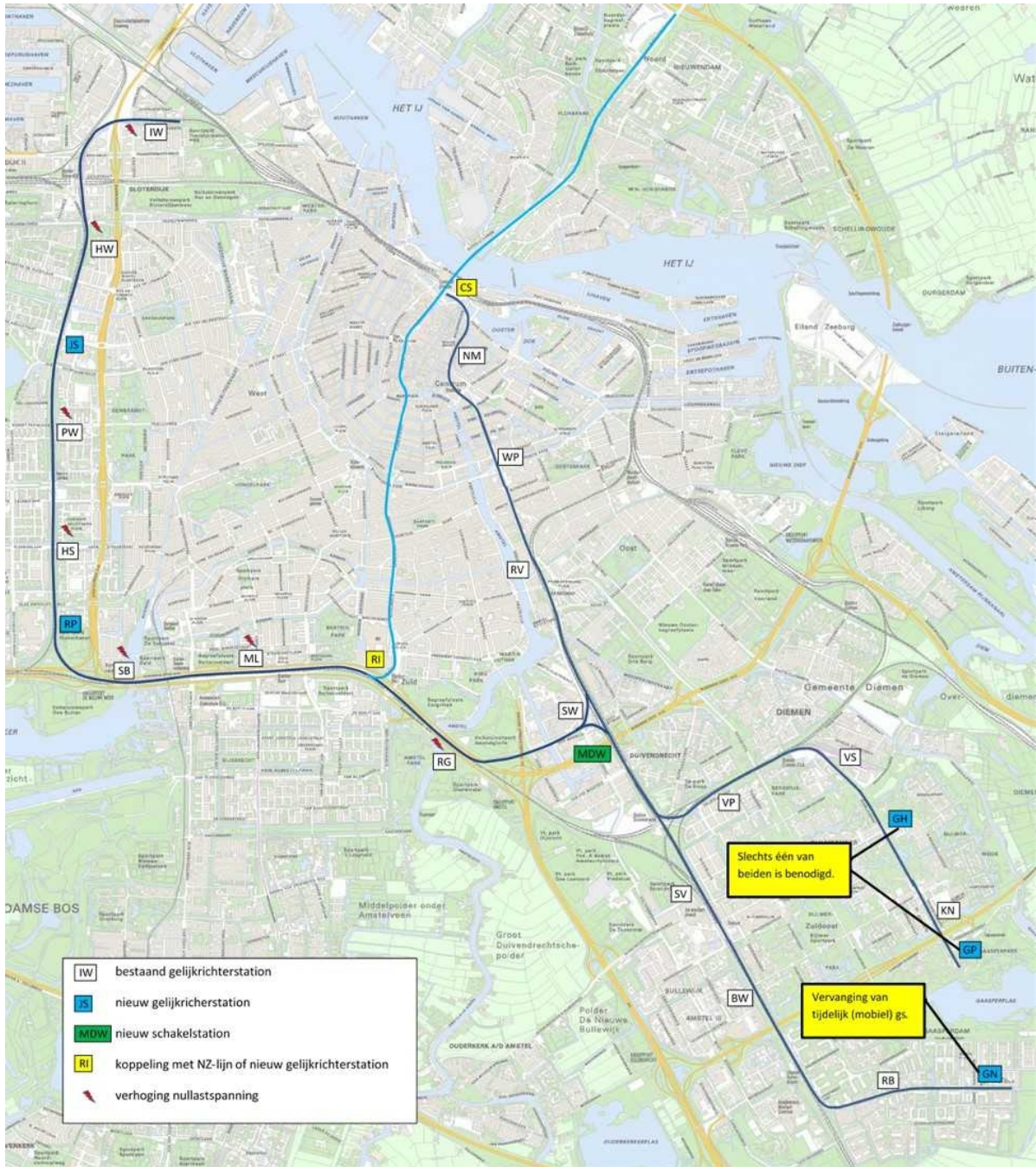


Figure A.1: Locations of substations

Appendix B

Profile of free space

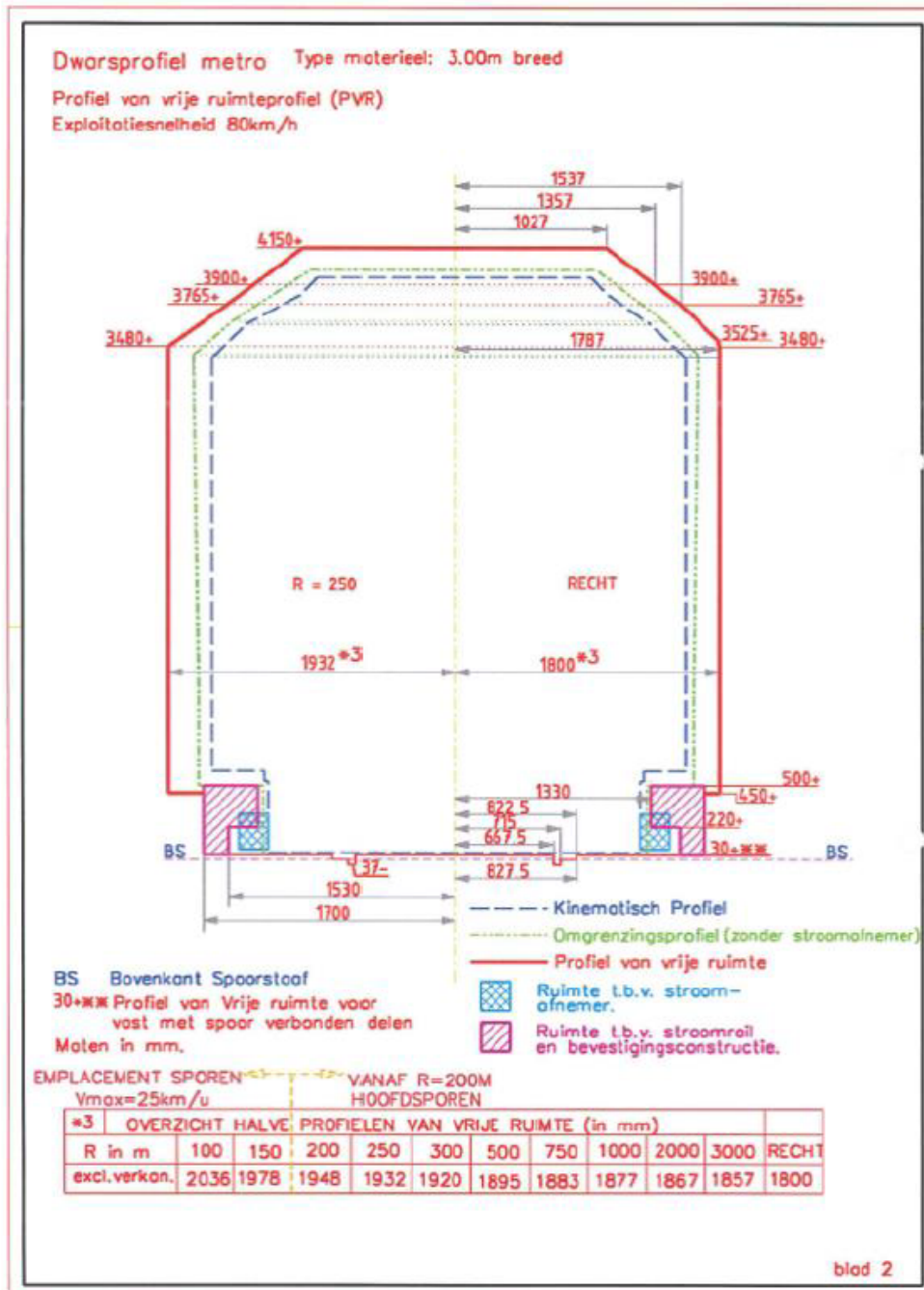


Figure B.1: Profile of free space

Appendix C

Power consumption and ohmic losses

(See next page)

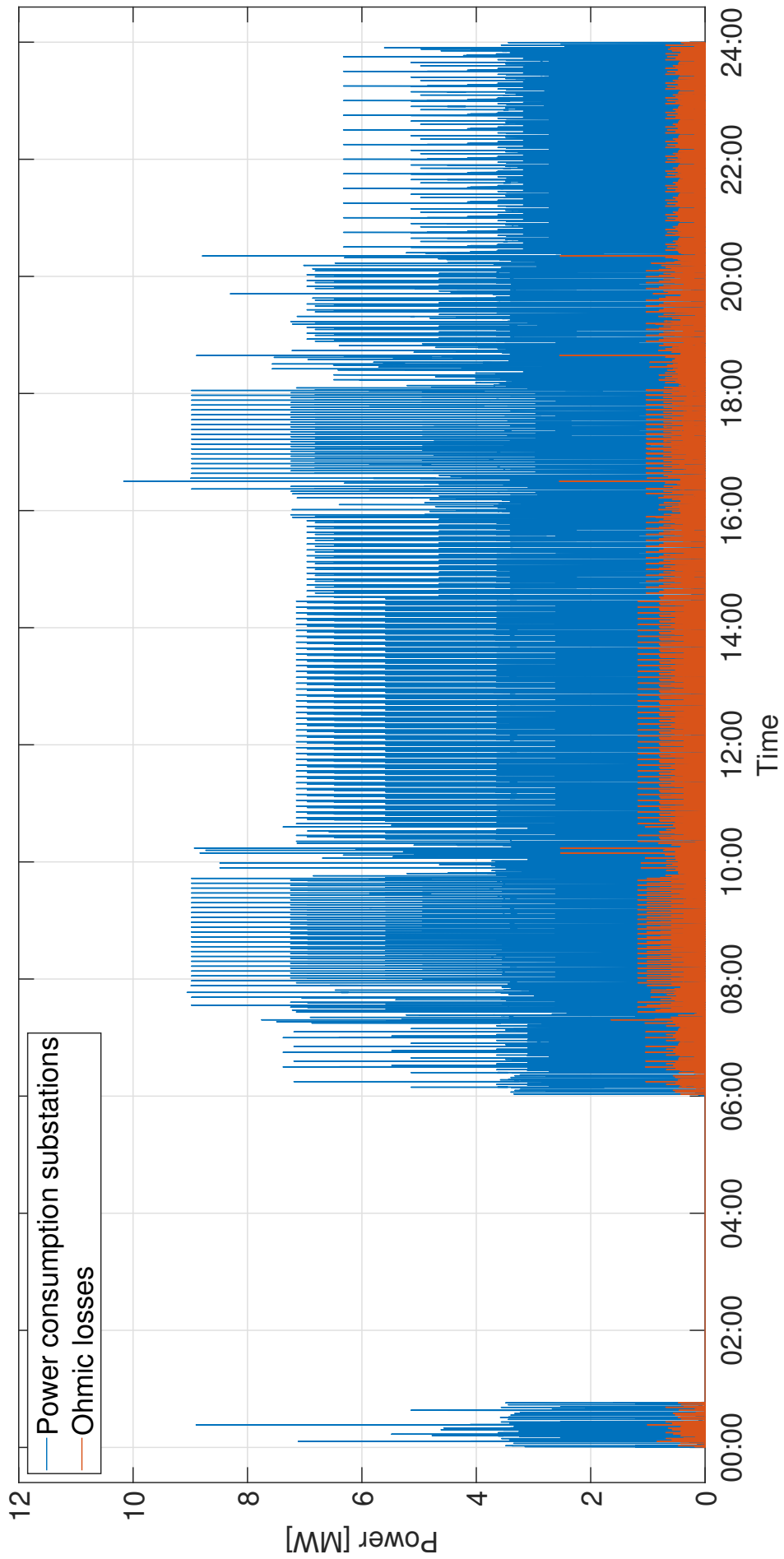


Figure C.1: Power consumption and ohmic losses in traction network during an entire day

Appendix D

Main results from PVsyst simulation

(See next page)



Main results

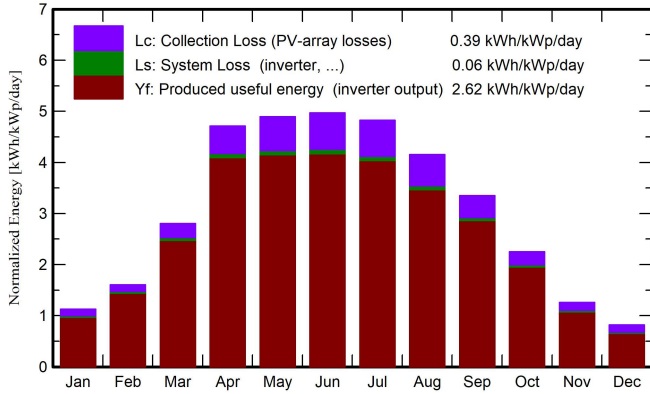
System Production

Produced Energy 191.3 MWh/year

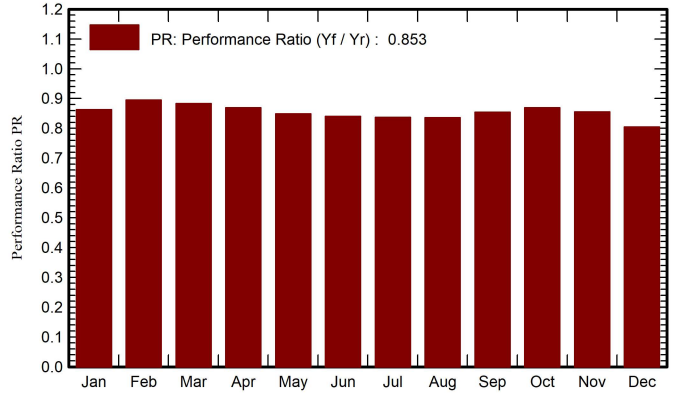
Specific production
Performance Ratio PR

956 kWh/kWp/year
85.31 %

Normalized productions (per installed kWp)



Performance Ratio PR



Balances and main results

	GlobHor kWh/m ²	DiffHor kWh/m ²	T_Amb °C	GlobInc kWh/m ²	GlobEff kWh/m ²	EArray MWh	E_Grid MWh	PR ratio
January	19.7	13.46	4.23	34.9	32.0	6.22	6.03	0.863
February	30.4	19.65	4.47	45.0	42.9	8.28	8.07	0.896
March	69.5	43.47	6.21	86.9	82.6	15.70	15.36	0.883
April	121.4	62.59	9.80	141.3	134.8	25.08	24.60	0.870
May	147.4	79.22	13.81	151.7	143.5	26.29	25.76	0.849
June	150.5	87.26	16.09	149.0	140.9	25.57	25.04	0.840
July	150.0	90.46	18.26	149.6	141.2	25.59	25.06	0.837
August	118.9	66.89	18.22	128.8	122.1	22.00	21.53	0.836
September	83.6	52.39	15.05	100.6	95.6	17.56	17.20	0.854
October	49.5	33.19	11.41	69.8	65.9	12.42	12.14	0.870
November	22.0	14.20	7.63	37.8	34.9	6.66	6.46	0.855
December	14.5	11.04	4.15	25.4	21.8	4.24	4.09	0.805
Year	977.4	573.84	10.82	1120.9	1058.2	195.61	191.34	0.853

Legends

- GlobHor Global horizontal irradiation
- DiffHor Horizontal diffuse irradiation
- T_Amb Ambient Temperature
- GlobInc Global incident in coll. plane
- GlobEff Effective Global, corr. for IAM and shadings
- EArray Effective energy at the output of the array
- E_Grid Energy injected into grid
- PR Performance Ratio

Appendix E

Costs and profit for three different systems

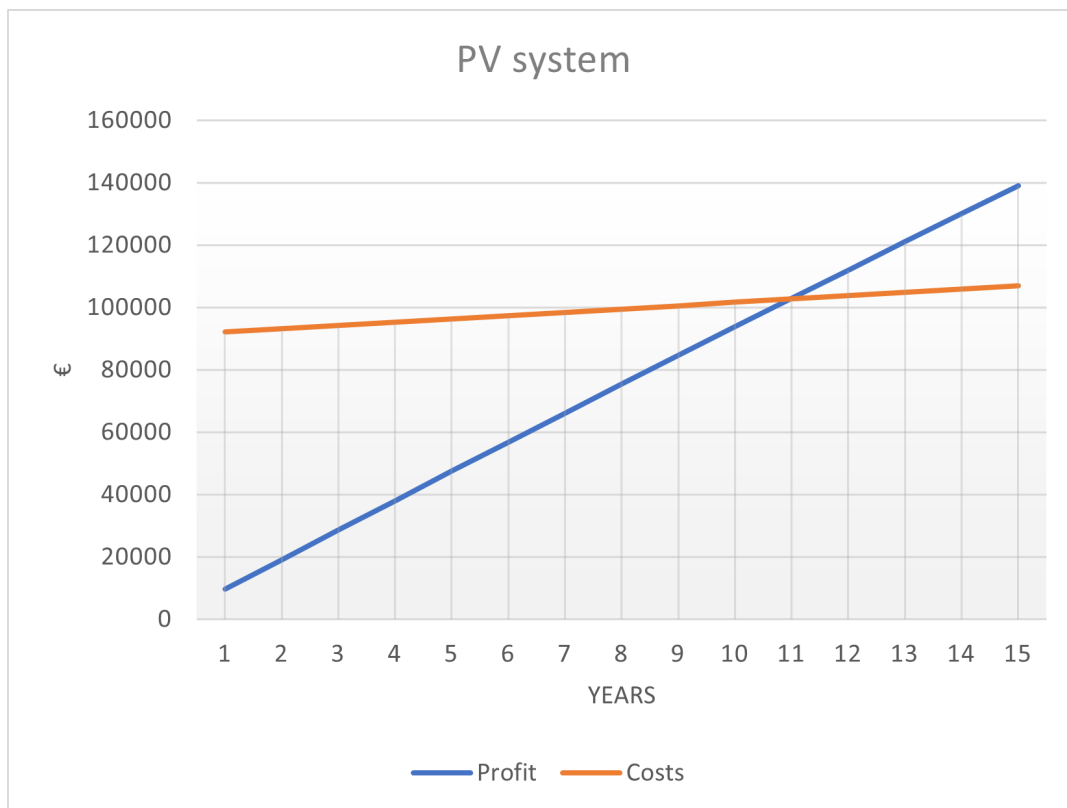


Figure E.1: Profit and costs for PV system

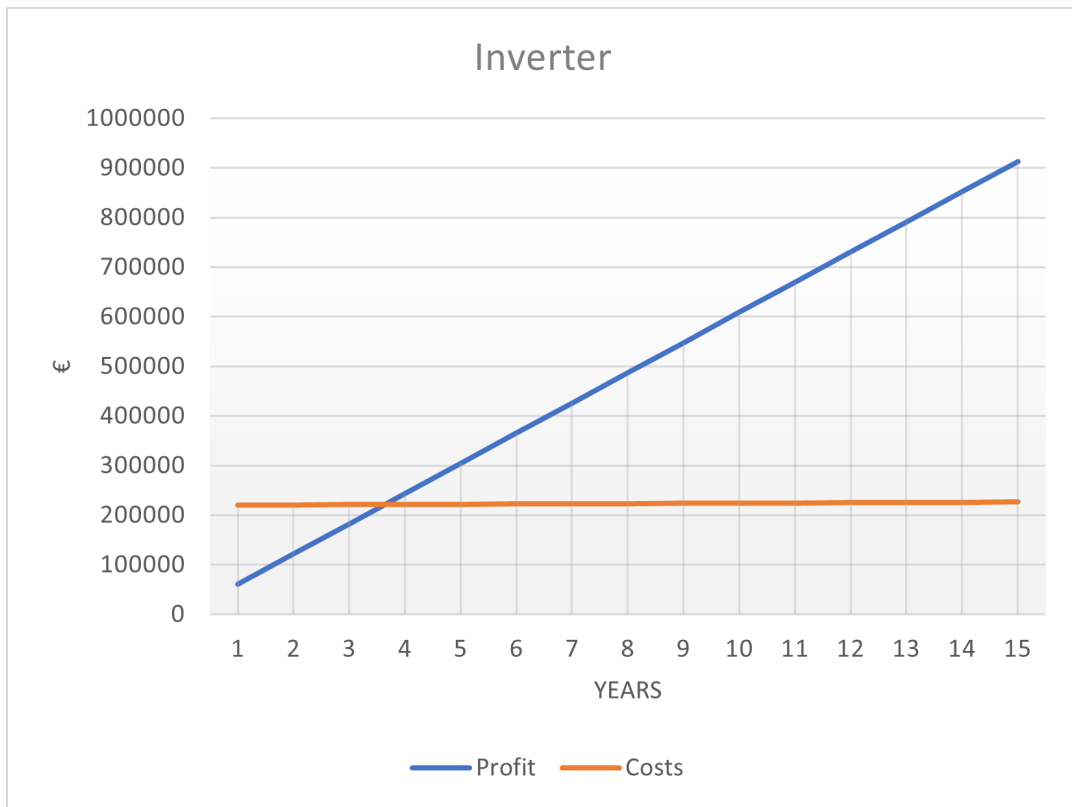


Figure E.2: Profit and costs for inverter

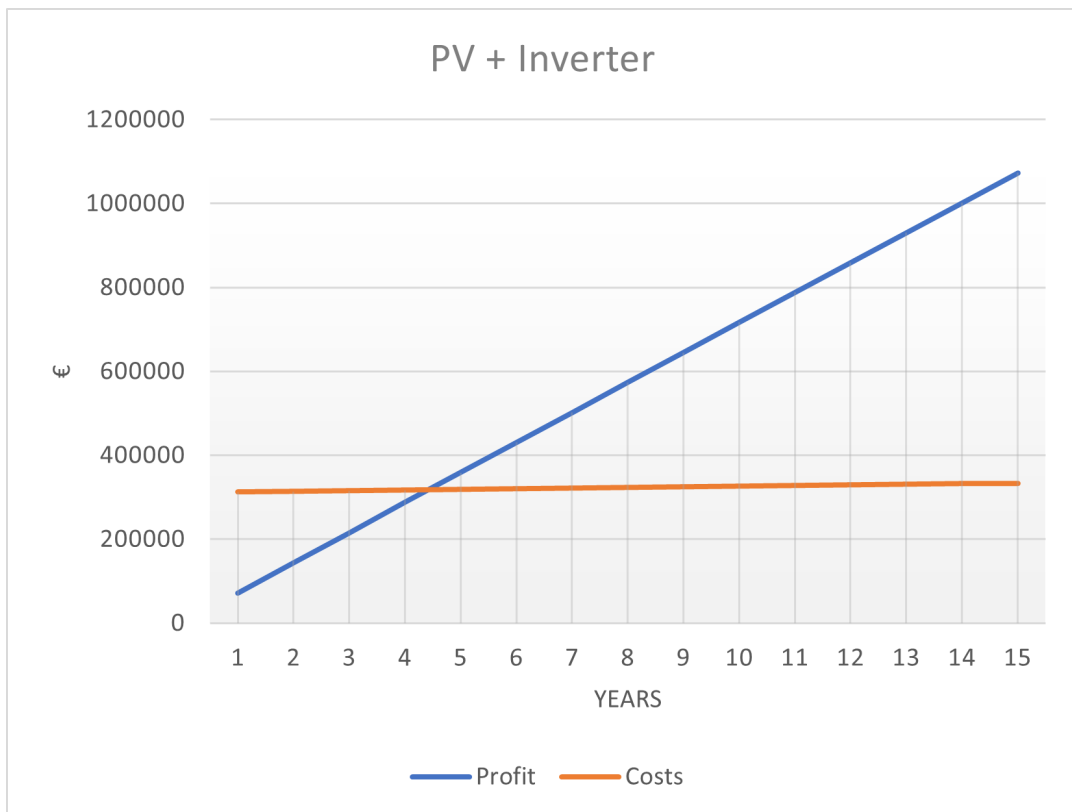


Figure E.3: Profit and costs for PV system + inverter